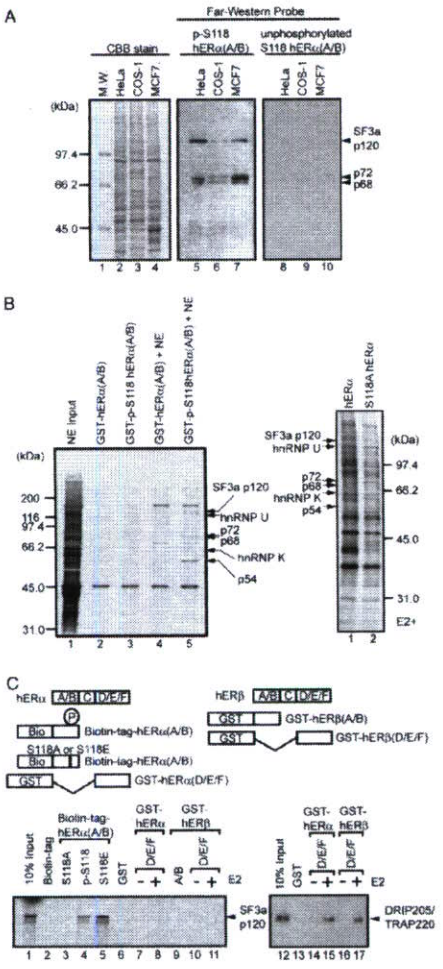

Fig. 1. SF3a p120 directly binds phosphorylated Ser-118 hERα (A/B) domains. (*A*) Endogenous interactants of the hERα (A/B) domain. Three endogenous interactants (p120, p72, and p68, as indicated) were detected in 10 μg of nuclear extracts from HeLa, COS-1, and MCF7 cells lines with Ser-118 phosphorylated or nonphosphorylated hERα (A/B) domain probes by using the Far-Western technique (20). (*Left*) Coomassie brilliant blue R-250 (CBB)-stained gel. (*B*) Identification of phosphorylated hERα (A/B) domain-interacting proteins. Nuclear extracts prepared from HeLa S3 cells were incubated with immobilized GST-hERα (A/B) or GST-*p*-Ser-118 hERα (A/B) domains. (*Left*) Proteins eluted from the columns by 1 M KCl were subjected to SDS/PAGE followed by staining with CBB. (*Right*) Products of FLAG-M2 resin affinity purification from nuclear extracts of HeLa cells stably expressing FLAG-hERα or FLAG-Ser-118–Ala hERα were examined by MS. Identified proteins are indicated at the right. (*C*) Selective binding of SF3a p120 to hERα in a pull-down assay. *In vitro*-translated SF3a p120 protein was tested for direct interaction with biotin-tagged hERα (A/B), chimeric GST-fused A/B domain of hERβ, or D/E/F domains of hERα or hERβ. DRIP205/TRAP220 was used as a positive control and exhibited ligand-induced association with the hERα D/E/F domain.

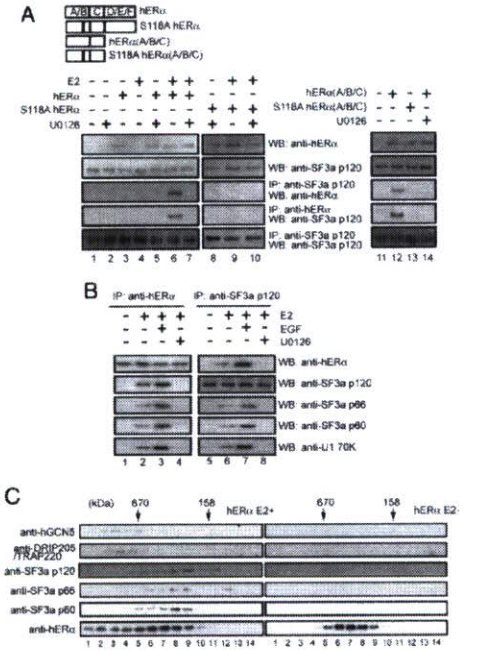

Fig. 2. Association of hERα AF-1 domain with spliceosome complex through SF3a p120. (*A*) *In vivo* association of hERα and SF3a p120. The 293T cells were transfected with hERα expression vectors (0.1 μg) and then incubated with or without E2 (10^{-8} M). Cells were then lysed in TNE buffer (10 mM Tris·HCl, pH 7.5, 150 mM NaCl, 1 mM EDTA, 1% NP-40) and immunoprecipitated with anti-hERα or anti-Flag SF3a p120 Ab. Immunoprecipitates were subjected to SDS/PAGE followed by Western blotting with the indicated Abs. (*B*) Ligand-induced association of full-length hERα with U1/U2 components was further characterized by using endogenous proteins in MCF7 cells. Cells were treated with E2 (10^{-8} M), EGF (100 ng/ml), and MAPK inhibitor U0126 (20 μM), as indicated, and then immunoprecipitated with anti-hERα or anti-SF3a p120 Ab. Immunoprecipitates were subjected to SDS/PAGE followed by Western blotting with the indicated Abs. (*C*) hERα associates with a complex containing SF3a spliceosome components. Nuclear extracts from a stable transformant of FLAG-tagged full-length hERα with or without E2 (10^{-7} M) were applied to FLAG-M2 resin, and eluted proteins were separated by using Superose 6 gel filtration column (10, 14) and detected by the indicated Abs.

transient transfection experiment by using a luciferase reporter plasmid bearing estrogen response elements (10, 20) transfected into 293T cells. Although SF3a p120 enhanced the estrogen-induced transactivation function of full-length hERα (Fig. 3*A*, lane 5), with a 2- to 3-fold increase in hERα (A/B/C) AF-1 activity (Fig. 3*B*, lane 5), no potentiation of AF-2 activity of hERα (D/E/F) was observed (data not shown). Introduction of SF3a p120 siRNA significantly lowered the ligand-induced transactivation of hERα and dramatically attenuated MAPK signaling-induced potentiation (Fig. 3*A*, lanes 6, 9, and 12). To examine the AF-1-specific coactivator function of SF3a p120 for full-length hERα, we tested SF3a p120 activity on hERα bound to 4-hydroxy-tamoxifen (TAM), an AF-1 agonist/AF-2 antagonist (16). As expected, partial transactivation of TAM-bound ERα was observed, presumably via activated AF-1 (Fig. 3*A*, lanes 19–27). This transactivation was potentiated by both SF3a p120 and MAPK activators, with the simultaneous addition of MAPK activators and SF3a p120 resulting in additive potentiation (Fig. 3*A*, compare lane 19 and lanes 20, 23, and 26). To further examine the SF3a p120 hERα AF-1 coactivator function, possible interaction with known hERα AF-1 coactivators was tested by coimmunoprecipitation by using SF3a p120. p68/p72 and p300 were detected in the SF3a p120 coimmunoprecipitants (data not shown), and we then verified these associations by further testing the complexes that formed around the hERα AF-1 domain (Fig. 3*C*). Purification of the SF3a p120-containing complex that associated with hERα (A/B/C) by using sequential affinity columns identified p68/72 and p300, which raised the hypothesis that SF3a p120 was the associating component of the p68/72 and p300 hERα AF-1 coactivator complex (20).

To examine these *in vivo* associations, we performed a chromatin immunoprecipitation assay by using full-length hERα in MCF7 cells, spliceosome complex components, and a gene promoter region from human oxytocin that contained an estrogen-responsive element (26). Upon 17β-estradiol (E2) stimulation, the SF3a subunits and hERα all were recruited to the oxytocin promoter along with RNA polymerase II (Fig. 3*D*).

Phosphorylated hERα Associates with the Spliceosome Through SF3a p120. Because SF3a p120 is known to be a component of U2 small nuclear ribonucleoprotein particle, which forms the spliceosome along with the U1 complex (24, 25), we used coimmunoprecipitation to determine whether phosphorylated hERα associated with the spliceosome via SF3a p120. Coimmunoprecipitation experiments were performed with extracts from hERα-expressing MCF7 cells, and results indicated that all U1/U2 endogenous components tested (U2: SF3a p66, SF3a p60 small nuclear ribonucleoprotein particles; and U1: U1 70K small nuclear ribonucleoprotein particles) (27, 28) were coimmunoprecipitated with endogenous hERα, with these associations potentiated by EGF treatment (Fig. 2*B*, lanes 1–4). Similar results were obtained by using anti-SF3a p120 (Fig. 2*B*, lanes 5–8). Moreover, the U2 components were detected as a single complex by Western blotting after liganded hERα-associated complexes were biochemically isolated from HeLa nuclear extracts and fractionated by gel filtration (10, 14, 29) (Fig. 2*C Left*, lanes 8 and 9).

SF3a p120 Potentiates hERα-Mediated RNA Splicing. To test whether the phosphorylation-dependent association of hERα with spliceosome components modulated mRNA processing, we examined the effect of SF3a p120 on RNA splicing by using a test CD44 minigene, as reported (Fig. 4*A*) (22). Although estrogen (E2) stimulated transcription via hERα or hERβ (Fig. 4*B*, lanes 6 and 12), the ratio of skipped to unskipped transcripts was enhanced only by liganded ERα. SF3a p120 clearly potentiated hERα-mediated RNA splicing (Fig. 4*B*, lane 7). Unlike SF3a p120, neither p68 nor p72 was able to potentiate intron excision. Indeed, p68/p72 inhibited exon skipping in the CD44 minigene (Fig. 4*B*, lane 8), as expected from previous studies (22, 30), despite the finding that p68/p72 coactivated ERα-mediated transcription (see Fig. 3*A*, lane 16–18, for p72 activity as a representative of p68/p72) (19, 20). Similar results were observed by using a human β-globin minigene and a mutant ERα AF-1 domain fused to the yeast GAL4-DNA binding domain. In

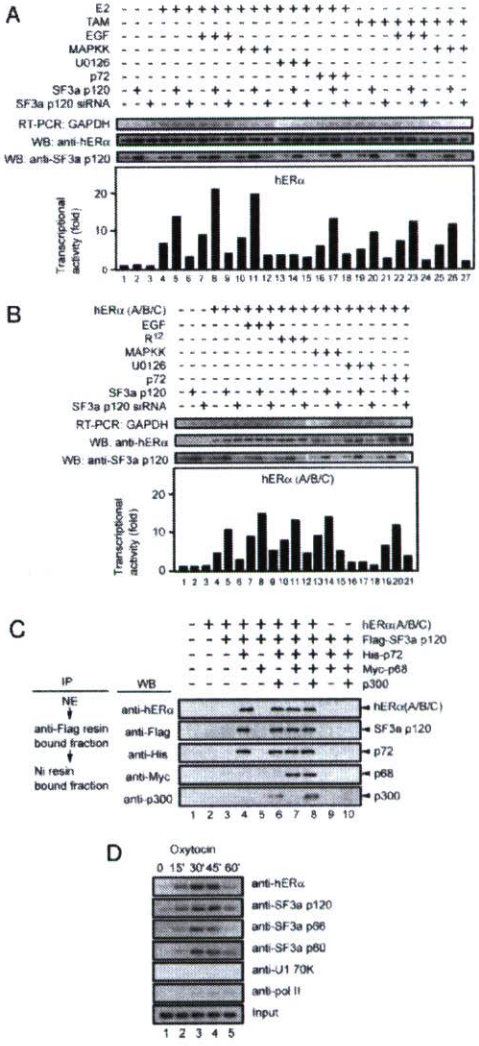

Fig. 3. SF3a p120 coactivates the transactivation function of hERα AF-1. (*A* and *B*) SF3a p120 potentiates the transactivation function of hERα AF-1 in a Ser-118 phosphorylation-dependent manner. The 293T cells were transfected with expression vectors of full-length hERα (50 ng), hERα (A/B/C) (50 ng), Ki-Ras^{val12} (R^{12}) (100 ng), MAPKK (100 ng), SF3a p120 (300 ng), or combinations as indicated, in either the absence or presence of E2 (10^{-8} M), TAM (10^{-7} M), U0126 (20 μM), or combinations as indicated, along with pGL-estrogen response element-tk (1.0 μg) and pRL-CMV (10 ng). Cultured cells were also transfected with 100 pmol dsRNA for SF3a p120 siRNA (5′-AGACGGAAUGGAAACUGAAUGGGCAAG-3′ and 5′-UGCCCAUUCAGUUUCCAUUCCGUCUAU-3′) by using Lipofectamine 2000 (Invitrogen). Assays were performed 24 h after transfection. (*Upper*) Cell extracts were used in luciferase assays (20) and Western blotting. (*C*) SF3a p120 enhances the association of hERα AF-1 with p68, p72, and p300. The 293T cells were transfected with indicated plasmids. The complex associated with A/B/C domains of hERα were analyzed to detect SF3a p120, p68, p72, and p300 by purification from the cell extracts with anti-Flag M2 resin and Ni resin, followed by Western blotting by using the anti-hERα, anti-Flag, anti-His, anti-Myc, or anti-p300 Abs (lanes 1–10). (*D*) Occupancy of human oxytocin promoter by hERα and spliceosome components in MCF7 cells was determined by chromatin immunoprecipitation analysis (14, 23).

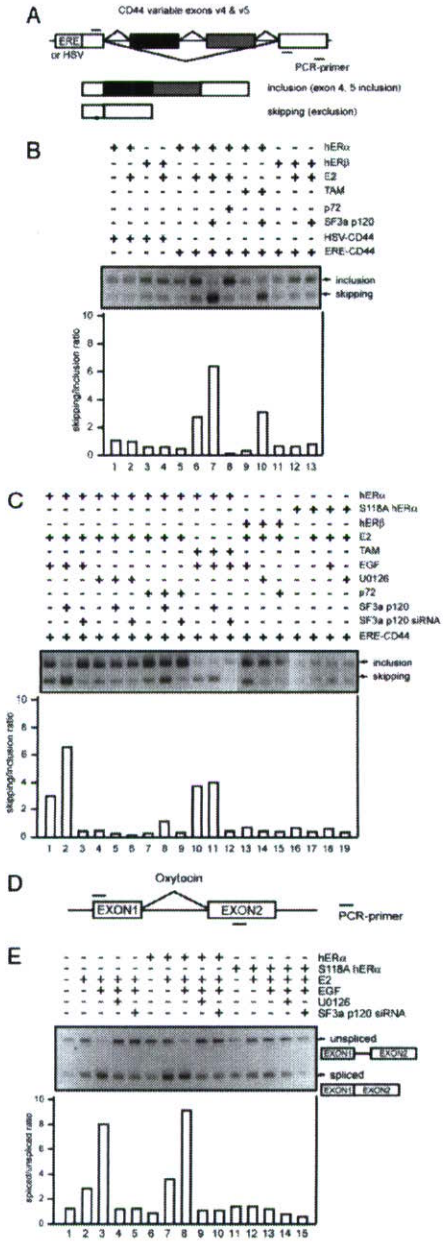

Fig. 4. hERα AF-1-specific potentiation of mRNA processing by SF3a p120. (*A*) Schematic representation of the estrogen response element-CD44 construct used in the *in vivo* splicing assay (22). (*B* and *C*) SF3a p120 regulation of CD44 mRNA processing depends on hERα Ser-118 phosphorylation state. The 293T cells were transfected with the indicated plasmids and siRNA (SF3a p120; 100 pmol). After transfection, cells were treated with E2 (10−8 M), TAM (10−7 M), EGF (100 ng/ml), and U0126 (20 μM) as indicated. Total RNA was extracted with Isogen 24 h after transfection and subjected to RT-PCR analysis (22). (*D*) Schematic representation of the human oxytocin gene exon 1 and 2 used in the *in vivo* splicing assay. (*E*) MCF7 cells were transfected with the indicated plasmids and treated as in *B* and *C*. After the treatment, total RNA was extracted. Splicing patterns were evaluated by RT-PCR by using oxytocin-specific primers.

that system, the hERα AF-1 domain alone was able to potentiate RNA splicing (data not shown).

RNA Splicing Augmented by hERα Depends on hERα Ser-118 Phosphorylation by MAPK. Reflecting the Ser-118 phosphorylation-dependent association between hERα and SF3a p120 (Fig. 2*A*), both Ala substitution in the AF-1 domain (S118A) (Fig. 4*C*, lanes 16–19) and SF3a p120 siRNA (Fig. 4*C*, lanes 3, 6, and 9) abrogated the potentiation of intron excision by hERα. The efficiency of RNA splicing from the CD44 minigene mediated by hERα appeared to depend on SF3a p120 expression level and activated MAPK signaling via EGF treatment (Fig. 4*C*, compare lanes 1 and 4). TAM treatment (20) further confirmed the AF-1 specificity of SF3a p120 on hERα (Fig. 4*B*, compare lanes 9 and 10). Neither potentiation of exon skipping by SF3a p120 nor increased RNA splicing caused by activated MAPK was observed for the full-length hERα Ser-118–Ala mutant (Fig. 4*C*, lanes 16–19). Reflecting the phosphorylation-dependent association of SF3a p120 with hERα through the A/B AF-1 domain, activation of MAPK by Ki-Ras^{val12}, MAPKK, or EGF also potentiated the effects of SF3a p120 on RNA splicing mediated by the hERα A/B-AF-1 domain alone (data not shown). Such potentiation via activated MAPK signaling was not detectable in the hERα Ser-118–Ala mutant A/β-GAL-DNA binding domain (data not shown). Notably, neither a significant increase in spliced transcript stability nor specific intracellular localization was observed when transcription was potentiated under any of the conditions tested (data not shown).

Finally, to address the physiological relevance of our findings, we screened several known endogenous ERα target genes that show ERα-regulated splicing. We found that the human oxytocin gene generated a transcript that retained intron 1 sequence (see Fig. 4*D*). In response to E2 treatment, intron 1 splicing was increased along with enhanced transcription in MCF7 cells (Fig. 4*E*, compare lanes 1 and 2). EGF-mediated MAPK activation further enhanced RNA splicing mediated by hERα (Fig. 4*E*, lanes 3 and 8). However, Ser-118–Ala hERα expression abrogated this increase in RNA splicing after EGF treatment (Fig. 4*E*, lane 13). Thus, our findings suggested that the potentiation of splicing efficiency mediated via the association of phosphorylated hERα with SF3a p120 occurred in at least some hERα target genes.

Cross-Talk Between Estrogen and Growth Factor Signaling Mediates the Control of RNA Splicing. Our study uncovered a unique mechanism by which RNA splicing is potentiated by MAPK-mediated growth factor signaling through Ser-118 phosphorylation of hERα, such that augmented RNA splicing may, at least in part, account for the effects of SF3a p120 coactivation on the ligand-induced transactivation functions of hERα. Based on our findings, it is also possible that phosphorylated, but DNA-unbound, hERα may serve as a coregulator of RNA splicing in some estrogen-responsive gene promoters. Recent reports have shown that the RNA splicing process is coupled with transcriptional events under the control of sequence-specific activators, such as peroxisome proliferator-activated receptor (PPAR)γ and steroid receptors (22, 30–35). Thus, given the current view that the progression from transcription to splicing is a sequential, yet rapid process (36), it is likely that the spliceosome functionally associates, directly or indirectly, with activator molecules, presumably including coregulators and transcription elongation factors. The efficiency of RNA splicing is then modulated via the association between transcription-related factors and the spliceosome. The present study provides an example of coordinated regulation of transcription and intron excision modulated by growth factor signaling via the association of an activator with the spliceosome. This mechanism may support, at least in part, growth factor-mediated gene regulation.

We thank Dr. C. Will (Max Planck Institute, Gottingen, Germany) for the kind gift of the U1 70K plasmid; Drs. M. Saitoh, K. Goto, and H. Nawata for technical help; Drs. P. Chambon, D. Metzger, and H. Kawate for helpful suggestions and plasmids; and H. Higuchi for manuscript preparation. This work was supported in part by the Program for Promotion of Basic Research Activities for Innovative Biosciences and priority areas from the Ministry of Education, Science, Sports and Culture of Japan (to S.K.) and National Institutes of Health Grant 08818 (to B.W.O.).

1. Parker, M. G. (1998) *Biochem. Soc. Symp.* **63,** 45–50.
2. Kushner, P. J., Agard, D. A., Greene, G. L., Scanlan, T. S., Shiau, A. K., Uht, R. M. & Webb, P. (2000) *J. Steroid Biochem. Mol. Biol.* **74,** 311–317.
3. Onate, S. A., Tsai, S. Y., Tsai, M. J. & O'Malley, B. W. (1995) *Science* **270,** 1354–1357.
4. Chen, H., Lin, R. J., Schiltz, R. L., Chakravarti, D., Nash, A., Nagy, L., Privalsky, M. L., Nakatani, Y. & Evans, R. M. (1997) *Cell* **90,** 569–580.
5. Kamei, Y., Xu, L., Heinzel, T., Torchia, J., Kurokawa, R., Gloss, B., Lin, S. C., Heyman, R. A., Rose, D. W., Glass, C. K., *et al.* (1996) *Cell* **85,** 403–414.
6. Spencer, T. E., Jenster, G., Burcin, M. M., Allis, C. D., Zhou, J., Mizzen, C. A., McKenna, N. J., Onate, S. A., Tsai, S. Y., Tsai, M. J., *et al.* (1997) *Nature* **389,** 194–198.
7. Lanz, R. B., McKenna, N. J., Onate, S. A., Albrecht, U., Wong, J., Tsai, S. Y., Tsai, M. J. & O'Malley, B. W. (1999) *Cell* **97,** 17–27.
8. McKenna, N. J. & O'Malley, B. W. (2002) *Cell* **108,** 465–474.
9. Spiegelman, B. M. & Heinrich, R. (2004) *Cell* **119,** 157–167.
10. Yanagisawa, J., Kitagawa, H., Yanagida, M., Wada, O., Ogawa, S., Nakagomi, M., Oishi, H., Yamamoto, Y., Nagasawa, H., McMahon, S. B., *et al.* (2002) *Mol. Cell* **9,** 553–562.
11. Fondell, J. D., Ge, H. & Roeder, R. G. (1996) *Proc. Natl. Acad. Sci. USA* **93,** 8329–8333.
12. Rachez, C., Lemon, B. D., Suldan, Z., Bromleigh, V., Gamble, M., Naar, A. M., Erdjument-Bromage, H., Tempst, P. & Freedman, L. P. (1999) *Nature* **398,** 824–828.
13. Naar, A. M., Beaurang, P. A., Zhou, S., Abraham, S., Solomon, W. & Tjian, R. (1999) *Nature* **398,** 828–832.
14. Ohtake, F., Takeyama, K., Matsumoto, T., Kitagawa, H., Yamamoto, Y., Nohara, K., Tohyama, C., Krust, A., Mimura, J., Chambon, P., *et al.* (2003) *Nature* **423,** 545–550.
15. Couse, J. F. & Korach, K. S. (1999) *Endocr. Rev.* **20,** 358–417.
16. Kato, S., Endoh, H., Masuhiro, Y., Kitamoto, T., Uchiyama, S., Sasaki, H., Masushige, S., Gotoh, Y., Nishida, E., Kawashima, H., *et al.* (1995) *Science* **270,** 1491–1494.
17. Feng, W., Webb, P., Nguyen, P., Liu, X., Li, J., Karin, M. & Kushner, P. J. (2001) *Mol. Endocrinol.* **15,** 32–45.
18. Chen, D., Riedl, T., Washbrook, E., Pace, P. E., Coombes, R. C., Egly, J. M. & Ali, S. (2000) *Mol. Cell* **6,** 127–137.
19. Endoh, H., Maruyama, K., Masuhiro, Y., Kobayashi, Y., Goto, M., Tai, H., Yanagisawa, J., Metzger, D., Hashimoto, S. & Kato, S. (1999) *Mol. Cell. Biol.* **19,** 5363–5372.
20. Watanabe, M., Yanagisawa, J., Kitagawa, H., Takeyama, K., Ogawa, S., Arao, Y., Suzawa, M., Kobayashi, Y., Yano, T., Yoshikawa, H., *et al.* (2001) *EMBO J.* **20,** 1341–1352.
21. Kobayashi, Y., Kitamoto, T., Masuhiro, Y., Watanabe, M., Kase, T., Metzger, D., Yanagisawa, J. & Kato, S. (2000) *J. Biol. Chem.* **275,** 15645–15651.
22. Auboeuf, D., Honig, A., Berget, S. M. & O'Malley, B. W. (2002) *Science* **298,** 416–419.
23. Shang, Y., Hu, X., DiRenzo, J., Lazar, M. A. & Brown, M. (2000) *Cell* **103,** 843–852.
24. Brosi, R., Groning, K., Behrens, S. E., Luhrmann, R. & Kramer, A. (1993) *Science* **262,** 102–105.
25. Brosi, R., Hauri, H. P. & Kramer, A. (1993) *J. Biol. Chem.* **268,** 17640–17646.
26. Stedronsky, K., Telgmann, R., Tillmann, G., Walther, N. & Ivell, R. (2002) *J. Neuroendocrinol.* **14,** 472–485.
27. Nilsen, T. W. (2003) *BioEssays* **25,** 1147–1149.
28. Soret, J. & Tazi, J. (2003) *Prog. Mol. Subcell. Biol.* **31,** 89–126.
29. Kitagawa, H., Fujiki, R., Yoshimura, K., Mezaki, Y., Uematsu, Y., Matsui, D., Ogawa, S., Unno, K., Okubo, M., Tokita, A., *et al.* (2003) *Cell* **113,** 905–917.
30. Cramer, P., Caceres, J. F., Cazalla, D., Kadener, S., Muro, A. F., Baralle, F. E. & Kornblihtt, A. R. (1999) *Mol. Cell* **4,** 251–258.
31. Monsalve, M., Wu, Z., Adelmant, G., Puigserver, P., Fan, M. & Spiegelman, B. M. (2000) *Mol. Cell* **6,** 307–316.
32. Iwasaki, T., Chin, W. W. & Ko, L. (2001) *J. Biol. Chem.* **276,** 33375–33383.
33. Zhao, Y., Goto, K., Saitoh, M., Yanase, T., Nomura, M., Okabe, T., Takayanagi, R. & Nawata, H. (2002) *J. Biol. Chem.* **277,** 30031–30039.
34. Brand, M., Moggs, J. G., Oulad-Abdelghani, M., Lejeune, F., Dilworth, F. J., Stevenin, J., Almouzni, G. & Tora, L. (2001) *EMBO J.* **20,** 3187–3196.
35. Honig, A., Auboeuf, D., Parker, M. M., O'Malley, B. W. & Berget, S. M. (2002) *Mol. Cell. Biol.* **22,** 5698–5707.
36. Orphanides, G. & Reinberg, D. (2002) *Cell* **108,** 439–451.

The EMBO Journal (2005) 24, 3881–3894 | © 2005 European Molecular Biology Organization | All Rights Reserved 0261-4189/05
www.embojournal.org

THE EMBO JOURNAL

Ligand-induced transrepression by VDR through association of WSTF with acetylated histones

Ryoji Fujiki[1], Mi-sun Kim[1], Yasumasa Sasaki[1], Kimihiro Yoshimura[1], Hirochika Kitagawa[1] and Shigeaki Kato[1,2,*]

[1]The Institute of Molecular and Cellular Biosciences, The University of Tokyo, Bunkyo-ku, Tokyo, Japan and [2]ERATO, Japan Science and Technology, Kawaguchi, Saitama, Japan

We have previously shown that the novel ATP-dependent chromatin-remodeling complex WINAC is required for the ligand-bound vitamin D receptor (VDR)-mediated transrepression of the 25(OH)D_3 1α-hydroxylase (1α(OH)ase) gene. However, the molecular basis for VDR promoter association, which does not involve its binding to specific DNA sequences, remains unclear. To address this issue, we investigated the function of WSTF in terms of the association between WINAC and chromatin for ligand-induced transrepression by VDR. Results of *in vitro* experiments using chromatin templates showed that the association of unliganded VDR with the promoter required physical interactions between WSTF and both VDR and acetylated histones prior to VDR association with chromatin. The acetylated histone-interacting region of WSTF was mapped to the bromodomain, and a WSTF mutant lacking the bromodomain served as a dominant-negative mutant in terms of ligand-induced transrepression of the 1α(OH)ase gene. Thus, our findings indicate that WINAC associates with chromatin through a physical interaction between the WSTF bromodomain and acetylated his tones, which appears to be indispensable for VDR/promoter association for ligand-induced transrepression of 1α(OH)ase gene expression.

The EMBO Journal (2005) **24**, 3881–3894. doi:10.1038/sj.emboj.7600853; Published online 27 October 2005
Subject Categories: chromatin & transcription
Keywords: acetylated histone; transrepression; VDIR; VDR; WSTF

Introduction

Lipophilic ligands, such as fat-soluble vitamins A and D, as well as thyroid/steroid hormones, are thought to exert their physiological effects through transcriptional control of target genes via cognate nuclear receptors (NRs) (Mangelsdorf *et al*, 1995). NRs form a gene superfamily, and they act as ligand-inducible activators. A number of coregulator complexes that support ligand-dependent transcription control have been identified, and these complexes can be classified into three categories according to function (Glass and Rosenfeld, 2000). The first coregulator complex class regulates transcriptional control directly, through a physical interaction with general transcription factors and RNA polymerase II (Rachez *et al*, 1998; Gu *et al*, 1999). Members of the second coregulator complex class modify histone tails covalently, for example by acetylation, in promoter nucleosomal arrays (Onate *et al*, 1995; Kamei *et al*, 1996; Heinzel *et al*, 1997; Yanagisawa *et al*, 2002). The major function of the last class of complexes is chromatin remodeling, which involves the ATP-dependent dynamic remodeling of chromatin structure (Ito *et al*, 1997; Fyodorov and Kadonaga, 2001; Lemon *et al*, 2001; Narlikar *et al*, 2002; Kitagawa *et al*, 2003). Chromatin-remodeling complexes utilize energy from ATP hydrolysis to rearrange nucleosomal arrays in a non-covalent manner. As chromosomal DNA is generally packed as nucleosomal arrays, chromatin-remodeling complexes are thought to render specific promoter regions accessible to other coregulator complex classes and sequence-specific regulators.

Recently, we identified a novel, multifunctional, ATP-dependent chromatin-remodeling complex, designated WINAC, which consists of 13 subunits (Kitagawa *et al*, 2003). It contains SWI/SNF chromatin-remodeling complex components and DNA replication-related factors. Vitamin D receptor (VDR) interacts with WINAC in a ligand-independent manner through the Williams syndrome transcription factor (WSTF). WSTF belongs to bromodomain adjacent to a zinc-finger motif (BAZ) protein family. Members of this family harbor both a PHD finger and a bromodomain in their C-terminal domain (Jones *et al*, 2000). As bromodomains have been recently shown to bind acetylated histones, it is possible that WSTF serves as an adaptor protein for acetylated histones, facilitating the association between WINAC and chromatin (Dhalluin *et al*, 1999; Winston and Allis, 1999; Jacobson *et al*, 2000; Hassan *et al*, 2002).

Expression of the 25(OH)D_3 1α-hydroxylase (1α(OH)ase) gene, a key enzyme in vitamin D biosynthesis, is negatively regulated by vitamin D (Takeyama *et al*, 1997; Yoshizawa *et al*, 1997; Murayama *et al*, 1998). We recently reported that a bHLH-type activator, VDR-interacting repressor (VDIR), directly binds to the negative vitamin D response element (1αnVDRE) in the human 1α(OH)ase gene promoter, thus activating transcription (Murayama *et al*, 2004). However, ligand-induced association between VDR and VDIR results in ligand-induced transrepression of 1α(OH)ase gene expression. This occurs through the switching of coregulator complexes from histone acetyltransferase (HAT) coactivator complexes to histone deacetylase (HDAC) corepressors upon VDIR binding to 1αnVDRE (Murayama *et al*, 2004). However, the molecular basis of VDR targeting to 1αnVDRE in the chromatinized 1α(OH)ase gene promoter remained unclear.

In the present study, we demonstrate, using chromatin templates *in vitro*, that both ligand-free VDR and WINAC avidly associate with the 1α(OH)ase gene promoter when the promoter region is reconstituted as a nucleosomal array. The WSTF bromodomain in WINAC appears to serve as a chromatin-targeting module that escorts ligand-free VDR to the promoter via a physical interaction with acetylated histones. Thus, our findings show that WINAC associates with chromatin through a physical interaction between the WSTF bromodomain and acetylated histones. This apparently contributes to the association between unliganded VDR and the promoter, resulting in a ligand-induced transrepression of human 1α(OH)ase gene expression.

*Corresponding author. The Institute of Molecular and Cellular Biosciences, The University of Tokyo, 1-1-1 Yayoi, Bunkyo-ku, Tokyo 113-0032, Japan. Tel.: +81 3 5841 8478; Fax: +81 3 5841 8477; E-mail: uskato@mail.ecc.u-tokyo.ac.jp

Received: 23 May 2005; accepted: 6 October 2005; published online: 27 October 2005

Results

Involvement of WSTF in ligand-induced transrepression by VDR/VDIR of the 1α(OH)ase gene promoter

It has previously been shown that VDIR activates transcription via specific binding to 1αnVDRE in the promoter (Murayama *et al*, 2004). The association of liganded VDR with VDIR then inhibits VDIR transactivation function through recruitment of an HDAC corepressor complex, resulting in ligand-induced transrepression (Murayama *et al*, 2004). Although WSTF was previously shown to be involved in 1α(OH)ase gene regulation (Kitagawa *et al*, 2003; Kato *et al*, 2004), the function of WSTF, with respect to ligand-induced VDR/VDIR transrepression, remained unclear.

We employed a transient expression assay using MCF7 cells, which express the 1α(OH)ase gene endogenously, and a luciferase reporter gene plasmid containing two consensus 1αnVDRE sequences recognized by VDIR. These sequences confer negative responsiveness to 1α,25(OH)$_2D_3$ in gene repression. 1α,25(OH)$_2D_3$ transrepressed transcription of the reporter gene, and this repression was enhanced in the presence of VDR/RXR expression (Figure 1A).

We further assessed whether endogenous VDR, VDIR and WSTF were responsible for ligand-induced negative responsiveness of the 1α(OH)ase gene, using RNAi in a transient expression assay, in which a reporter gene was driven by the native promoter. The analysis confirmed that RNAi down-regulated expression of the target endogenous factors without modulating the expression levels of the other factors (Figure 1B). We confirmed that WSTF-RNAi and VDIR-RNAi are able to abrogate the transrepression function of VDIR and WSTF, respectively, and VDR-RNAi eliminates both of them (Figure 1C). These results show that it is likely that WSTF mediates the ligand-induced transrepression of the 1α(OH)ase gene, together with VDR and VDIR.

WSTF associates with VDIR in a ligand-dependent manner

Based on our findings that WSTF appears to play a role in ligand-induced VDR/VDIR transrepression, we further examined the complex formed by these three factors in MCF-7 cells using an immunoprecipitation assay. As unliganded VDR was reported to associate with NCoR corepressor complex (Glass and Rosenfeld, 2000), the corepressor dissociation of exogenous VDR was observed in response to ligand binding (Figure 2A, lanes 3 and 4). As previously reported (Kitagawa *et al*, 2003; Kato *et al*, 2004; Murayama *et al*, 2004), while VDR associated with WSTF irrespective of 1α,25(OH)$_2D_3$ binding, 1α,25(OH)$_2D_3$ binding enhanced the interaction between VDR and VDIR (Figure 2A, lanes 3–8). Exogenous WSTF co-immunoprecipitated with exogenous VDIR in a ligand-dependent manner, and with endogenous NCoR corepressor complex components (NCoR, mSin3 and HDAC2) in the presence of 1α,25(OH)$_2D_3$ (Figure 2A, lanes 7 and 8). Furthermore, we found that an HDAC inhibitor trichostatin A (TSA)-released HDAC activity was contained in immunoprecipitates of exogenous FLAG-WSTF, and this activity was enhanced in a ligand-dependent manner (Figure 2B). The ligand-dependent association of VDR/WSTF with VDIR was also observed for endogenous proteins in MCF7 cells (Figure 2C). This ligand binding is presumably required for the association between VDR/WSTF and VDIR, and it results in recruitment of an HDAC corepressor complex.

We tested this hypothesis using an *in vitro* GST pull-down assay on a series of bacterially expressed GST-fused WSTF mutants (Figure 2D). The WSTF m1 domain (aa 163–576, illustrated as a shaded box above the panel) was found to interact with *in vitro*-translated VDR, irrespective of 1α,25(OH)$_2D_3$ binding (Figure 2E, upper panel). No clear association of VDR with the other regions was detected, even in the presence of 1α,25(OH)$_2D_3$. We then assessed the interaction of VDIR with the WSTF mutants. While none of the WSTF regions exhibited physical interaction with VDIR, in the presence of 1α,25(OH)$_2D_3$-bound VDR, an association between WSTF and VDIR was detected (Figure 2E, middle and lower panels). Together, these findings suggest that while WSTF interacts with VDR, VDIR is stably recruited only when VDR is liganded.

WSTF mediates 1α(OH)ase gene promoter occupancy of ligand-unbound VDR

To test whether WSTF was recruited to VDIR via liganded VDR in the nuclei of living cells, we performed a chromatin immunoprecipitation (ChIP) assay using endogenous proteins and the native 1α(OH)ase gene promoter. In agreement with previous reports (Kitagawa *et al*, 2003; Murayama *et al*, 2004), VDIR was constitutively bound to 1αnVDRE, while the NCoR corepressor complex components were recruited to the promoter 45 min after the addition of 1α,25(OH)$_2D_3$

Figure 1 WSTF enhances 1α,25(OH)$_2D_3$-induced transrepression of 1α(OH)ase gene expression, but not transactivation by VDIR. (**A**) Coordinate transrepression of the 1α(OH)ase gene by VDR, WSTF and VDIR in a luciferase reporter assay. MCF7 cells were transfected with a luciferase reporter gene expression vector containing 1αnVDRE (× 2) driven by a TATA promoter (0.4 μg), pML-CMV (2 ng), and either pSG5-rat VDR and pSG5-rat RXRα (0.2 μg each), pcDNA3-VDIR (0.1 μg), pcDNA3-WSTF (0.1[+], 0.3[++] μg), or combinations thereof in the presence or absence of 1α,25(OH)$_2D_3$ (10^{-8} M) (Kitagawa *et al*, 2003; Murayama *et al*, 2004). Bars in each graph show the fold change in luciferase activity relative to basal activity obtained in the absence of ligand. All values are means±s.d. for at least three independent experiments. (**B**) Gene-specific knockdown of WSTF, VDIR or VDR by RNAi was confirmed by Western blots using anti-WSTF, -VDIR, -VDR and β-actin (as a control). Whole-cell extracts were prepared from MCF7 cells transfected with 0.3 μg of double-stranded siRNA and further cultured for 48 h. (**C**) Effect of gene-specific knockdown of endogenous factors, WSTF, VDIR and VDR on 1α(OH)ase gene expression in a luciferase reporter assay. MCF7 cells were transfected with 0.3 μg of the indicated siRNAs, 48 h after the transfection luciferase reporter gene containing 1α(OH)ase native promoter was transfected again into the cells. Luciferase activity was assessed after 12 h culture in the presence or absence of 1α,25(OH)$_2D_3$ (10^{-8} M).

(Figure 3A). SNF2h, an ISWI chromatin-remodeling complex ATPase, was used as a negative control. As WSTF RNAi remarkably attenuated the promoter occupancy of VDR in the absence of ligand, WSTF appeared to facilitate the binding of ligand-unbound VDR to the 1αnVDRE region (Figure 3A). The occupancy of VDR and WSTF was undetectable in the 1α(OH)ase-distal region, confirming promoter-specific binding of the factors. A Re-ChIP assay was performed to

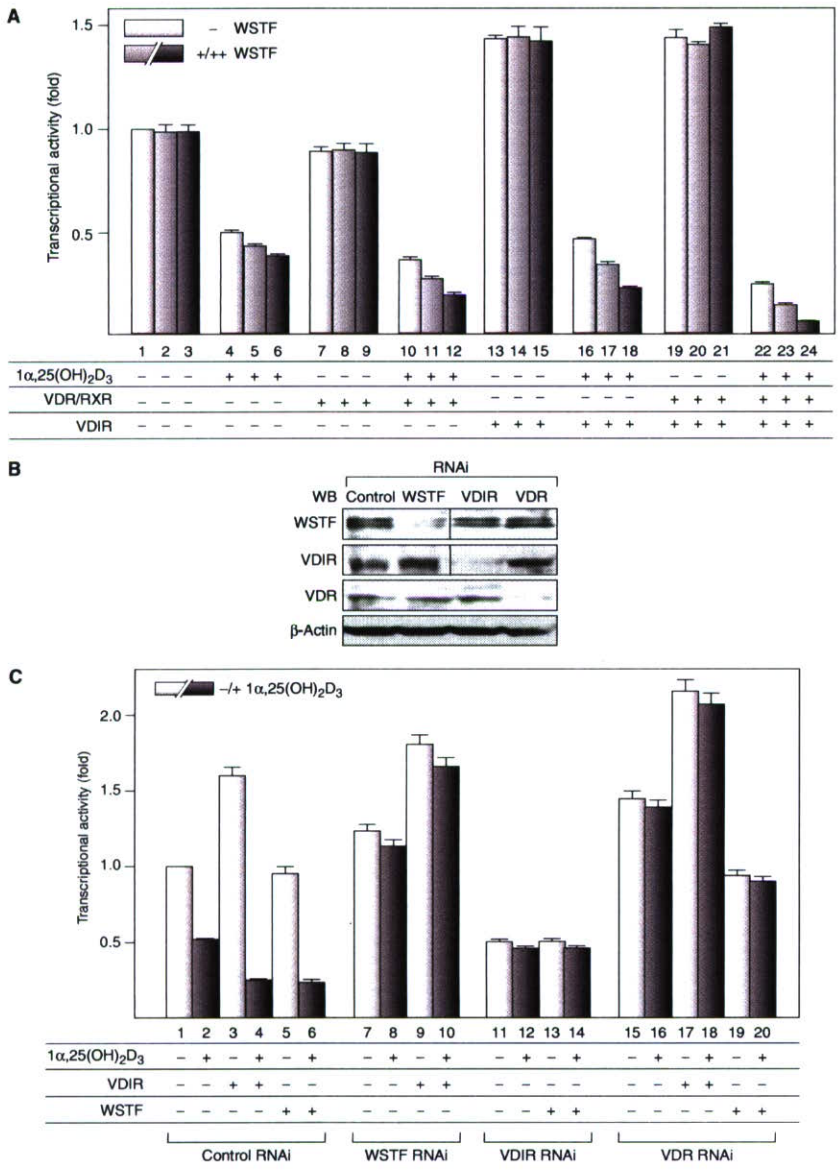

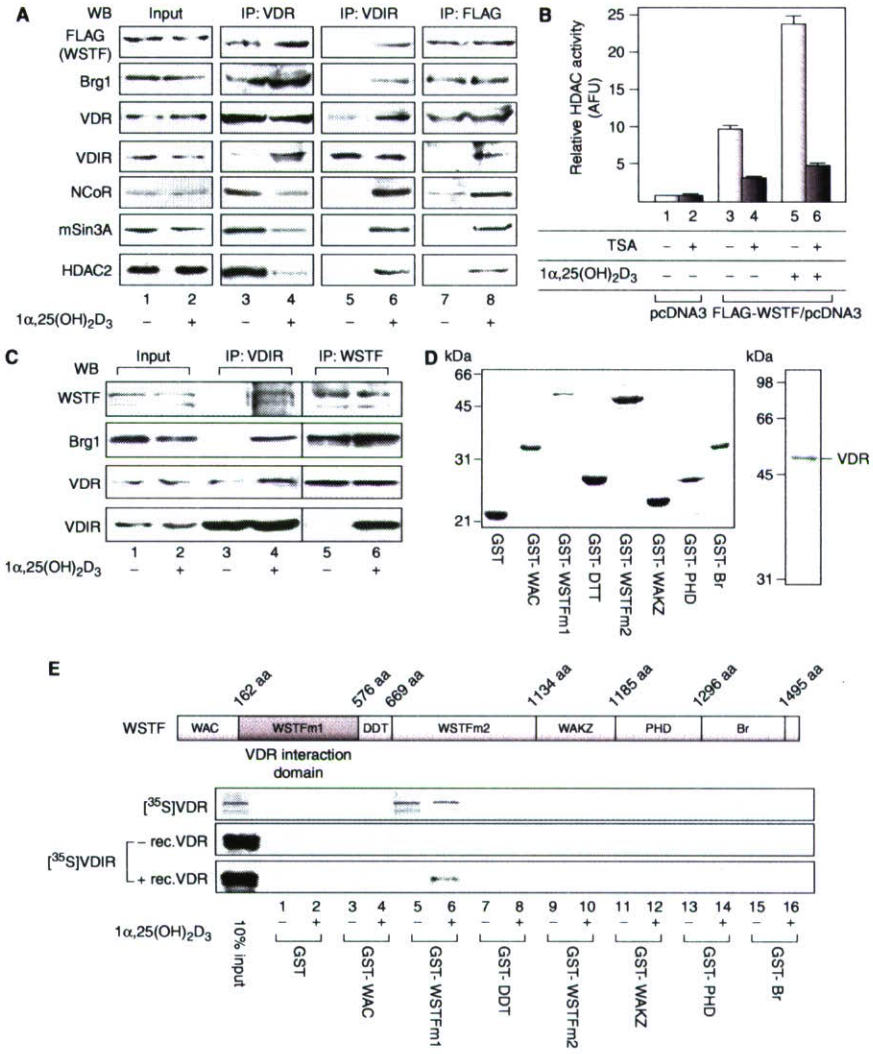

Figure 2 WSTF interacts with VDIR through 1α,25(OH)2D3-bound VDR. (**A**) Exogenous WSTF interacted with exogenous VDIR and endogenous corepressors in an $1\alpha,25(OH)_2D_3$-dependent manner *in vivo*. MCF7 cells were transfected with 0.3 μg of WSTF, VDR and VDIR expression vector. The panels show results of immunoprecipitation with anti-VDR, -VDIR or -FLAG (WSTF) antibodies, followed by Western blot analysis using the indicated antibodies. (**B**) WSTF associates with HDAC activity in a ligand-dependent manner. MCF7 cells were transfected with pcDNA3 or FLAG-WSTF/pcDNA3 and the extracted cell lysates were then immunoprecipitated with anti-FLAG M2 resin. HDAC activity in the immunoprecipitates was measured by fluorometric detection using an HDAC assay kit. (**C**) $1\alpha,25(OH)_2D_3$-dependent interaction between endogenous WSTF and VDIR *in vivo*. MCF7 cells cultured with or without $1\alpha,25(OH)_2D_3$ for 12 h were subjected to immunoprecipitation with anti-WSTF or anti-VDIR antibodies. Immunoprecipitates were Western blotted with specific antibodies as shown on the left. (**D**) SDS–PAGE gels of a series of GST-fused WSTF deletion mutants (left panel) and recombinant VDR (right panel) were visualized by CBB staining. Recombinant proteins were expressed in *Escherichia coli* and purified by affinity chromatography. (**E**) GST pull-down assay. Schematic diagrams of the WSTF deletion mutants used are illustrated. ^{35}S-labeled VDR translated *in vitro* was incubated with deletion mutants immobilized onto glutathione-Sepharose beads in the presence or absence of $1\alpha,25(OH)_2D_3$ (10^{-6} M). Bound proteins were resolved by SDS–PAGE followed by autoradiography (upper panel). Autoradiographs show ^{35}S-labeled VDIR, preincubated with (lower panel) or without (middle panel) cold recombinant VDR, bound to the GST-fused mutants immobilized on beads (Murayama *et al*, 2004).

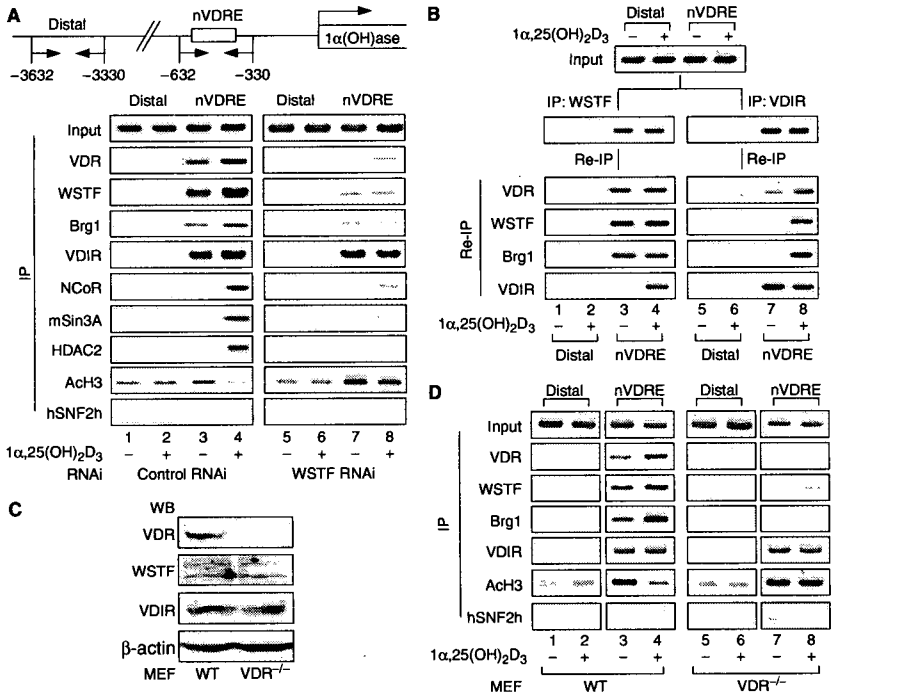

Figure 3 VDR is indispensable for ligand-induced promoter assembly of the WINAC and HDAC corepressor complex. (**A**) Recruitment of VDR, WSTF, VDIR and other coregulators to the 1α(OH)ase gene promoter *in vivo*, as shown by ChIP analysis. Soluble chromatin was prepared from MCF7 cells treated with $1\alpha,25(OH)_2D_3$ (10^{-8} M) for 45 min and immunoprecipitated with the indicated antibodies. Extracted DNA samples were amplified using primer pairs that covered the 1α(OH)ase negative VDRE region (1αnVDRE) (Kitagawa *et al*, 2003; Murayama *et al*, 2004) or a distal region (3 kb upstream of 1αnVDRE) as a control. (**B**) Recruitment of ligand-free VDR/WSTF complexes to the 1α(OH)ase gene promoter, shown by the re-chromatin immunoprecipitation (Re-ChIP) assay. Chromatin prepared from MCF7 cells cultured in the presence or absence of $1\alpha,25(OH)_2D_3$ (10^{-8} M) for 45 min was subjected to the ChIP procedure with the indicated antibodies and immunoprecipitated using the antibodies as shown on the left. (**C**) Cessation of VDR expression in $VDR^{-/-}$ MEF cells was confirmed by Western blot analysis. $VDR^{-/-}$ and wild-type (WT) MEF cells were generated from $VDR^{-/-}$ knockout mouse embryos and WT littermates (E 13.5). (**D**) Effect of VDR disruption in recruitment of WSTF and VDIR to the 1α(OH)ase gene promoter *in vivo* by ChIP analysis. Soluble chromatin was prepared from $VDR^{-/-}$ and WT MEF cells treated with $1\alpha,25(OH)_2D_3$ (10^{-8} M) for 45 min and subjected to the ChIP procedure as described in panel A.

verify the formation of the unliganded VDR, WSTF and VDIR complex at 1αnVDRE. Ligand-independent association of VDR and WSTF was observed in the 1αnVDRE region, while clear association of VDR with VDIR required ligand binding (Figure 3B). Finally, to verify a physiological role for VDR in WINAC promoter targeting, isolated primary mouse embryonic fibroblasts (MEFs) derived from VDR knockout mice were used, after confirming the ablation of VDR protein without changes in the expression level of VDIR and WSTF by Western blotting analysis (Figure 3C). In a ChIP assay using $VDR^{-/-}$ MEFs, VDR appeared to mediate the recruitment of these factors to the 1αnVDRE-proximal region (Figure 3D). Based on these findings, it appeared that WSTF requires VDR to target the promoter nucleosomes, and WSTF facilitates the subsequent retention of unliganded VDR. Furthermore, $1\alpha,25(OH)_2D_3$ binding appears to induce association of VDR with VDIR together with an HDAC complex to trigger ligand-induced transrepression.

Promoter targeting of unliganded VDR via WSTF requires chromatin structures

To clarify the mechanism by which WSTF targets unliganded VDR to the promoter *in vitro*, we addressed which factors are indispensable for the promoter targeting of unliganded VDR by employing an immobilized DNA/chromatin template recruitment assay. DNA fragments containing either 1αnVDRE (−60 to −615) or the 1α(OH)ase distal region (−3632 to −3032) were end-biotinylated to allow their immobilization onto streptavidin beads. These fragments were reconstituted as highly regular nucleosome arrays using recombinant dNAP1 protein and dACF complexes, along with purified histone octamers from HeLa cells and bacterially expressed histone octamers as unmodified histones for negative control (Figure 4A), as previously reported (Nakagawa *et al*, 2001; Kitagawa *et al*, 2003). The expected functions of the chromatin reconstitution factors were verified by supercoiling or standard micrococcal nuclease (MNase) digestion assays

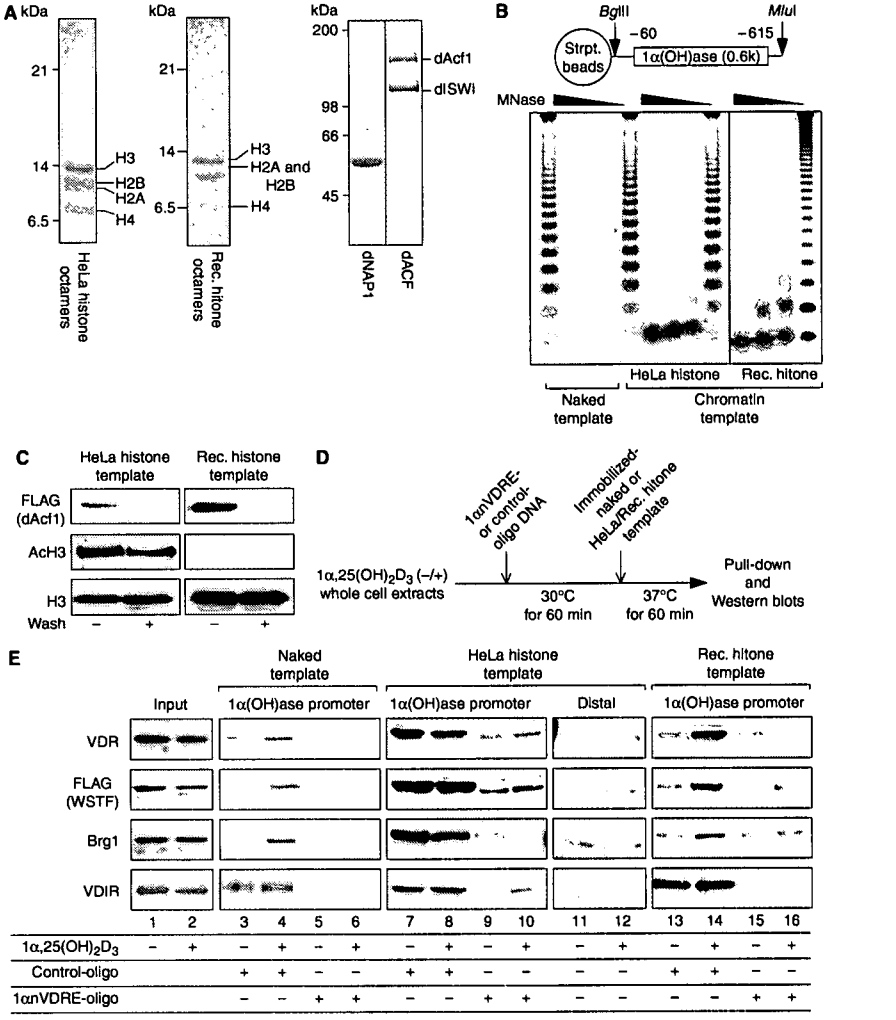

Figure 4 Chromatin structures are required to target unliganded VDR to the 1α(OH)ase promoter. (**A**) SDS–PAGE analysis of purified HeLa histone octamers, recombinant histone octamers, recombinant *Drosophila* NAP1 (dNAP1) and *Drosophila* ACF (dACF) complexes. HeLa histone octamers were purified from HeLa nuclear pellets by traditional hydroxylapatite chromatography, as described in Materials and methods. Each component of the recombinant histone octamer, H2A, H2B, H3 and H4, was expressed in an insoluble form in *E. coli* and extracted with guanidine hydrochloride. Extracted crude proteins were further purified by traditional gel filtration and ion exchange chromatography, as described previously (Luger *et al*, 1999). Affinity-tagged recombinant dNAP1 and dACF complex components (FLAG-dAcf1 and dISWI) were expressed in Sf9 cells by infection with recombinant baculoviruses and purified by affinity chromatography as described in Materials and methods. (**B**) Chromatin template containing the 1α(OH)ase gene promoter immobilized to streptavidin beads. Schematic representation of the DNA template containing the 1α(OH)ase gene promoter is illustrated above. Chromatinized template reconstituted *in vitro* was confirmed using the standard MNase digestion assay. The 123 bp ladder DNA was used as a size marker. (**C**) Immobilized template was subjected to Western blot analysis with an anti-FLAG antibody. To eliminate possible contamination by recombinant dACF complexes, immunoblotting of the beads using anti-FLAG, acetylated histone H3 and unmodified histone H3 (as a control) antibodies was performed after extensive washing with high-salt buffer. (**D**) Schematic diagram of the *in vitro*-immobilized DNA/chromatin template assay. (**E**) Stabilization of the ligand-free VDR/WSTF complex on the 1α(OH)ase promoter required chromatin structure *in vitro*. Whole-cell extracts from MCF7 cells stably expressing FLAG-WSTF treated with or without $1\alpha,25(OH)_2D_3$ (10^{-8} M) were mixed with immobilized templates. The template beads were then concentrated using a magnet and analyzed by Western blotting using the indicated antibodies.

(data not shown). Using these factors, the end-biotinylated DNA fragments were correctly reconstituted into nucleosome arrays according to the MNase digestion assay (Figure 4B). As dAcf-1 in the dACF complex is highly homologous to WSTF, chromatin templates were analyzed by Western blots to confirm the absence of dAcf-1 after final washing (Figure 4C).

Whole-cell extracts from MCF-7 cells that stably expressed FLAG-tagged WSTF treated with or without $1\alpha,25(OH)_2D_3$ were incubated with either naked or chromatin DNA templates containing 1αnVDRE. Proteins bound to the DNA templates were then analyzed by immunoblotting (Figure 4D). WSTF and VDR bound to naked DNA templates only in the presence of ligand, while VDIR stably associated with naked DNA templates even in the absence of ligand (Figure 4E, lanes 3 and 4). The specific recruitment of WSTF, together with VDR and VDIR, to 1αnVDRE was confirmed by the finding that addition of excessive synthetic 1αnVDRE oligonucleotides blocked recruitment (Figure 4E, lanes 5 and 6). In contrast, for the chromatin templates with HeLa histone octamers, recruitment of WSTF and VDR was ligand-independent (Figure 4E, lanes 7 and 8). However, WSTF and VDR were removed to significant extents from chromatinized templates by the addition of excess 1αnVDRE oligonucleotides (Figure 4E, lanes 9 and 10), indicating a role for DNA-bound VDIR in the stable association of VDR/WSTF with chromatin. This significant association of WSTF and VDR with chromatin template was not seen when the distal 1α(OH)ase gene promoter region was used (Figure 4E, lanes 11 and 12), or when the promoter region with the octamers of the unmodified histones was used (Figure 4E, lanes 13–16). This supported the significance of WSTF function in unliganded VDR recruitment to the native 1α(OH)ase promoter.

WSTF associates with acetylated nucleosomes and facilitates transcriptional repression through its C-terminal region, which contains the bromodomain

As a member of the BAZ protein family, WSTF harbors two characteristic domains, designated the bromodomain and the PHD finger, in its C-terminal region. Because these domains are present in a number of chromatin-remodeling factors (Ito *et al*, 1997; Dhalluin *et al*, 1999; Winston and Allis, 1999; Jacobson *et al*, 2000; Hassan *et al*, 2002), we speculated that the WSTF bromodomain and the PHD finger play a role in the observed association between WSTF and chromatin. To address whether these domains served as the direct contact site for histone octamers, we performed *in vitro* histone binding experiments with purified histone octamers from HeLa cells, and GST fusion proteins containing the bromodomain and PHD finger regions. We also prepared anti-FLAG immunoprecipitates having HDAC activity from whole lysates of MCF7 cells with $1\alpha,25(OH)_2D_3$ (Figure 2B), in order to deacetylate the HeLa histone octamers (Figure 5A). The results indicated that the WSTF bromodomain bound to the histone octamers only when histones were preincubated with the anti-FLAG immunoprecipitates and TSA, while the PHD finger bound the octamers only weakly (Figure 5B, even number lanes). Because bromodomains are generally known to serve as a motif responsible for binding acetylated lysine in histone tails, we reasoned that histone acetylation mediates the interaction between the WSTF bromodomain and HeLa histone octamers. This idea was supported by the observed *in vitro* association between the WSTF bromodomain and histone octamers, which was indeed abrogated when histone octamers were deacetylated using anti-FLAG immunoprecipitates (Figure 5B, odd number lanes).

To determine whether the histone acetylation was sufficient to promote this interaction, we established an *in vitro* histone binding assay using recombinant histone octamers. The integrity and HAT activity of purified recombinant p300 were assessed by CBB stain of the protein and *in vitro* acetylation of recombinant histone octamers (Figure 5C). The WSTF bromodomain bound to recombinant histone octamers only when the histones were acetylated (Figure 5D). We then further analyzed selective recognition of acetylated lysine residues in histone N-terminal tails by WSTF. Among biotin-conjugated tail peptides, WSTF selectively recognized some of the known acetylated lysine residues, histone AcH2BK12, AcH3K14, AcH4K16. However, ablation of the WSTF bromodomain (WSTFΔC) resulted in loss of the WSTF interaction with acetylated histones (Figure 5E). Our results thus suggested that the WSTF C-terminal region selectively associated with post-translationally acetylated lysine residues in the histone tails through the WSTF bromodomain.

Physical interactions between the WSTF C-terminal region and acetylated histones are required for the ligand-induced transrepression of the 1α(OH)ase gene

We next examined the role of WSTF in binding to acetylated histones during VDR-mediated gene repression. A WSTFΔC construct was first assessed in MCF7 cells by immunoprecipitation using anti-FLAG antibodies and Western blotting with anti-acetylated lysine 14 of histone H3 (AcH3K14), anti-acetylated histone H3 (AcH3), anti-Brg1 and anti-VDR antibodies. Both WT WSTF and the WSTFΔC mutant appeared to associate with VDR and Brg1, which is an ATPase subunit of WINAC, as well as the other SWI/SNF chromatin-remodeling complex subtypes. However, the WSTFΔC mutant exhibited no clear association with AcH3 and AcH3K14 (Figure 6A). These findings imply that the highly acetylated state of histones induces a stable association between WSTF and chromatin *in vivo*.

To further characterize this association, a ChIP assay was performed. TSA treatment potentiated histone H3 and H3K14 acetylation around 1αnVDRE (nVDRE), as expected, with increased recruitment of VDR and WSTF (Figure 6B, left panel). In the distal region of the 1α(OH)ase gene promoter, histone H3 acetylation was partially enhanced by TSA, though WSTF, VDR or VDIR was undetectable. As expected from the previous findings of $1\alpha,25(OH)_2D_3$-induced recruitment of HDAC to 1αnVDRE via VDIR/VDR (Murayama *et al*, 2004), $1\alpha,25(OH)_2D_3$ treatment caused clear deacetylation of histone H3 around 1αnVDRE. The WSTFΔC mutant was again unable to associate with the 1αnVDRE region, regardless of the hyperacetylated state of histone H3 (Figure 6B, right panel). A reporter assay using the luciferase gene driven by the 1α(OH)ase promoter showed that WSTF expression potentiated the $1\alpha,25(OH)_2D_3$-induced transrepression along with Brg1 (Figure 6C), whereas the WSTFΔC mutant acted as a dominant-negative factor in terms of the ligand-induced transrepression (Figure 6C, black bars). Thus, it appears that WSTF interacts with acetylated histones via the bromodomain *in vivo*, and that this interaction is indispensable for VDR-mediated transrepression through 1αnVDRE.

Discussion

Role of WINAC in the ligand-dependent corepressor recruitment

Transcription control by NRs encompasses multiple steps with the help of a large number of coregulator complexes (Glass and Rosenfeld, 2000; McKenna and O'Malley, 2002). ATP-dependent chromatin-remodeling complexes are considered to support the promoter-specific recruitment of other coregulator complexes (Emerson, 2002; Narlikar *et al*, 2002). We have previously reported that the WINAC dysfunction resulted in a failure of proper transcriptional regulation by

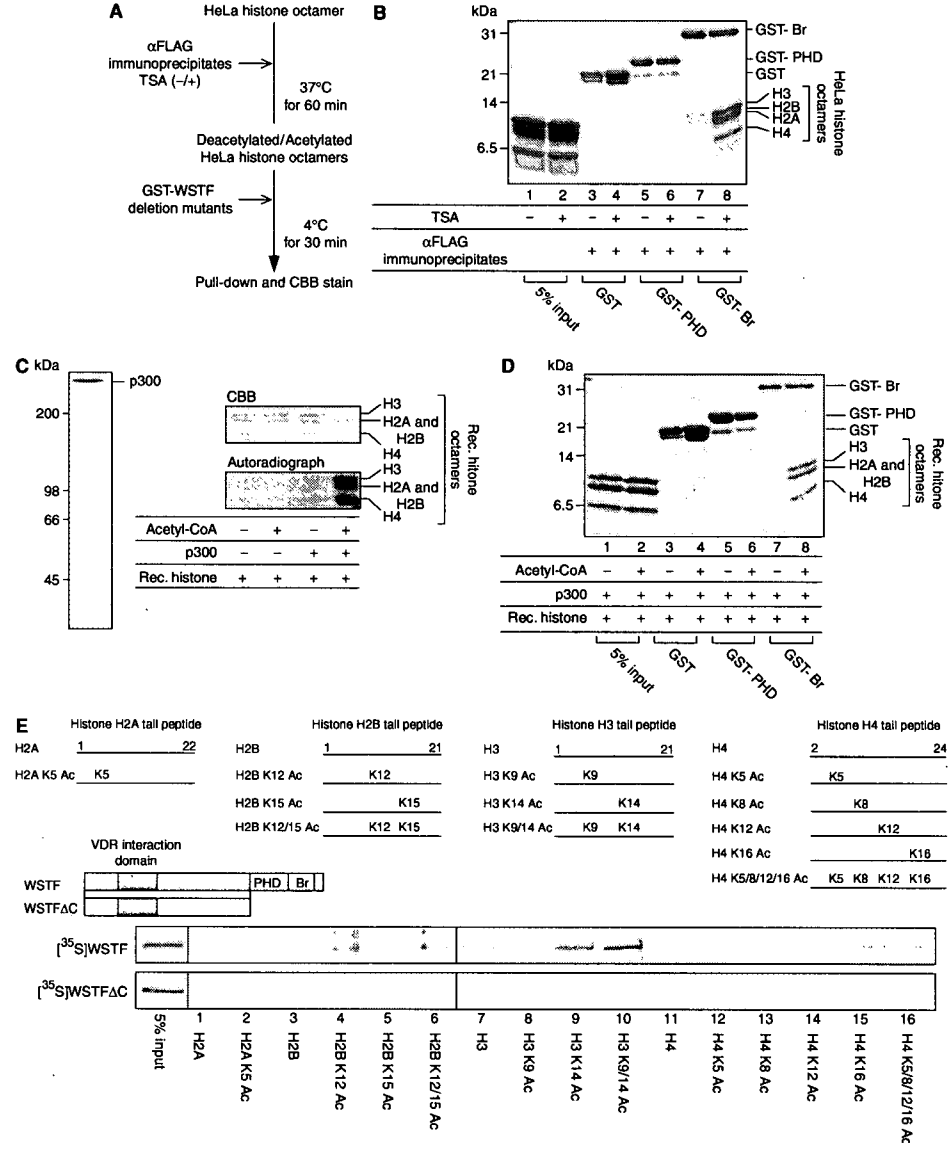

VDR, possibly because of impairment of coregulator recruitment to VDR target gene promoter. These findings strongly suggested that ATP-dependent chromatin-remodeling activity is indispensable for subsequent coregulator recruitment in response to ligand binding. However, the molecular mechanism in ligand-induced transrepression has not been well understood.

It has been considered that ligand-unbound VDR/RXR on VDRE mainly associates with HDAC complex to actively repress target genes. Reflecting this model, ligand binding led to corepressor dissociation from VDR (Figure 2A). In contrast, we also showed that WINAC assisted promoter recruitment of HDAC corepressor complex in VDIR-mediated transrepression on a negative VDRE (Figure 3A). These results may indicate a difference in the set of associating factors/complexes with unliganded VDR on negative VDREs from positive VDREs on the VDR target gene promoters. Indeed, ligand binding significantly increases the interaction of VDR/WINAC with HDAC complex (Figure 2A and B). A WSTF mutant with a deleted C-terminal region containing bromodomains functions as a dominant-negative mutant in terms of ligand-induced transrepression by VDR (Figure 6C), although this mutant could interact with VDR (Figure 6A). Moreover, this mutant abrogated ligand-dependent histone deacetylation, considering loss of acetylated histone recognition and subsequent HDAC corepressor recruitment. Hence, in addition to ligand-induced transactivation by VDR, WINAC has an important role in VDR-mediated transrepression mechanism. The proposed mechanism of the ligand-induced transrepression by VDR in the present study appears to be dependent on the promoter content, since it is unlikely that all of the VDR target gene promoters for vitamin D-induced transrepression harbor VDIR binding sites. The other mode and mechanism of ligand-induced transrepression might be unrevealed in the other promoters for VDR and the other NRs.

Promoter targeting of VDR requires chromatin structures

In this report, we investigated the role of WINAC in the recruitment of VDR to 1αnVDRE in the 1α(OH)ase gene promoter with consequent ligand-induced transrepression. We showed *in vitro* that WINAC potentiated association of VDR with 1αnVDRE, irrespective of the ligand binding, when the promoter DNA was configured as a nucleosome array (Figure 4). In contrast, in naked DNA fragments, only liganded VDR was recruited to 1αnVDRE via association with VDIR. Moreover, biochemical mapping experiments demonstrated that the WSTF bromodomain has an interaction surface with histone octamers (Figure 5B and E). These results suggest that WINAC aids promoter occupancy by unliganded VDR, acting as a tether between VDR and promoter nucleosomal arrays. This model was further supported by the *in vivo* observation that a decrease in WSTF levels due to RNAi expression attenuated VDR retention on the endogenous 1α(OH)ase gene promoter (Figure 3A). As VDR directly interacts with WSTF in a ligand-independent manner, VDR could be targeted to the promoter irrespective of ligand binding through its association with WSTF.

Transition from the transactivation state to the transrepression state

1α(OH)ase gene expression is induced by calciotropic peptide hormones such as parathyroid hormone (PTH) (Brenza *et al*, 1998; Murayama *et al*, 1998). It has been previously shown that VDIR is phosphorylated by PKA as a downstream effect of PTH activity, which then leads to HAT p300/CBP complex binding and transactivation (Murayama *et al*, 2004). The recruited HAT coactivator complex is presumed to acetylate the nucleosomal array around 1αnVDRE, and consequently this acetylation renders the 1α(OH)ase promoter accessible to the $1\alpha,25(OH)_2D_3$-unbound VDR/WINAC complex. Furthermore, the weak interaction between unliganded VDR and VDIR, shown in Figure 3B, uncovered the existence of this transition stage (see Figure 7). In this study, we show that a WSTF mutant with a deletion of the C-terminal region, which includes bromodomains, abolished the retention of the WINAC complex on the acetylated 1α(OH)ase gene promoter. This deletion mutant also functions as a dominant-negative form of WSTF to carry out ligand-induced transrepression (Figure 6). These results indicate that assembly of these factors prior to ligand binding is indispensable to initiate ligand-induced transrepression. Upon VDR binding to $1\alpha,25(OH)_2D_3$, VDR stably associates with VDIR, leading to recruitment of the HDAC corepressor complex with the assistance of WINAC chromatin-remodeling activity. Alternatively, it is also possible to presume that WINAC stabilizes the association of VDR with the HDAC corepressor complex. In any case, ligand binding to VDR results in transcriptional repression of these gene expressions through DNA-bound VDIR and the WINAC complex.

Several pieces of evidence support our finding of a physical interaction between acetylated histones and ATP-dependent chromatin-remodeling complexes. For instance, histone acetylation by Gcn5 has been shown to recruit SWI/SNF complexes during activation of the interferon-β promoter (Agalioti *et al*, 2000). Likewise, ligand-induced transactivation by RAR/RXR also requires histone acetylation prior to chromatin remodeling by SWI/SNF complexes *in vitro* (Dilworth *et al*, 2000). However, all of these studies focused on the role of histone acetylation in transcriptional activation. Thus, we have revealed a novel mechanism by which histone acetylation may be linked with transcriptional repression, even though the acetylation of nucleosomes is generally considered to enhance eukaryotic gene expression.

Figure 5 WSTF bromodomains in its C-terminal region interact with acetylated histone octamers. (**A**) Schematic diagram of a histone binding assay. HDAC immunoprecipitate was prepared using an anti-FLAG antibody from whole-cell extracts of $1\alpha,25(OH)_2D_3$-treated MCF7 cells transiently expressing FLAG-WSTF (see Figure 2B). (**B**) An *in vitro* histone binding assay showed that the interaction between WSTF bromodomains and HeLa histone octamers is decreased after deacetylation of the HeLa histone octamers. HeLa histone octamers were incubated with HDAC complexes, mixed with GST-fused WSTF bromodomain and PHD finger regions and then immobilized onto glutathione-Sepharose beads. Bound materials were eluted from the resin and resolved by 18% SDS–PAGE. Proteins were visualized by CBB staining. (**C**) SDS–PAGE analysis of recombinant p300 and *in vitro* histone acetylation of recombinant histone octamers. Affinity-tagged recombinant p300 was expressed in Sf9 cells using a baculovirus system and purified by affinity chromatography as described in Materials and methods. Histone octamers were acetylated *in vitro* by p300 with radiolabeled acetyl-CoA and the gels were visualized by CBB staining following exposure to film. (**D**) Interaction between recombinant histone octamers and WSTF bromodomains is enhanced after *in vitro* histone acetylation by p300. Recombinant histone octamers were preincubated with p300 in the absence (upper panel) or presence (lower panel) of acetyl-CoA and subjected to histone binding assay. (**E**) Site-specific recognition between the WSTF bromodomain and histones with tail modification. Schematic diagrams of the WSTF deletion mutants used are illustrated (upper panel). ^{35}S-labeled WSTF and a WSTFΔC mutant translated *in vitro* were incubated with a series of acetylated N-terminal histone tails immobilized onto streptavidin beads. Histone tail peptides were tested for WSTF binding (middle panel). Bound WSTF was resolved by SDS–PAGE, followed by autoradiography (lower panel).

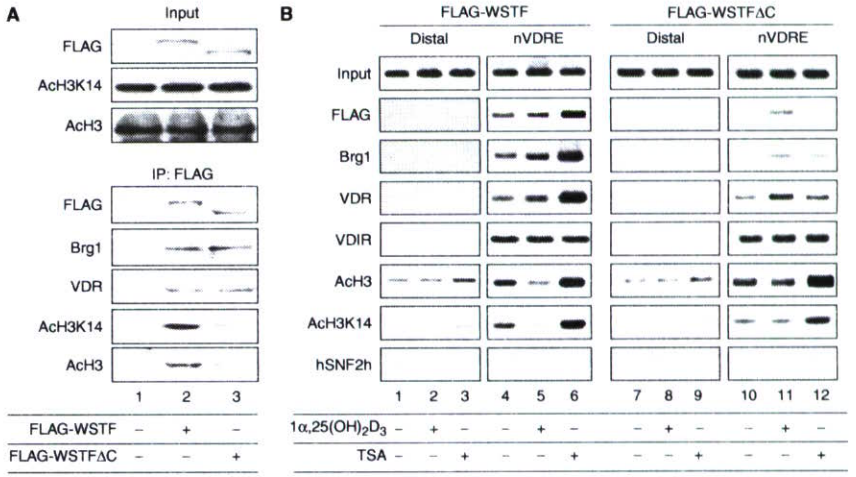

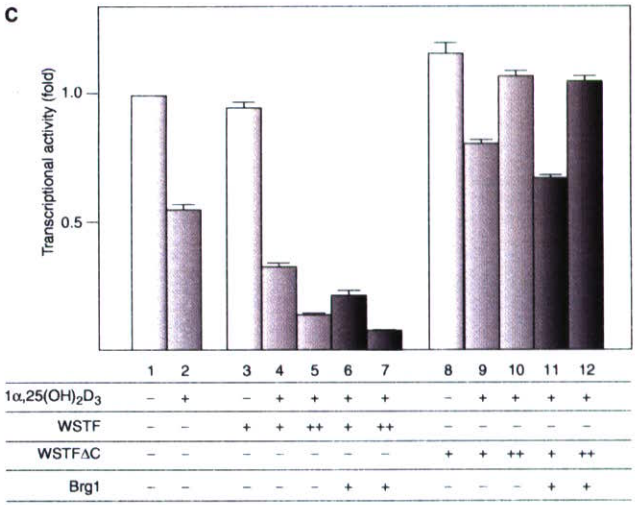

Figure 6 The WSTF C-terminal region is indispensable for the promoter targeting of ligand-unbound VDR and for VDR-mediated transrepression of the 1α(OH)ase gene. (**A**) WSTFΔC shows no binding to acetylated histone H3. MCF7 cells transfected with FLAG-tagged WSTF, FLAG-tagged WSTFΔC or pcDNA3 vector as a control were lysed and subjected to immunoprecipitation with anti-FLAG. Immunoprecipitates were Western blotted with indicated antibodies (lower panel). (**B**) Histone acetylation-dependent recruitment of WSTF to the 1αnVDRE region. MCF7 cells transfected with FLAG-tagged WSTF or FLAG-tagged WSTFΔC were treated with either $1\alpha,25(OH)_2D_3$ (10^{-8} M) for 45 min or TSA (10^{-7} M) for 120 min and then subjected to ChIP analysis. (**C**) A WSTF mutant with a deleted C-terminal bromodomain and PHD finger (WSTFΔC) exerted a partial dominant-negative effect on the ligand-induced transrepression function of VDR. The amounts of each transfected plasmid are described in Figure 1A.

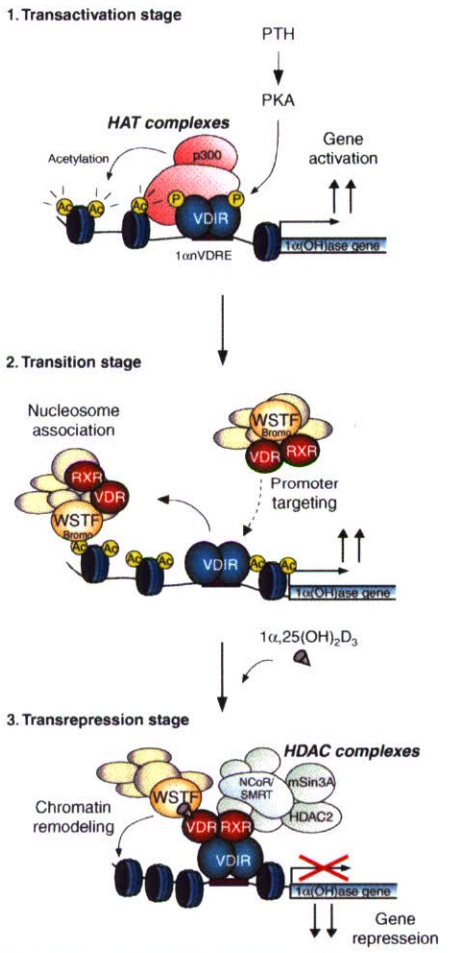

Figure 7 Model demonstrating the role of WINAC in the ligand-induced transrepression function of VDR at the 1α(OH)ase gene promoter. p300 is recruited to VDIR, which was phosphorylated via PKA signaling, and it acetylates the nucleosomes around the 1α(OH)ase gene promoter region (transactivation stage). WINAC, along with VDR, sequentially targets VDIR through interaction between unliganded VDR and VDIR, and is retained on the acetylated promoter via the WSTF bromodomain. VDR becomes receptive to $1\alpha,25(OH)_2D_3$ binding (transition stage). Upon $1\alpha,25(OH)_2D_3$ binding, HDAC corepressor complexes are recruited to the ligand-bound VDR/VDIR complex, and they then deacetylate the nucleosomes. WINAC then exerts its ATP-dependent chromatin-remodeling activity (transrepression stage).

VDR/WINAC targets VDIR on 1αnVDRE and anchors on the promoter via a physical interaction between the WSTF bromodomain and acetylated histones

In this report, we showed that the WSTF bromodomain physically interacts with acetylated histone octamers *in vitro* (Figure 5), and that the WSTF bromodomain is indispensable for ligand-induced transrepression by VDR (Figure 6). Physical interaction of acetylated histones with the bromodomains harbored in ATP-dependent chromatin-remodeling complex components is considered to be a critical step in the activation of chromatin, modulating its architecture by rearrangement of nucleosome arrays (Winston and Allis, 1999; Jones *et al*, 2000). Hassan *et al* (2002) found that both the SAGA and SWI/SNF complexes are capable of anchoring to promoter nucleosomes through direct contact of acetylated histones with the bromodomains. However, it remained unclear how these chromatin-remodeling complexes selectively discriminate their target chromosomal areas from others through their chromatin recognition modules. To address this point, we have examined two aspects of WINAC promoter targeting. One is the mechanism by which specific chromatin areas are recognized by WSTF through association with sequence-specific regulators, and the other is the preference of WSTF for a specific chromatin condition.

To address the first aspect of WINAC promoter targeting, we investigated the role of VDR by using $VDR^{-/-}$ MEF cells. Our experiments showed *in vivo* that WSTF recruitment to the 1α(OH)ase promoter was significantly impaired in $VDR^{-/-}$ MEF cells, even though the acetylation level of histones and VDIR occupancy in the promoter were unchanged when compared to WT MEF cells (Figure 3D). These results suggested that the association between the WSTF bromodomain and acetylated nucleosomes itself is not stable enough to anchor the VDR/WINAC complex on the promoters. Indeed, clear VDR/WSTF retention on the chromatin templates required VDIR bound to 1αnVDRE (Figure 4F, lanes 11 and 12). Previous reports have shown that SWI/SNF complexes are able to associate with promoter nucleosomes, but the association was somewhat unstable on an unmodified nucleosomal array (Cote *et al*, 1998). Therefore, ATP-dependent chromatin-remodeling complexes may require a physical interaction with the sequence-specific regulators to maintain their promoter occupancy. In this respect, VDIR could be considered as a hallmark for targeting of VDR/WINAC to the specific chromosomal areas.

The second aspect of WINAC promoter targeting was addressed by showing a preferential interaction of WSTF with acetylated amino-acid residues in histones. Acetylation of lysines on the histone tails is thought to establish a distinct histone code that directs molecular processes, including gene regulation (Strahl and Allis, 2000). A number of factors have turned out to harbor bromodomains, and these are believed to utilize diverse histone codes to carry out different cellular functions. We found that the WSTF bromodomain preferentially binds to acetylated Lys^{14} of histone H3 (Figure 5F). This lysine residue is considered to be the best HAT substrate for p300, as a previous study showed that p300 effectively acetylates Lys^{14} in histone H3 in a nucleosomal context (Schiltz *et al*, 1999; Lau *et al*, 2000). Together with our previous findings that p300/CBP is a HAT coactivator for VDIR bound to 1αnVDRE, this suggests that interaction of the WSTF bromodomain with acetylated H3 Lys^{14} by p300 enables WINAC to discriminate, at least to some extent, the target promoter regions from other nonspecific acetylated regions.

Thus, considering all of these results, we conclude that WINAC facilitates VDR-mediated transrepression of the 1α(OH)ase gene through a physical interaction between the WSTF bromodomain and an acetylated nucleosomal array. This mechanism is likely indispensable for the biological functions of the VDR, such as a negative feedback control in the $1\alpha,25(OH)_2D_3$ biosynthesis pathway.

Materials and methods

Plasmids and RNAi

For transfection studies, the two 1αnVDRE sequences (5′-CAT TTT AGC CCA TTA ACC CAC CTG CCA TCT GCC C-3′) and the 1α(OH)ase promoter (nucleotides −615 to −60 relative to the RNA start site) were inserted into the pGL3-Luciferase vector (Promega) under the control of a TATA promoter. Expression vectors for full-length rat VDR, rat RXR and human FLAG-tagged WSTF were as previously described (Kitagawa *et al*, 2003). Full-length mouse VDIR cDNA tagged with 6 × His was inserted into pcDNA3 (Invitrogen). cDNA encoding a human WSTF deletion mutant (amino acids 1–1185, WSTFΔC) N-terminally tagged with FLAG was cloned into pcDNA3. A series of human WSTF deletion mutants fused with GST were cloned into pGEX-4T (Pharmacia) (Kitagawa *et al*, 2003). For an immobilized template recruitment assay, the human 1α(OH)ase promoter distal region (nucleotides −3615 to −3060 relative to the RNA start site) was cloned into the pGL3 vector.

The two short RNA oligomers denatured at 90°C were annealed for 1 h at 60°C (Kitagawa *et al*, 2003). The RNAi sequences used were as follows: WSTF (5′-GAG UAU GAA GCC CGC UUG GTT-3′ and 5′-CCA AGC GGG CUU CAU ACU CTT-3′); VDR (5′-UCA AUG CUA UGA CCU GUG AUU-3′ and 5′-UCA CAG GUC AUA GCA UUG AUU-3′); VDIR (5′-GAA CCU GAA UCC CAA AGC AUU-3′ and 5′-UGC UUU GGG AUU CAG GUU CUU-3′); lamin A/C Duplex (as a control; Dharmacon) (5′-CUG GAC UUC CAG AAG AAC ATT-3′ and 5′-TTG ACC UGA AGG UCU UCU UGU-3′).

Protein purification

HeLa histone octamers were prepared from HeLa nuclear pellets as previously described (Hassan *et al*, 2002). HeLa cells (3 l culture) were lysed in lysis buffer (20 mM HEPES, pH 7.5, 0.25 M sucrose, 3 mM $MgCl_2$, 0.2% Nonidet-P40 (NP-40), 3 mM 2-mercaptoethanol, 0.4 mM PMSF, 1 μM pepstatin A and 1 μM leupeptin) by Dounce homogenization with pestle B. After washing the pellet with buffer B (20 mM HEPES, pH 7.5, 3 mM $MgCl_2$, 0.2 mM EGTA, 3 mM 2-mercaptoethanol, 0.4 mM PMSF, 1 μM pepstatin A and 1 μM leupeptin), nuclear proteins were extracted with buffer B containing 0.3 M KCl and 5% glycerol. The nuclear pellets were resuspended in HAP buffer (50 mM sodium phosphate, pH 6.8, 0.6 M NaCl, 1 mM 2-mercaptoethanol and 0.5 mM PMSF). To remove extra DNA fragments and histone H1, 20 g of dry BioGel HTP powder (Bio-Rad) was added to the suspension and the slurries were poured into a column (2.5 × 20 cm). After washing the resin extensively with HAP buffer, HeLa histone octamers were eluted with HAP buffer containing 2.5 M NaCl. Purified histone octamers were concentrated using Centriprep-3 (Amicon).

Recombinant *Xenopus* histones (H2A, H2B, H3, H4) were expressed and purified as previously described (Luger *et al*, 1999; Dyer *et al*, 2004). Recombinant p300, dNAP1 and dACF complexes were prepared essentially as described previously (Ito *et al*, 1997; Dilworth *et al*, 2000; Nakagawa *et al*, 2001). Briefly, His_6-tagged p300 and His_6-tagged dNAP1 were purified from baculovirus-infected Sf9 cells using Ni-NTA resin (Qiagen), followed by conventional anion exchange chromatography using SOURCE 15Q (Pharmacia) for dNAP1. Recombinant dACF complexes were prepared from Sf9 cells infected with baculovirus vectors encoding dACF complex components, FLAG-tagged dAcf-1 and dISWI, by affinity chromatography using anti-FLAG M2 agarose (Sigma). All proteins were dialyzed against HEG buffer (HEPES, pH 7.6, 1 mM EDTA, 10% glycerol, 0.15 M NaCl, 1 mM DTT and 0.5 mM PMSF), and protein concentrations were evaluated by SDS–PAGE and visualized with CBB R-250, using BSA as a standard.

Establishment and maintenance of WT and $VDR^{-/-}$ MEF cell lines

MEF cell lines were obtained from WT or $VDR^{-/-}$ 13.5-day-old embryos and used at the 10th generation (Ito *et al*, 2000). The MEF cell lines were replated at a density of 1×10^6 cells on gelatin-coated 10-cm dishes and maintained in DMEM supplemented with 10% FBS at 37°C in 5% CO_2.

Immunoprecipitation

After washing MCF7 cells with ice-cold PBS, cells were collected and resuspended in 100 μl lysis buffer (20 mM Tris–HCl, pH 7.9, 1% NP-40, 1 mM EDTA, 150 mM NaCl, 2.5 mM $MgCl_2$, 5% glycerol, 5 mM DTT, 10 μg/ml aprotinin and 1 mM PMSF) containing 0.1% SDS, incubated on ice for 30 min and then centrifuged for 30 min at 12 000 *g*. After centrifugation, the supernatants were diluted 10 times with lysis buffer and used as MCF7 whole-cell extracts for immunoprecipitation using anti-FLAG (Sigma), anti-VDR (Neomarkers), anti-WSTF (Cell signaling) or anti-VDIR (Santa Cruz) antibodies (Yanagisawa *et al*, 2002; Kitagawa *et al*, 2003; Murayama *et al*, 2004).

ChIP and Re-ChIP assay

ChIP analysis was performed using the ChIP assay kit (Upstates) (Yanagisawa *et al*, 2002; Kitagawa *et al*, 2003), according to the manufacturer's instructions. Intact MCF7 cells or transfected cells, and WT or $VDR^{-/-}$ MEF cells were cultured in the presence of ligand. Soluble chromatin prepared from 1×10^6 cells was immunoprecipitated with antibodies against the indicated proteins, including anti-NCoR (Alexis), anti-AcH3 (Upstates) or hSNF2h (Santa Cruz) as a negative control.

Immobilized DNA/chromatin template recruitment assays

Recruitment assays were performed as previously described (Hassan *et al*, 2002). The 1α(OH)ase promoter or distal fragment was cleaved from the 1α(OH)ase promoter/pGL3 or 1a(OH)ase distal region/pGL3 with *MluI* and *BglII*, end-labeled with biotin-14-dATP (Gibco) and gel purified. The fragments (0.2 μg DNA) were then reconstituted as chromatin with purified HeLa histone octamers (0.15 μg), recombinant histone octamers (0.3 μg), purified recombinant dNAP1 (2.5 μg), and purified recombinant dACF complexes (10 ng) and ATP (5 mM; Sigma) as described previously (Kitagawa *et al*, 2003). Biotinylated DNA or nucleosomal arrays were incubated at room temperature for 1 h with paramagnetic beads coupled to streptavidin (Dynabeads streptavidin, Dynal) in binding buffer (10 mM Tris–HCl, pH 7.9, 0.3 M KCl, 5 mM DTT, 5 mM PMSF, 5% glycerol and 0.25 mg/ml BSA) and washed extensively with binding buffer supplemented with 0.5 M KCl. Whole-cell extracts, prepared from three 75 cm^3 dishes of MCF-7 cells stably expressing FLAG-hWSTF treated with or without 10^{-8} M $1\alpha,25(OH)_2D_3$, were preincubated with 1 μg of circular competitor chromatin for 30 min and then added to the prepared templates and further incubated in lysis buffer for 1 h at 37°C. Either 100 pmol of double-stranded 1αnVDRE-oligo (5′-TAA CCC ACC TGC CAT CTG CCC AGT-3′) as a competitor or 100 pmol of double-stranded DR5-oligo (5′-TAA GGG TTC ACC GAA AGT TCA CTC GCA T-3′) as a control was then added and samples were further incubated for 1 h at 30°C. Subsequently, templates were concentrated using a magnet and washed twice in binding buffer containing 50 mM KCl before being used in Western blot analysis.

In vitro histone acetylation and histone deacetylation

For *in vitro* histone acetylation experiments, recombinant histone octamers (0.5 μg) were incubated with or without recombinant p300 (200 ng) in HEG buffer. Acetyl-CoA mix (1 μM radiolabeled and 9 μM cold acetyl-CoA) was then added and histone acetylation was carried out at 30°C for 30 min. After stopping the reaction by incubating on ice for 30 min, samples were analyzed on an 18% SDS–PAGE gel, which was visualized with Coomassie staining before immersion in Enhance (NEN) fluorography reagent as the manufacturer's instructions. The gel was then dried and visualized by autoradiography.

For *in vitro* histone deacetylation, anti-FLAG immunoprecipitates were prepared from whole extracts of MCF7 cells transfected with empty pcDNA3 vector or FLAG-WSTF/pcDNA3 and cultured with or without 10^{-8} M $1\alpha,25(OH)_2D_3$ for 48 h. HDAC activity of the immunoprecipitates was measured using an HDAC assay kit (Fluorometric detection, Upstate Biotech.) according to the manufacturer's instructions. HeLa histone octamers were deacetylated by incubation with immunoprecipitates containing HDAC activity in the presence or absence of 10^{-6} M TSA at 37°C for 60 min.

Peptide binding assay

Peptide binding assay was performed as previously reported (Dey *et al*, 2003). Briefly, ^{35}S-labeled proteins translated *in vitro* were incubated with 2 μg of biotin-labeled synthetic peptides corresponding to the N-terminal tails of histone H2A, H2B, H3 and H4 (purchased from Upstate, or synthesized from Genemed Synthesis) in a binding buffer (50 mM Tris–HCl (pH 7.5), 15 mM $MgCl_2$, 150 mM NaCl, 0.5 mM DTT and 0.1% NP-40) for 2 h at 4°C, followed by incubation with 20 μl of M-280 streptavidin beads (Dynal). Bound materials were subjected to SDS–PAGE, followed by autoradiography.

Acknowledgements

We thank Dr Timothy J Richmond for kindly providing the xHistone expression vector, Dr JT Kadonaga for the recombinant baculovirus expressing human p300 and Dr K Luger for technical discussions. We also thank Mr Y Mezaki and Dr AP Kouzmenko for technical support, and Ms H Higuchi for manuscript preparation. This work was supported in part by a grant-in-aid for Basic Research Activities for Innovative Biosciences (BRAIN) and priority areas from the Ministry of Education, Science, Sports, and Culture of Japan (to SK).

References

Agalioti T, Lomvardas S, Parekh B, Yie J, Maniatis T, Thanos D (2000) Ordered recruitment of chromatin modifying and general transcription factors to the IFN-beta promoter. *Cell* **103:** 667–678

Brenza HL, Kimmel-Jehan C, Jehan F, Shinki T, Wakino S, Anazawa H, Suda T, DeLuca HF (1998) Parathyroid hormone activation of the 25-hydroxyvitamin D3-1alpha-hydroxylase gene promoter. *Proc Natl Acad Sci USA* **95:** 1387–1391

Cote J, Peterson CL, Workman JL (1998) Perturbation of nucleosome core structure by the SWI/SNF complex persists after its detachment, enhancing subsequent transcription factor binding. *Proc Natl Acad Sci USA* **95:** 4947–4952

Dey A, Chitsaz F, Abbasi A, Misteli T, Ozato K (2003) The double bromodomain protein Brd4 binds to acetylated chromatin during interphase and mitosis. *Proc Natl Acad Sci USA* **100:** 8758–8763

Dhalluin C, Carlson JE, Zeng L, He C, Aggarwal AK, Zhou MM (1999) Structure and ligand of a histone acetyltransferase bromodomain. *Nature* **399:** 491–496

Dilworth FJ, Fromental-Ramain C, Yamamoto K, Chambon P (2000) ATP-driven chromatin remodeling activity and histone acetyltransferases act sequentially during transactivation by RAR/RXR *in vitro*. *Mol Cell* **6:** 1049–1058

Dyer PN, Edayathumangalam RS, White CL, Bao Y, Chakravarthy S, Muthurajan UM, Luger K (2004) Reconstitution of nucleosome core particles from recombinant histones and DNA. *Methods Enzymol* **375:** 23–44

Emerson BM (2002) Specificity of gene regulation. *Cell* **109:** 267–270

Fyodorov DV, Kadonaga JT (2001) The many faces of chromatin remodeling: SWItching beyond transcription. *Cell* **106:** 523–525

Glass CK, Rosenfeld MG (2000) The coregulator exchange in transcriptional functions of nuclear receptors. *Genes Dev* **14:** 121–141

Gu W, Malik S, Ito M, Yuan CX, Fondell JD, Zhang X, Martinez E, Qin J, Roeder RG (1999) A novel human SRB/MED-containing cofactor complex, SMCC, involved in transcription regulation. *Mol Cell* **3:** 97–108

Hassan AH, Prochasson P, Neely KE, Galasinski SC, Chandy M, Carrozza MJ, Workman JL (2002) Function and selectivity of bromodomains in anchoring chromatin-modifying complexes to promoter nucleosomes. *Cell* **111:** 369–379

Heinzel T, Lavinsky RM, Mullen TM, Soderstrom M, Laherty CD, Torchia J, Yang WM, Brard G, Ngo SD, Davie JR, Seto E, Eisenman RN, Rose DW, Glass CK, Rosenfeld MG (1997) A complex containing N-CoR, mSin3 and histone deacetylase mediates transcriptional repression. *Nature* **387:** 43–48

Ito M, Yuan CX, Okano HJ, Darnell RB, Roeder RG (2000) Involvement of the TRAP220 component of the TRAP/SMCC coactivator complex in embryonic development and thyroid hormone action. *Mol Cell* **5:** 683–693

Ito T, Bulger M, Pazin MJ, Kobayashi R, Kadonaga JT (1997) ACF, an ISWI-containing and ATP-utilizing chromatin assembly and remodeling factor. *Cell* **90:** 145–155

Jacobson RH, Ladurner AG, King DS, Tjian R (2000) Structure and function of a human TAFII250 double bromodomain module. *Science* **288:** 1422–1425

Jones MH, Hamana N, Nezu J, Shimane M (2000) A novel family of bromodomain genes. *Genomics* **63:** 40–45

Kamei Y, Xu L, Heinzel T, Torchia J, Kurokawa R, Gloss B, Lin SC, Heyman RA, Rose DW, Glass CK, Rosenfeld MG (1996) A CBP integrator complex mediates transcriptional activation and AP-1 inhibition by nuclear receptors. *Cell* **85:** 403–414

Kato S, Fujiki R, Kitagawa H (2004) Vitamin D receptor (VDR) promoter targeting through a novel chromatin remodeling complex. *J Steroid Biochem Mol Biol* **89-90:** 173–178

Kitagawa H, Fujiki R, Yoshimura K, Mezaki Y, Uematsu Y, Matsui D, Ogawa S, Unno K, Okubo M, Tokita A, Nakagawa T, Ito T, Ishimi Y, Nagasawa H, Matsumoto T, Yanagisawa J, Kato S (2003) The chromatin-remodeling complex WINAC targets a nuclear receptor to promoters and is impaired in Williams syndrome. *Cell* **113:** 905–917

Lau OD, Kundu TK, Soccio RE, Ait-Si-Ali S, Khalil EM, Vassilev A, Wolffe AP, Nakatani Y, Roeder RG, Cole PA (2000) HATs off: selective synthetic inhibitors of the histone acetyltransferases p300 and PCAF. *Mol Cell* **5:** 589–595

Lemon B, Inouye C, King DS, Tjian R (2001) Selectivity of chromatin-remodelling cofactors for ligand-activated transcription. *Nature* **414:** 924–928

Luger K, Rechsteiner TJ, Richmond TJ (1999) Preparation of nucleosome core particle from recombinant histones. *Methods Enzymol* **304:** 3–19

Mangelsdorf DJ, Thummel C, Beato M, Herrlich P, Schutz G, Umesono K, Blumberg B, Kastner P, Mark M, Chambon P, Evans RM (1995) The nuclear receptor superfamily: the second decade. *Cell* **83:** 835–839

McKenna NJ, O'Malley BW (2002) Combinatorial control of gene expression by nuclear receptors and coregulators. *Cell* **108:** 465–474

Murayama A, Kim MS, Yanagisawa J, Takeyama KI, Kato S (2004) Transrepression by a liganded nuclear receptor via a bHLH activator through co-regulator switching. *EMBO J* **23:** 1598–1608

Murayama A, Takeyama K, Kitanaka S, Kodera Y, Hosoya T, Kato S (1998) The promoter of the human 25-hydroxyvitamin D3 1 alpha-hydroxylase gene confers positive and negative responsiveness to PTH, calcitonin, and 1 alpha,25(OH)2D3. *Biochem Biophys Res Commun* **249:** 11–16

Nakagawa T, Bulger M, Muramatsu M, Ito T (2001) Multistep chromatin assembly on supercoiled plasmid DNA by nucleosome assembly protein-1 and ATP-utilizing chromatin assembly and remodeling factor. *J Biol Chem* **276:** 27384–27391

Narlikar GJ, Fan HY, Kingston RE (2002) Cooperation between complexes that regulate chromatin structure and transcription. *Cell* **108:** 475–487

Onate SA, Tsai SY, Tsai MJ, O'Malley BW (1995) Sequence and characterization of a coactivator for the steroid hormone receptor superfamily. *Science* **270:** 1354–1357

Rachez C, Suldan Z, Ward J, Chang CP, Burakov D, Erdjument-Bromage H, Tempst P, Freedman LP (1998) A novel protein complex that interacts with the vitamin D3 receptor in a ligand-dependent manner and enhances VDR transactivation in a cell-free system. *Genes Dev* **12:** 1787–1800

Schiltz RL, Mizzen CA, Vassilev A, Cook RG, Allis CD, Nakatani Y (1999) Overlapping but distinct patterns of histone acetylation by the human coactivators p300 and PCAF within nucleosomal substrates. *J Biol Chem* **274:** 1189–1192

Strahl BD, Allis CD (2000) The language of covalent histone modifications. *Nature* **403:** 41–45

Takeyama K, Kitanaka S, Sato T, Kobori M, Yanagisawa J, Kato S (1997) 25-Hydroxyvitamin D3 1alpha-hydroxylase and vitamin D synthesis. *Science* **277:** 1827–1830

Winston F, Allis CD (1999) The bromodomain: a chromatin-targeting module? *Nat Struct Biol* **6:** 601–604

Yanagisawa J, Kitagawa H, Yanagida M, Wada O, Ogawa S, Nakagomi M, Oishi H, Yamamoto Y, Nagasawa H, McMahon SB, Cole MD, Tora L, Takahashi N, Kato S (2002) Nuclear receptor function requires a TFTC-type histone acetyl transferase complex. *Mol Cell* **9:** 553–562

Yoshizawa T, Handa Y, Uematsu Y, Takeda S, Sekine K, Yoshihara Y, Kawakami T, Arioka K, Sato H, Uchiyama Y, Masushige S, Fukamizu A, Matsumoto T, Kato S (1997) Mice lacking the vitamin D receptor exhibit impaired bone formation, uterine hypoplasia and growth retardation after weaning. *Nat Genet* **16:** 391–396

THE JOURNAL OF BIOLOGICAL CHEMISTRY
Vol. 280, No. 4, Issue of January 28, pp. 2543–2549, 2005
Printed in U.S.A.

Circulating FGF-23 Is Regulated by 1α,25-Dihydroxyvitamin D_3 and Phosphorus *in Vivo**

Received for publication, August 4, 2004, and in revised form, September 27, 2004
Published, JBC Papers in Press, November 5, 2004, DOI 10.1074/jbc.M408903200

Hitoshi Saito‡§, Akira Maeda‡, Shu-ichi Ohtomo‡, Michinori Hirata‡, Kenichiro Kusano‡, Shigeaki Kato¶, Etsuro Ogata‖, Hiroko Segawa, Ken-ichi Miyamoto**, and Naoshi Fukushima‡**

*From the ‡Pharmaceutical Research Department II, Chugai Pharmaceutical Co., Ltd., Gotemba, Shizuoka 412-8513, Japan, the ¶Institute of Molecular and Cellular Biosciences, Tokyo University, 1-1-1 Yayoi, Bunkyo-ku, Tokyo 113-0032, Japan, the ‖Cancer Institute Hospital, 1-37-1 Kami-ikebukuro, Toshima-ku, Tokyo 170-8455, Japan, and the **Department of Molecular Nutrition, Institute of Health Bioscience, University of Tokushima Graduate School, 3-18-15 Kuramoto-cho, Tokushima 770-8503, Japan*

Fibroblast growth factor-23 (FGF-23), a novel phosphate-regulating factor, was elevated in hypophosphatemic patients with X-linked hypophosphatemic rickets/osteomalacia and also in patients with chronic kidney disease. These observations suggested the pathophysiological importance of FGF-23 on phosphate homeostasis. However, regulation of FGF-23 production is still unclear. We investigated effects of both dietary phosphorus and 1α,25-dihydroxyvitamin D_3 (1α,25$(OH)_2D_3$) on circulating FGF-23 *in vivo*. Administration of 1α,25$(OH)_2D_3$ dose-dependently increased serum FGF-23 in thyroparathyroidectomized rats without correlating with serum inorganic phosphorus or serum parathyroid hormone. On the other hand, vitamin D receptor null mice had very low serum FGF-23 and did not respond to the 1α,25$(OH)_2D_3$ administration. These observations suggested 1α,25$(OH)_2D_3$ directly or indirectly regulates circulating FGF-23. Serum FGF-23 had a strong correlation with serum inorganic phosphorus controlled by dietary phosphorus in 5/6 nephrectomized rats. High phosphate diet elicited a 5-fold increase in serum FGF-23 compared with sham-operated rats, whereas serum FGF-23 did not correlate with serum calcium or serum creatinine in 5/6 nephrectomized rats. Administration of 1α,25-dihydroxyvitamin D_3 also elicited a severalfold increase in serum FGF-23 in the uremic rats. Taken together, this shows that both serum phosphorus and 1α,25$(OH)_2D_3$ regulate circulating FGF-23 independent of each other. Therefore, we proposed there was a feedback loop existing among serum phosphorus, 1α,25$(OH)_2D_3$, and FGF-23, in which the novel phosphate-regulating bone-kidney axis integrated with the parathyroid hormone-vitamin D_3 axis in regulating phosphate homeostasis.

The parathyroid hormone-vitamin D_3 endocrine system, as well as dietary phosphorus, plays an important role in regulating renal and gastrointestinal absorption of phosphate. Recently, emerging evidence suggests that other systemic and/or paracrine/autocrine factors are present in bones for maintaining phosphate homeostasis, such as fibroblast growth factor-23 (FGF-23),[1] frizzled-related protein-4 (FRP-4), and matrix extracellular phosphoglycoprotein (MEPE) (1–11). These three factors were highly expressed in tumors isolated from oncogenic osteomalacia patients and reduced phosphate transport in kidney. Among these factors, FGF-23 strongly suppressed 1α,25$(OH)_2D_3$ production and elicited hypophosphatemia. Administration of the recombinant FGF-23 protein reduced serum phosphorus without affecting serum calcium, as well as increasing renal phosphorus excretion in mice (12). Mice bearing FGF-23-expressing Chinese hamster ovary cells showed suppressed 25-hydroxyvitamin D_3 1α-hydroxylase mRNA expression in the kidney (3). FGF-23 mRNA is expressed in a variety of tissues such as thymus, brain, bone, thyroid/parathyroid gland, and heart (2, 3, 13). Recent studies (13, 14) indicated FGF-23 mRNA as well as FGF-23 protein was elevated in bones from patients with McCune-Albright syndrome and also in bones from HYP mouse, mouse homologue to X-linked hypophosphatemic (XLH) rickets. However, the level of serum FGF-23 in hypophosphatemic patients with XLH is still controversial (15–17). Hyperphosphatemic patients with chronic kidney disease showed significant elevation in circulating FGF-23, which correlated with serum phosphorus and creatinine (16, 18–20), suggesting (*a*) serum phosphorus was a possible regulator of FGF-23 production or (*b*) circulating FGF-23 accumulated in chronic renal failure.

The purpose of this study was to evaluate the effects of dietary phosphorus and 1α,25$(OH)_2D_3$ on FGF-23 production. Administration of FGF-23 protein or overexpression of *Fgf23* gene in rodent suppressed 1α,25$(OH)_2D_3$ production by reducing 25-hydroxyvitamin D_3 1α-hydroxylase in the proximal tubules (12, 21–23). On the contrary, *Fgf23*-null mice reported increased circulating 1α,25$(OH)_2D_3$ despite hyperphosphatemia, hypercalcemia, and low PTH levels (24). Administration of 1α,25$(OH)_2D_3$ increased serum FGF-23 in normal mice (25). These observations suggested mutual regulation between FGF-23 and 1α,25$(OH)_2D_3$; however, 1α,25$(OH)_2D_3$ administration also increases intestinal phosphate uptake and suppresses PTH. Thus, we used thyroparathyroidectomized rats as well as 5/6 nephrectomized rats fed a diet with various kinds of phosphorus content to examine the direct effect of 1α,25$(OH)_2D_3$ administration on serum FGF-23.

* The costs of publication of this article were defrayed in part by the payment of page charges. This article must therefore be hereby marked "*advertisement*" in accordance with 18 U.S.C. Section 1734 solely to indicate this fact.

§ To whom correspondence should be addressed. Tel.: 81-550-87-6735; Fax: 81-550-87-5326; E-mail: saitohts@chugai-pharm.co.jp.

[1] The abbreviations used are: FGF-23, fibroblast growth factor-23; P_i, phosphate; IP, inorganic phosphorus; TPTX, thyroparathyroidectomy; XLH, X-linked hypophosphatemia; *PHEX*, phosphate-regulating gene with homologies to endopeptidases on the X chromosome; 1α,25$(OH)_2D_3$, 1α,25-dihydroxyvitamin D_3; 1α-OHase, 25-hydroxyvitamin D_3 1α-hydroxylase; PTH, parathyroid hormone; ELISA, enzyme-linked immunosorbent assay; VDRKO, vitamin D receptor null(−/−).

Dietary phosphate deprivation or loading rapidly induces activation or repression of phosphate absorption in kidney and in intestine, mainly by inducing or suppressing type II sodium-dependent phosphate (Na/P_i) cotransporter expression (26, 27). Therefore, the serum phosphorus level is not susceptible to the change in dietary phosphorus content in normal animals *in vivo*. We investigated the effects of dietary phosphorus on FGF-23 production *in vivo* using 5/6 nephrectomized uremic rats, in which the serum phosphorus level can be easily manipulated by dietary phosphorus due to reduced kidney function. We also examined the correlations between serum FGF-23 and (*a*) serum inorganic phosphorus, (*b*) serum calcium, (*c*) serum creatinine, and (*d*) serum PTH in 5/6 nephrectomized rats.

EXPERIMENTAL PROCEDURES

Normal Rat—Eight-week-old male Sprague-Dawley rats (CREA Japan, Inc., Shizuoka, Japan) were given either vehicle, 10, 30, 100, or 300 ng of 1α,25$(OH)_2D_3$/kg of bodyweight intravenously, three times a week for 2 weeks. Blood samples were obtained from the vena cava under ether anesthesia on day 14. Serum calcium, serum inorganic phosphorus, and serum creatinine were measured by an automatic analyzer (Type 7170E, Hitachi Corp.). Serum FGF-23 was determined by the Human FGF-23 ELISA kit (Kinos Inc., Tokyo, Japan).

Thyroparathyroidectomized (TPTX) Rats and PTH-infused TPTX Rats—Eight-week-old male Sprague-Dawley rats purchased from Charles River (Tokyo, Japan) were TPTX under ether anesthesia. After confirming hypocalcemia had been induced, rats were divided to two groups, the TPTX group and the TPTX + PTH group. Rats in the TPTX + PTH group were subcutaneously implanted with ALZET® osmotic pumps (model 2ML2, Durect Corp., Cupertino, CA) and administered human PTH-(1–34) at a constant rate of 2.4 μg/day for 14 days. Rats in the TPTX group were intravenously injected with vehicle, 50 ng/kg or 300 ng/kg 1α,25$(OH)_2D_3$, three times a week for 2 weeks; rats in the TPTX + PTH group were injected with either vehicle or 50 ng/kg 1α,25$(OH)_2D_3$ three times a week for 2 weeks. Blood samples were collected and various parameters analyzed as described above.

Vitamin D Receptor Null(−/−) (VDRKO) Mice—VDRKO mice and their littermates kept on a high calcium and high phosphorus diet (28) were administered vehicle or 300 ng/kg 1α,25$(OH)_2D_3$ three times a week for 2 weeks. Blood samples were collected and analyzed as described above.

5/6 Subtotally Nephrectomized Uremic Rat Models and Diets—Male Sprague-Dawley rats weighing 180–200 g were purchased from CREA Japan and maintained under specific pathogen-free conditions with a 12-h light/dark cycle. After acclimating for 1 week, the rats were 5/6 nephrectomized and then allowed unlimited access to normal rodent chow (CE-2, CREA Japan Inc.) and tap water. The phosphate (P_i)-controlled diets and 1α,25$(OH)_2D_3$ injection started when rat serum creatinine reached within the range of 1.1–1.5 mg/dl. Three P_i-controlled diets (Oriental Yeast Co., Ltd., Osaka, Japan) were used in the present study: a high P_i diet, containing 0.9% phosphorus, 0.6% calcium; a midrange P_i diet, containing 0.6% phosphorus, 0.6% calcium; and a low P_i diet, containing 0.2% phosphorus, 0.6% calcium (26, 27).

The following groups of rats were studied: 1) 5/6 nephrectomized rats fed either the high, midrange, or low P_i diet for 4 weeks, 2) 5/6 nephrectomized rats fed the high, midrange, or low P_i diet and injected with 50 ng of 1α,25$(OH)_2D_3$/kg of bodyweight intravenously twice weekly for 4 weeks, and 3) age-matched sham-operated rats fed normal rat chow (CE-2, CREA Japan) used as a control. Blood samples were obtained from the vena cava under ether anesthesia at day 28 and various parameters analyzed as described above. Serum PTH was determined using a Rat Intact PTH ELISA kit (Immutopics, Inc., San Clemente, CA).

All animal procedures were conducted in accordance with Chugai Pharmaceutical's ethical guidelines for animal care, and all experimental protocols were approved by the Animal Care Committee of the institution.

Statistical Analysis—Data were expressed as means ± S.E., and statistical significance was determined using Student's *t* test or Dunnett's *t* test (SAS Preclinical Package, Version 5.0, SAS Institute Japan, Tokyo) unless otherwise indicated. A p value of <0.05 was considered statistically significant.

RESULTS

Effect of 1α,25$(OH)_2D_3$ on Serum FGF-23 in Normal Rats—Intravenous administration of 1α,25$(OH)_2D_3$, three times a week for 2 weeks, dose-dependently increased serum FGF-23 (Fig. 1A); however, it also increased serum inorganic phosphorus (Fig. 1*B*). Therefore, 1α,25$(OH)_2D_3$ administration increased both serum FGF-23 and serum phosphorus in normal rats.

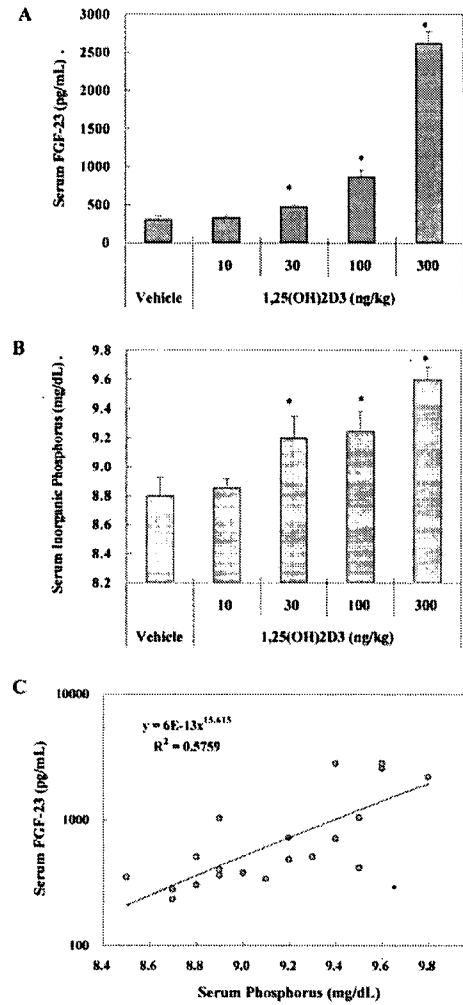

FIG. 1. Administration of 1α,25-dihydroxyvitamin D_3 dose-dependently increased both (*A*) serum FGF-23 as well as (*B*) serum inorganic phosphorus in normal rats. Correlation between serum FGF-23 and serum inorganic phosphorus in normal rats (*C*). Eight-week-old rats were given intravenously either vehicle, 10, 30, 100, or 300 ng/kg 1α,25-dihydroxyvitamin D_3 three times a week for 2 weeks. Serum inorganic phosphorus and FGF-23 were determined as described in the text. Each column represents mean ± S.E. (n = 4). *, statistically significant *versus* vehicle; $p < 0.05$, by Dunnett's *t* test.

Effects of 1α,25$(OH)_2D_3$ on Serum FGF-23 in TPTX Rats—As shown in Fig. 2, *A–C*, Thyroparathyroidectomized rats induced hyperphosphatemia, hypocalcemia, and also a slight but signif-

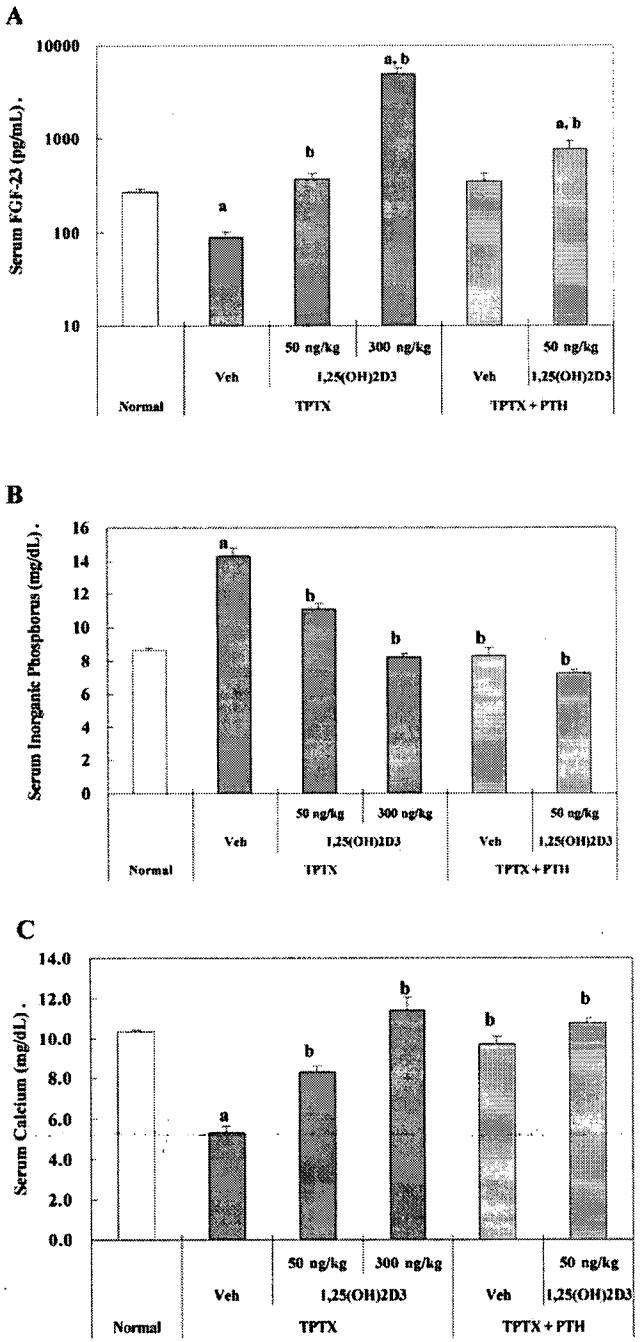

FIG. 2. **Effect of 1α,25-dihydroxyvitamin D_3 on serum FGF-23 (*A*), serum inorganic phosphorus (*B*), and serum calcium (*C*) in TPTX rats.** TPTX or PTH-infused TPTX rats were given intravenously vehicle (*Veh*) or 1α,25-dihydroxyvitamin D_3 three times a week for 2 weeks. Serum inorganic phosphorus, calcium, and FGF-23 were determined as described under "Experimental Procedures." Each column represents mean ± S.E. (n = 4–5). *a*, statistically significant *versus* normal; *b*, *versus* TPTX vehicle treatment; $p < 0.05$, by Student's t test.

icant decrease in serum FGF-23 in comparison with normal rats. Administration of $1\alpha,25(OH)_2D_3$ dose-dependently increased serum FGF-23 as well as serum calcium in TPTX rats. Also $1\alpha,25(OH)_2D_3$ suppressed serum inorganic phosphorus in TPTX rats. PTH infusion to TPTX rats normalized serum calcium, serum inorganic phosphorus, and serum FGF-23. $1\alpha,25(OH)_2D_3$ increased serum FGF-23; however, unlike TPTX rats, no significant change was observed in serum inorganic phosphorus and serum calcium in PTH-infused TPTX rats. These observations suggested that $1\alpha,25(OH)_2D_3$ increased serum FGF-23 independent of serum inorganic phosphorus and PTH.

Effect of $1\alpha,25(OH)_2D_3$ on Serum FGF-23 in VDRKO Mice—VDRKO mice kept on high calcium (2%) and high phosphorus (1.25%) diets showed considerably low serum FGF-23 (<3 pg/ml, below detection limit) and low serum calcium (5.8 ± 0.6 mg/dl) in comparison with the wild-type littermates (FGF-23, 254 ± 35.6 pg/ml; calcium, 9.5 ± 0.1 mg/dl). $1\alpha,25(OH)_2D_3$ administration did not affect either serum FGF-23 (<3 pg/ml, below detection limit) or serum calcium (5.1 ± 0.2 mg/dl).

Effects of P_i-controlled Diets on Serum FGF-23 and Serum Inorganic Phosphorus in 5/6 Nephrectomized Rats—Serum inorganic phosphorus correlated with the dietary phosphorus contents (Fig. 3*A*) in 5/6 nephrectomized rats. On the contrary, serum calcium correlated with serum phosphorus in a reciprocal fashion (Fig. 3*B*). The 5/6 nephrectomy induced a significant increase in serum FGF-23 in rats, regardless of the dietary phosphorus contents (Fig. 3*C*). Serum FGF-23 of sham-operated rats was 305 ± 23 pg/ml. Whereas, serum FGF-23 increased in high, midrange, and low P_i diet groups (5108 ± 989 pg/ml, 1815 ± 200 pg/ml, and 1133 ± 121 pg/ml, respectively). Serum FGF-23 showed a clear correlation with serum phosphorus (Fig. 4*A*) and a weak inverse correlation with serum calcium (Fig. 4*B*) in 5/6 nephrectomized rats. However, serum FGF-23 did not correlate with serum creatinine (Fig. 4*C*).

Effect of $1\alpha,25(OH)_2D_3$ on Serum FGF-23 and Serum Inorganic Phosphorus in 5/6 Nephrectomized Rats—Serum FGF-23 in the 5/6 nephrectomized rats on each P_i-controlled diet was augmented significantly by the administration of $1\alpha,25(OH)_2D_3$ (Fig. 5). $1\alpha,25(OH)_2D_3$ administration also increased serum inorganic phosphorus, serum calcium, and serum creatinine and decreased serum PTH in all diet groups (data not shown). Serum inorganic phosphorus weakly correlated with serum FGF-23 in the nephrectomized rats with or without $1\alpha,25(OH)_2D_3$ treatment (Fig. 6*A*). However, the other three parameters did not have a strong correlation with serum FGF-23 (Fig. 6, *B–D*).

In normal rats, 30 and 100 ng/kg $1\alpha,25(OH)_2D_3$ injection increased serum FGF-23 only by 1.5- and 3-fold, respectively. Whereas, in the 5/6 nephrectomized rats, 50 ng/kg $1\alpha,25(OH)_2D_3$ increased serum FGF-23 by 3–9-fold, suggesting that $1\alpha,25(OH)_2D_3$ had a more profound effect on increasing serum FGF-23 in rats with chronic renal failure.

DISCUSSION

Shimada *et al.* reported that a single injection of $1\alpha,25(OH)_2D_3$ increased serum FGF-23 and suggested the increase in FGF-23 by $1\alpha,25(OH)_2D_3$ was independent of serum inorganic phosphorus (25). We confirmed their result that intravenous administration of $1\alpha,25(OH)_2D_3$ dose-dependently increased serum FGF-23 (Fig. 1*A*). However, we also observed an increase in serum inorganic phosphorus (Fig. 1*B*). There was a strong significant correlation between serum FGF-23 and serum phosphorus (Fig. 1*C*) in the normal rats given $1\alpha,25(OH)_2D_3$. Since $1\alpha,25(OH)_2D_3$ stimulates intestinal phosphate uptake and suppresses PTH production, this experiment indicated that $1\alpha,25(OH)_2D_3$ increased serum FGF-23 as well

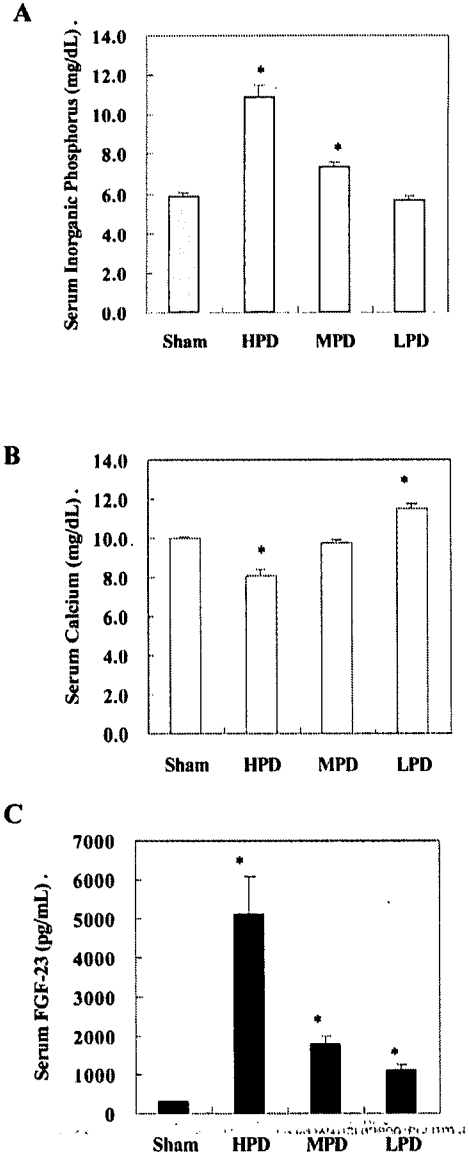

FIG. 3. **Effect of P_i-controlled diet on serum inorganic phosphorus, serum calcium, and serum FGF-23 in 5/6 nephrectomized rats.** 5/6 nephrectomized rats were fed either high P_i (0.9% P_i, 0.6% calcium) diet (*HPD*), midrange P_i (0.6% P_i, 0.6% calcium) diet (*MPD*), or low P_i (0.2% P_i, 0.6% calcium) diet (*LPD*) for 4 weeks. Blood samples were taken on day 28 from the vena cava under ether anesthesia. Serum inorganic phosphorus, serum calcium, and serum FGF-23 were determined as described under "Experimental Procedures." Data represents means ± S.E. (sham-operated group, n = 5; 5/6 nephrectomized groups, n = 10). *, statistically significant in comparison with the sham-operated group, $p < 0.05$ by Student's t test.

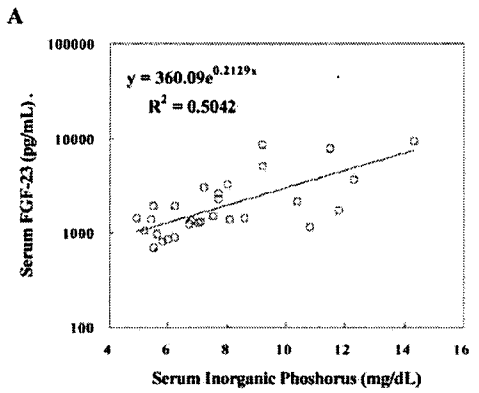

FIG. 4. **Correlations between serum FGF-23 and serum inorganic phosphorus (*A*), serum calcium (*B*), and serum creatinine (*C*) in 5/6 nephrectomized rats fed with P_i-controlled diet.** 5/6 nephrectomized rats were fed either high P_i, midrange P_i, or low P_i diet for 4 weeks. Serum creatinine, serum inorganic phosphorus, and serum FGF-23 were determined as described under "Experimental Procedures." Open circles represent the data from individual rats.

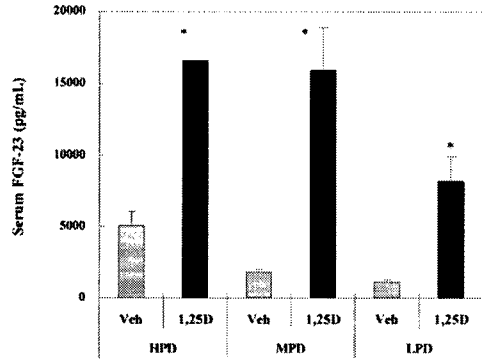

FIG. 5. **1α,25-Dihydroxyvitamin D_3 administration increased circulating FGF-23 in 5/6 nephrectomized rats.** 5/6 nephrectomized rats fed P_i-controlled diets were given either vehicle or 50 ng/kg 1α,25-dihydroxyvitamin D_3 intravenously, twice a week for 4 weeks. Serum FGF-23 was determined by ELISA. 1α,25-Dihydroxyvitamin D_3 injection to 5/6 nephrectomized rats induced a drastic increase in circulating FGF-23 among all diet groups. Each column represents mean ± S.E. (n = 10 rats/group). *, statistically significant difference between vehicle and $1\alpha,25(OH)_2D_3$ treated in each diet, $p < 0.05$ by Student's t test. *HPD*, high P_i diet; *MPD*, midrange P_i diet; *LPD*, low P_i diet.

as serum phosphorus. To evaluate the effect of $1\alpha,25(OH)_2D_3$ apart from serum phosphorus on FGF-23 production, $1\alpha,25(OH)_2D_3$ was administered to thyroparathyroidectomized rats with or without PTH infusion. $1\alpha,25(OH)_2D_3$ also increased serum FGF-23 in thyroparathyroidectomized, and the effect was independent of serum phosphorus (Fig. 2, *A–C*). The direct effect of $1\alpha,25(OH)_2D_3$ on FGF-23 production was confirmed by the fact that VDRKO mice did not respond to the $1\alpha,25(OH)_2D_3$ administration.

Larsson *et al.* (18) reported phosphate deprivation and/or phosphate loading to normal subjects did not affect serum FGF-23; however, serum phosphorus weakly correlated with serum FGF-23 in predialysis patients with chronic kidney disease. Recent studies also revealed that serum FGF-23 was elevated in patients with end-stage renal disease (16, 20, 28). In the present study, we investigated the effect of dietary phosphorus on FGF-23 production using 5/6 nephrectomized rats fed the diets with various kinds of phosphorus content. Serum FGF-23 was elevated in uremic rats; however, serum FGF-23 did not clearly correlate with serum creatinine in those rats as was observed in human subjects. Serum phosphorus was well controlled by the dietary phosphorus in 5/6 nephrectomized rats (Fig. 3*A*). Serum FGF-23 positively correlated with serum phosphorus in those rats (Fig. 3*C*). In the physiological condition, a high serum phosphorus suppresses $1\alpha,25(OH)_2D_3$ production in kidney. Thus, the elevation of serum FGF-23 induced by a high P_i diet was independent of serum $1\alpha,25(OH)_2D_3$. Moreover, serum FGF-23 was drastically elevated by $1\alpha,25(OH)_2D_3$ administration in 5/6 nephrectomized rats fed with various P_i-controlled diets (Fig. 5). However, serum FGF-23 did not correlate with serum calcium, serum creatinine, or serum PTH in those rats (Fig. 6, *B–D*). These observations suggested that FGF-23 production was mainly regulated by serum phosphorus and serum $1\alpha,25(OH)_2D_3$.

Recent studies (16, 17) reported that FGF-23 was elevated in some patients with XLH. Serum phosphorus concentrations were negatively correlated with circulating FGF-23 levels in patients with XLH. Moreover, FGF-23 mRNA expression was

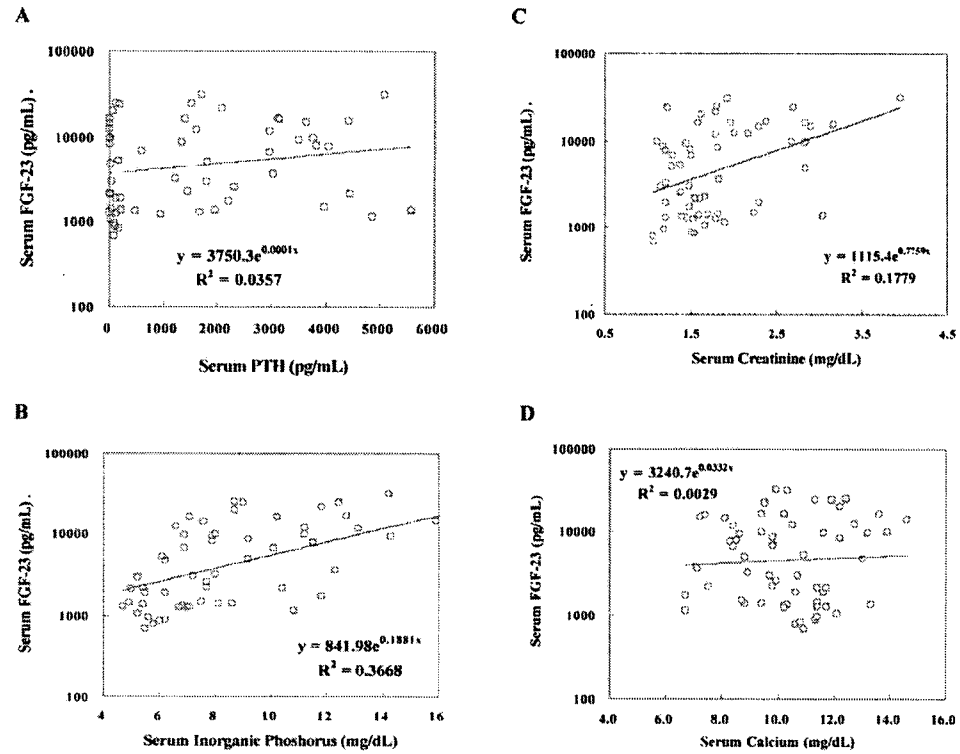

FIG. 6. **Correlations between serum FGF-23 and serum inorganic phosphorus (*A*), serum calcium (*B*), serum creatinine (*C*), and serum PTH (*D*) in 5/6 nephrectomized rats with or without 1α,25-dihydroxyvitamin D_3 administration.** 5/6 nephrectomized rats fed P_i-controlled diets were given intravenously either vehicle or 50 ng/kg 1α,25-dihydroxyvitamin D_3 for 4 weeks. Serum creatinine, serum inorganic phosphorus, and serum FGF-23 were determined as described under "Experimental Procedures." *Open circles* represent the data from individual rats.

enhanced in the calvarial and mandible bones of *Hyp*-mouse, which is a homologue of human XLH (13). Mutations in *PHEX*, a phosphate-regulating gene with homology to endopeptidase on the X-chromosome, are responsible for XLH. *PHEX* mRNA is predominantly expressed in bone and teeth. $1\alpha,25(OH)_2D_3$ decreased *PHEX* mRNA and *PHEX* protein in primary osteoblasts derived from newborn mouse calvaria as well as MC3T3-E1 cells, a mouse osteoblastic cell line, *in vitro* (29). In addition, *PHEX* mRNA expression in tibial bone was suppressed by $1\alpha,25(OH)_2D_3$ administration in 5/6 nephrectomized rats *in vivo* (30). It is plausible that administration of $1\alpha,25(OH)_2D_3$ up-regulated circulating FGF-23 levels in 5/6 nephrectomized rats at least partly by down-regulation of *PHEX* expression in bones.

FGF-23 induces hypophosphatemia by inhibiting both renal and intestinal P_i absorption by suppressing NaP_i-IIa and -IIb production (3, 12, 21, 22, 25). FGF-23 also inhibits $1\alpha,25(OH)_2D_3$ production in renal proximal tubules, which results in the reduction of intestinal P_i absorption and PTH secretion. On the contrary, $1\alpha,25(OH)_2D_3$ induced an increase in circulating FGF-23, and also loss of vitamin D signaling in VDRKO mice led to very low serum FGF-23. In 5/6 nephrectomized rats, serum phosphorus controlled by dietary phosphorus content positively correlated with serum FGF-23, suggesting an increase in serum phosphorus induces FGF-23 production. We propose that a feedback loop exists between serum phosphorus, $1\alpha,25(OH)_2D_3$, and FGF-23, in which the novel phosphate-regulating bone-kidney axis would be integrated with the parathyroid hormone-vitamin D_3 axis in regulating phosphate homeostasis.

Acknowledgments—We thank Keiko Kuroiwa and Yuko Azabu (Pharmaceutical Research Dept. II, Chugai Pharmaceutical Co., Ltd.) for their technical assistance. We also thank Dr. Paul Langman for his assistance with English usage.

REFERENCES

1. The ADHR Consortium (2000) *Nat. Genet.* **26**, 345–348
2. Yamashita, T., Yoshioka, M., and Ito, N. (2000) *Biochem. Biophys. Res. Commun.* **277**, 494–498
3. Shimada, T., Mizutani, S., Muto, T., Yoneya, T., Hino, R., Takeda, S., Takeuchi, Y., Fujita, T., Fukumoto, S., and Yamashita, T. (2001) *Proc. Natl. Acad. Sci. U. S. A.* **98**, 6500–6505
4. Berndt, T., Craig, T. A., Bowe, A. E., Vassiliadis, J., Reczek, D., Finnegan, R., Jan De Beur, S. M., Schiavi, S., and Kumar, R. (2003) *J. Clin. Invest.* **112**, 785–794
5. Rowe, P. S. N., de Zoysa, P. A., Dong, R., Wang, H. R., White, K. E., Econs, M. J., and Oudet, C. L. (2000) *Genomics* **67**, 54–68
6. Argiro, L. A., Desbarats, M., Glorieux, F. H., and Ecarot, B. (2001) *Genomics* **74**, 342–351
7. Jan De Beur, S. M., Finnegan, R., Vassiliadis, J., Cook, B., Barberion, D., Estes, S., Manavalan, P., Petroziello, J., Madden, S. L., Cho, J. Y., Kumar, R., Levine, M. A., and Schiavi, S. (2002) *J. Bone Miner. Metab.* **17**, 1102–1110
8. White, K. E., Jonsson, K. B., Carn, G., Hampton, G., Spector, T. D., Mannstadt, M., Lorenz-Depiereux, B., Miyauchi, A., Yang, M., Ljunggren, Ö., Meitinger, T., Strom, T. M., Jüppner, H., and Econs, M. J. (2001) *J. Clin.*

Endocrinol. Metab. **86,** 497–500
9. Gowen, L. C., Petersen, D. N., Mansolf, A. L., Qi, H., Stock, J. L., Tkalcevic, G. T., Simmons, H. A., Crawford, D. T., Chidsey-Frink, K. L., Ke, H. Z., McNeish, J. D., and Brown, T. A. (2003) *J. Biol. Chem.* **278,** 1998–2007
10. Quarles, L. D. (2003) *Am. J. Physiol.* **285,** E1–E9
11. Quarles, L. D. (2003) *J. Clin. Invest.* **112,** 642–646
12. Shimada, T., Muto, T., Urakawa, I., Yoneya, T., Yamazaki, Y., Okawa, K., Takeuchi, Y., Fujita, T., Fukumoto, S., and Yamashita, T. (2002) *Endocrinology* **143,** 3179–3182
13. Liu, S., Guo, R., Simpson, L. G., Xiao, Z-S., Burnham, C. E., and Quarles, L. D. (2003) *J. Biol. Chem.* **278,** 37419–37426
14. Riminucci, M., Collins, M. T., Fedaeko, N. S., Cherman, N., Corsi, A., White, K. E., Waguespack, S., Gupta, A., Hannon, T., Econs, M. J., Bianco, P., and Robey, P. G. (2003) *J. Clin. Invest.* **112,** 683–692
15. Yamazaki, Y., Okazaki, R., Shibata, M., Hasegawa, Y., Satoh, K., Tajima, T., Takeuchi, Y., Fujita, T., Nakahara, K., Yamashita, T., and Fukumoto, S. (2002) *J. Clin. Endocrinol. Metab.* **87,** 4957–4960
16. Webber, T. J., Liu, S., Indridason, O. S., and Quarles, L. D. (2003) *J. Bone Miner. Res.* **18,** 1227–1234
17. Jonsson, K. B., Zahradnik, R., Larsson, T., White, K. E., Sugimoto, T., Imanishi, Y., Yamamoto, T., Hampson, G., Koshiyama, H., Ljuggren, Ö., Oba, K., Yang, I. M., Miyauchi, A., Econs, M. J., Lavigne, J., and Jüppner, H. (2003) *N. Eng. J. Med.* **348,** 1656–1663
18. Larsson, T., Nisbeth, U., Ljunggren, Ö., Jüppner, H., and Jonsson, K. B. (2003) *Kidney Int.* **64,** 2272–2279
19. Imanishi, Y., Inaba, M., Nakatsuka, K., Nagasue, K., Okuno, S., Yoshihara, A., Miura, M., Miyauchi, A., Kobayashi, K., Miki, T., Shoji, T., Ishimura, E., and Nishizawa, Y. (2004) *Kidney Int.* **65,** 1943–1946
20. Shigematsu, T., Kazama, J. J., Yamashita, T., Fukumoto, S., Hosoya, T., Geyjo, F., Fukagawa, M. (2004) *Am. J. Kidney Dis.* **44,** 250–256
21. Saito, H., Kusano, K., Kinosaki, M., Ito, H., Hirata, M., Segawa, H., Miyamoto, K., and Fukushima, N. (2003) *J. Biol. Chem.* **278,** 2206–2211
22. Bai, X. Y., Miao, D., Goltzman, D., and Karaplis, A. C. (2003) *J. Biol. Chem.* **278,** 9843–9849
23. Shimada, T., Urakawa, I., Yamazaki, Y., Hasegawa, H., Hino, R., Yoneya, T., Takeuchi, Y., Fujita, T., Fukumoto, S., and Yamashita, T. (2004) *Biochem. Biophys. Res. Comm.* **314,** 409–414
24. Shimada, T., Kakitani, M., Yamazaki, Y., Hasegawa, H., Takeuchi, Y., Fujita, T., Fukumoto, S., Tomizuka, K., and Yamashita, T. (2004) *J. Clin. Invest.* **113,** 561–568
25. Shimada, T., Hasegawa, H., Yamazaki, Y., Muto, T., Hino, R., Takeuchi, Y., Fujita, T., Nakahara, K., Fukumoto, S., and Yamashita, T. (2004) *J. Bone Miner. Res.* **19,** 429–435
26. Katai, K., Miyamoto, K., Kishida, S., Segawa, H., Nii, T., Tanaka, H., Tani, Y., Arai, H., Tatsumi, S., Morita, K., Taketani, Y., Takeda, E. (1999) *Biochem. J.* **343,** 705–714
27. Katai, K., Segawa, H., Haga, H., Morita, K., Arai, H., Tatsumi, S., Taketani, Y., Miyamoto, K., Hisano, S., Fukui, Y., and Takeda, E. (1997) *J. Biochem. (Tokyo)* **121,** 50–55
28. Yoshizawa, T., Handa, Y., Uematsu, Y., Takeda, S., Sekine, K., Yoshihara, Y., Kawakami, T., Arioka, K., Sato, H., Uchiyama, Y., Masushige, S., Fukamizu, A., Matsumoto, T., and Kato, S. (1997) *Nat. Genet.* **6,** 391–396
29. Ecarot, B., and Desbarats, M. (1999) *Endocrinology* **140,** 1192–1199
30. Brewer, A. J., Canaff, L., Hendy, G. F., and Tennenhouse, H. S. (2004) *Am. J. Physiol.* **286,** F739–F748

THE JOURNAL OF BIOLOGICAL CHEMISTRY Vol. 280, No. 34, Issue of August 26, pp. 30511–30516, 2005

Printed in U.S.A.

Identification of the Amino Acid Residue of CYP27B1 Responsible for Binding of 25-Hydroxyvitamin D_3 Whose Mutation Causes Vitamin D-dependent Rickets Type 1*

Received for publication, May 12, 2005, and in revised form, June 22, 2005
Published, JBC Papers in Press, June 22, 2005, DOI 10.1074/jbc.M505244200

Keiko Yamamoto‡, Eriko Uchida§, Naoko Urushino§, Toshiyuki Sakaki¶‖, Norio Kagawa, Natsumi Sawada‡‡, Masaki Kamakura¶, Shigeaki Kato§§, Kuniyo Inouye§, and Sachiko Yamada‡¶¶**

*From the ‡Institute of Biomaterials and Bioengineering & School of Biomedical Sciences, Tokyo Medical and Dental University, 2-3-10 Kanda-Surugadai, Chiyoda-ku, Tokyo 101-0062, Japan, the §Division of Food Science and Biotechnology, Graduate School of Agriculture, Kyoto University, Sakyo-ku, Kyoto 606-8502, Japan, the ¶Biotechnology Research Center, Faculty of Engineering, Toyama Prefectural University, 5180 Kurokawa, Kosugi, Toyama 939-0398, Japan, the **Department of Biochemistry, Vanderbilt University School of Medicine, Nashville, Tennessee 37232-0146, the ‡‡Laboratory of Endocrinology and Molecular Metabolism, Graduate School of Nutritional Sciences, University of Shizuoka, 52-1 Yada, Shizuoka 422-8526, Japan, and the §§Institute of Molecular and Cellular Biosciences, Tokyo University, 1-1-1 Yayoi, Bunkyo, Tokyo 113-0032, Japan*

We previously reported the three-dimensional structure of human CYP27B1 (25-hydroxyvitamin D_3 1α-hydroxylase) constructed by homology modeling. Using the three-dimensional model we studied the docking of the substrate, 25-hydroxyvitamin D_3, into the substrate binding pocket of CYP27B1. In this study, we focused on the amino acid residues whose point mutations cause vitamin D-dependent rickets type 1, especially unconserved residues among mitochondrial CYPs such as Gln^{65} and Thr^{409}. Recently, we successfully overexpressed mouse CYP27B1 by using a GroEL/ES co-expression system. In a mutation study of mouse CYP27B1 that included spectroscopic analysis, we concluded that in a 1α-hydroxylation process, Ser^{408} of mouse CYP27B1 corresponding to Thr^{409} of human CYP27B1 forms a hydrogen bond with the 25-hydroxyl group of 25-hydroxyvitamin D_3. This is the first report that shows a critical amino acid residue recognizing the 25-hydroxyl group of the vitamin D_3.

The hormonally active form of vitamin D_3, 1,25-$(OH)_2D_3$,[1] plays essential roles in calcium homeostasis, immunology, and cell differentiation (1). 1,25-$(OH)_2D_3$ is produced by two-step hydroxylations at the 25-position in the liver by mitochondrial CYP27A1 and then at the 1α-position in the kidney by CYP27B1. The cDNA for CYP27B1 was first cloned in 1997 (2–5), and the sequence analysis of the CYP27B1 gene confirmed that defects in CYP27B1 cause vitamin D-dependent rickets type 1 (VDDR1). To date, 16 one-point mutants and several frameshift mutants have been reported (6–9). The mutated amino acid residues seemed to play important roles in the function of 1α-hydroxylase, such as substrate binding, activation of molecular oxygen, interaction with adrenodoxin, and folding of the P450 structure (10, 11).

To investigate the mutations in depth, spectral analyses including reduced CO-difference spectra and substrate-induced difference spectra are indispensable. However, the expression levels of wild type and CYP27B1 mutants were too low to carry out spectral analyses (11, 12). Thus, enhancement of the expression level of CYP27B1 is essential for structure-function analysis of CYP27B1. Recently, we successfully overexpressed mouse CYP27B1 by using a GroEL/ES co-expression system (13). The expression level of CYP27B1 is sufficient for the preparation of large amounts of wild type and CYP27B1 mutants for structural analyses. In addition, we successfully constructed a three-dimensional structure of CYP27B1 by the homology modeling technique using the structure of rabbit microsomal CYP2C5 as a template, which is the first solved x-ray structure as a eukaryotic CYP (14, 15). The three-dimensional model of CYP27B1 provided much information about the roles of amino acid residues at the mutated positions seen in VDDR1 patients. In this study, we focused on the mutants from VDDR1 whose mutated amino acids are not conserved among six mitochondorial P450s (Fig. 1). We demonstrate which amino acid residue is responsible for substrate binding by mutation studies that include spectral analysis of CYP27B1.

EXPERIMENTAL PROCEDURES

Materials—DNA modifying enzymes, restriction enzymes, and the DNA sequencing kit were purchased from Takara Shuzo Co., Ltd. (Kyoto, Japan). Primer DNAs for mutation were purchased from GENSET KK (Kyoto, Japan) (Table I). *Escherichia coli* DH5α (Takara Shuzo Co.) was used as a host strain. The pKSDdl was constructed from pkk223-3 as described previously (13). The GroEL/ES expression plasmid, pGro12, was kindly given by the HSP research laboratory (Kyoto, Japan). CHAPS was purchased from Dojindo (Kumamoto, Japan). NADPH was purchased from Oriental Yeast Co. (Tokyo, Japan). Bovine adrenodoxin and NADPH-adrenodoxin reductase were kindly given by Dr. Y. Nonaka of Koshien University. 25-$(OH)D_3$ was purchased from

* This work was supported in part by a grant-in-aid for Scientific Research from the Ministry of Education, Science and Culture of Japan and the Sankyo Foundation of Life Sciences. The costs of publication of this article were defrayed in part by the payment of page charges. This article must therefore be hereby marked "*advertisement*" in accordance with 18 U.S.C. Section 1734 solely to indicate this fact.

‖ To whom correspondence may be addressed: Biotechnology Research Center, Faculty of Engineering, Toyama Prefectural University, 5180 Kurokawa, Kosugi, Toyama 939-0398, Japan. Tel.: 81-766-56-7500; Fax: 81-766-56-7500; E-mail: tsakaki@pu-toyama.ac.jp.

¶¶ To whom correspondence may be addressed: Institute of Biomaterials and Bioengineering & School of Biomedical Sciences, Tokyo Medical and Dental University, 2-3-10 Kanda-Surugadai, Chiyoda-ku, Tokyo 101-0062, Japan. Tel.: 81-3-5280-8036; Fax: 81-3-5280-8005; E-mail: yamada.mr@tmd.ac.j.

[1] The abbreviations used are: 25-$(OH)D_3$, 25-hydroxyvitamin D_3; 1α,25-$(OH)_2D_3$, 1α,25-dihydroxyvitamin D_3; VDDR1, vitamin D-dependent rickets type 1; CYP, cytochrome P450; HPLC, high performance liquid chromatography; CHAPS, 3-[(3-cholamidopropyl)dimethylammonio]-1-propanesulfonic acid.

TABLE I
Oligonucleotides used as PCR primers to generate CYP27B1 mutants

Mutation	Oligonucleotides
S408I	5′-GATACGCTAGTCATCCTATGTCACTATGCC-3′
	5′-GGCATAGTGACATAGGATGACTAGCGTATC-3′
S408T	5′-GATACGCTAGTCACCCTATGTCACTATGCC-3′
	5′-GGCATAGTGACATAGGGTGACTAGCGTATC-3′
S408V	5′-GATACGCTAGTCGTCCTATGTCACTATGCC-3′
	5′-GGCATAGTGACATAGGACGACTAGCGTATC-3′
S408A	5′-GATACGCTAGTCGCCCTATGTCACTATGCC-3′
	5′-GGCATAGTGACATAGGGCGACTAGCGTATC-3′
Q65H	5′-GGCTGCATGAACTGCACGTGCATGGCGCTG-3′
	5′-CAGCGCCATGCACGTGCAGTTCATGCAGCC-3′
Q65E	5′-GGCTGCATGAACTGGAGGTGCATGGCGCTG-3′
	5′-CAGCGCCATGCACCTCCAGTTCATGCAGCC-3′
Q65A	5′-GGCTGCATGAACTGGCGGTGCATGGCGCTG-3′
	5′-CAGCGCCATGCACCGCCAGTTCATGCAGCC-3′
Q65L	5′-GGCTGCATGAACTGCTGGTGCATGGCGCTG-3′
	5′-CAGCGCCATGCACCAGCAGTTCATGCAGCC-3′
Q65N	5′-GGCTGCATGAACTGAATGTGCATGGCGCTG-3′
	5′-CAGCGCCATGCACATTCAGTTCATGCAGCC-3′

Wako Pure Chemical Industries, Ltd. (Osaka, Japan). Other chemicals used were of the highest quality commercially available.

Molecular Modeling and Substrate Docking—Molecular modeling and graphical manipulations were performed using SYBYL 6.9 (Tripos, St. Louis, MO). 25-Hydroxyvitamin D_3 was docked into the substrate binding pocket manually.

Construction of Expression Plasmids—The expression plasmid for mouse CYP27B1 with the His tag at the C terminus, pKCHis-m1α, was constructed as described (6). The expression plasmids for CYP27B1 mutants (S408I, S408T, S408V, S408A, Q65H, Q65E, Q65A, Q65L, Q65N) were generated by the QuikChange™ Site-directed Mutagenesis kit from Stratagene (Amsterdam, the Netherlands) according to the instruction manual. The oligonucleotide primers for mutagenesis are shown in Table I. Corrected generation of the desired mutations was confirmed by DNA sequencing.

Cultivation of the Recombinant E. coli Cells—*The E. coli* DH5α harboring pGro12 was transformed with the expression plasmid for wild type CYP27B1 (pKCHis-m1α) or its mutants. Recombinant *E. coli* cells were grown in TB media (pH 7.0) containing 50 μg/ml ampicillin and 25 μg/ml kanamycin at 26 °C under good aeration for 24 h. The induction of transcription of CYP27B1 cDNA and the GroEL/ES gene was initiated by addition of isopropyl 1-thio-β-D-galactopyranoside and arabinose at a final concentration of 1 mM and 4 mg/ml, respectively. δ-Aminolevulinic acid was also added at a final concentration of 1 mM.

Solubilization of Wild Type and CYP27B1 Mutants by CHAPS—The recombinant *E. coli* cells were suspended in 100 mM Tris-HCl buffer (pH 7.4) containing 1% CHAPS, 1 mM EDTA, 0.1 mM phenylmethylsulfonyl fluoride, and 20% glycerol, and disrupted by sonication for 15 min at 4 °C. Cell debris was removed at 1,200 × *g* for 10 min. Then the supernatant was ultracentrifugated at 100,000 × *g* for 1 h at 4 °C. The resultant supernatant was used for spectral and enzymatic analyses.

Measurement of Reduced CO-difference Spectra—Reduced CO-difference spectra were measured by a Shimadzu UV-2200 spectrophotometer (Kyoto, Japan) as described previously (16). The concentration of CYP27B1 was determined from the reduced CO-difference spectrum using a difference of extinction coefficient at 446 and 490 nm of 91 mM^{-1} cm^{-1} by Omura and Sato (17).

Measurement of Substrate-induced Difference Spectra—Substrate-induced difference spectra of wild type and CYP27B1 mutants were measured in the presence of 1.0 μM 25-$(OH)D_3$ by a Shimadzu UV-2200 spectrophotometer (Kyoto, Japan).

Western Blot Analysis of Gln^{65} Mutants—Anti-CYP27B1 antiserum was prepared using a purified sample of mouse CYP27B1 as antigen (13). The purified CYP27B1 (0.1 mg) was mixed with an equal volume of Freund's complete adjuvant and injected intradermally into a young male Japan White rabbit. At 2, 4, 6, and 8 weeks after the first injection, the rabbit was boosted with additional injections of 0.1 or 0.2 mg each of the antigen mixed with Freund's incomplete adjuvant.

The rabbit was bled 1 week after the final injection, and antiserum was prepared. The solubilized fractions of wild type and CYP27B1 mutants containing 0.6 μg of protein were subjected to electrophoresis on 5–20% linear gradient polyacrylamide sodium dodecyl sulfate gels, and transferred electrophoretically from the gel to poly(vinylidene difluoride) membrane. The membrane was probed with the anti-CYP27B1 antiserum mentioned above, and then reacted with horseradish peroxidase-labeled rabbit IgG. The immobilized proteins were detected by treating the membrane with a mixture of 4-chloro-1-naphtol and hydrogen peroxide.

	H	H	E	L	N	G,K,L	R	Y	P	S	C,H	I	P	C	G	R
VDDR	65	107	125	143	164	189	321	323	335	382	389	409	429	453	478	497
CYP27B1	Q	R	Q	P	D	E	T	S	R	P	R	T	R	R	V	P
CYP27A1	Q	R	Q	Q	D	L	T	S	K	P	R	V	Q	R	V	P
CYP24	L	R	G	K	D	E	T	A	R	P	R	M	R	R	I	P
CYP11A1	H	R	G	Q	D	D	T	S	R	P	R	Q	D	R	V	P
CyP11B1	V	R	G	P	D	S	T	V	R	P	R	R	N	R	V	P
CYP11B2	M	R	G	P	D	S	T	A	R	P	R	Q	N	R	V	P

FIG. 1. **Comparison of the amino acid sequences of human CYP27B1 with other mitochondrial cytochromes P450 at the mutated positions seen in patients with VDDR1.** The amino acid residues that are identical and homologous in all the CYPs are shaded *dark* and *light*, respectively. The amino acid residues at the non-conserved position are surrounded by *open boxes*.

Measurement of Hydroxylation Activity Toward 25-$(OH)D_3$, 1α-$(OH)D_3$, and Vitamin D_3—The 1α-hydroxylation activity toward 25-$(OH)D_3$ was measured in a reconstituted system consisting of the solubilized CYP27B1 or each of its mutants (0.5–6.0 nM), 2.0 μM adrenodoxin, 0.2 μM NADPH-adrenodoxin reductase, 0.025–1.0 μM substrate, 100 mM Tris-HCl (pH 7.4), 1 mM EDTA, 0.2% glycerol, and 0.1% CHAPS in a final volume of 0.5 ml. The 25-hydroxylation activity toward 1α-$(OH)D_3$ was measured in a similar manner except for the concentrations of 1α-$(OH)D_3$ (0.05–1.0 μM) and CYP27B1 (2.5 nM) or S408V (50 nM). The vitamin D_3 metabolism was measured in a reconstituted system consisting of 2.0 μM adrenodoxin, 0.2 μM NADPH-adrenodoxin reductase, 46 nM of the purified sample of the wild type (13), or 50 nM of the purified sample of S408V, 1.0 μM vitamin D_3, 100 mM Tris-HCl (pH 7.4), 1 mM EDTA, 0.2% glycerol, and 0.1% CHAPS. The concentration of CHAPS was determined on the basis of our previous study (13). After incubation at 37 °C for 3 min, the reaction was initiated by adding NADPH at a final concentration of 1 mM. The reaction was terminated by adding 2 ml of chloroform/methanol (3:1, v/v). After extraction, the organic phase was recovered and dried. The resulting residue was solubilized with acetonitrile and applied to HPLC under the following conditions: column, YMC-Pack ODS-AM (4.6 × 300 mm) (YMC Co., Tokyo, Japan); column temperature, 40 °C; mobile phase, linear gradient of 70–100% acetonitrile aqueous solution per 15 min; flow rate, 1.0 ml/min; UV detection, 265 nm. The kinetic parameters, K_m and k_{cat}, were calculated by the nonlinear regression analysis using the KaleidaGraph (Synergy software).

Other Methods—The concentrations of vitamin D_3 derivatives were estimated by their molar extinction coefficient of 1.80×10^4 M^{-1} cm^{-1} at 264 nm (18). Total protein concentrations were determined by the Bradford method using bovine serum albumin as a standard. Mouse CYP27B1, human CYP27B1, and rabbit CYP2C5 were aligned by using ClustalW interfaced with Clustal X (version 1.81) for Windows.

RESULTS

Docking of 25-$(OH)D_3$ into CYP27B1—The three-dimensional structure of CYP27B1, which was constructed and reported in our previous paper (14), gave abundant insights in regards to the function of each residue. We are greatly interested in how the CYP27B1 recognizes 25-$(OH)D_3$ and binds it as a substrate. We noted amino acid residues whose point mutant cause VDDR1 (Fig. 1). Fig. 1 shows comparison of the residues of CYP27B1 with other human mitochondrial CYPs at the mutated positions seen in patients with VDDR1. Residues conserved in these CYPs are thought to be responsible for common roles among mitochondrial CYPs, whereas residues not conserved are thought to be involved in specific roles of each enzyme such as substrate binding. Thus, we focused on mutants Q65H, P143L, E189L, S323Y, T409I, and R429P. The three-dimensional structure of CYP27B1 demonstrated that P143L, E189L, S323Y, and R429P are responsible for protein folding as previously reported (14) (Fig. 2*a*). On the other hand, Gln^{65} and Thr^{409} are lining the end of broad cavity above heme in the three-dimensional model of CYP27B1 (Fig. 2*a*).

In the docking study of 25-$(OH)D_3$ into the pocket, it is important to determine the substrate binding site and the conformation of 25-$(OH)D_3$. Considering the importance of

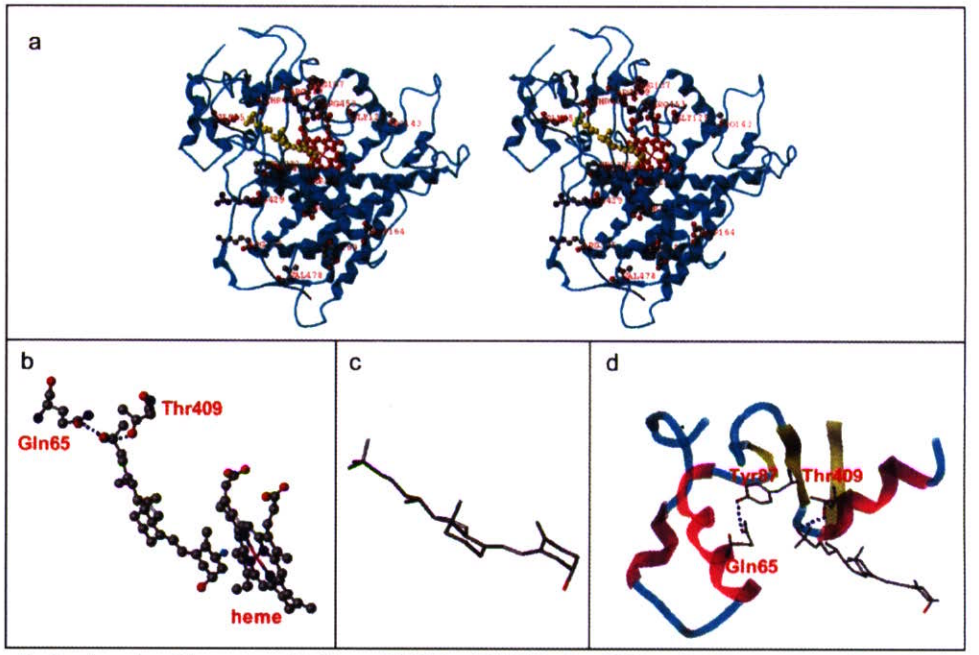

FIG. 2. *a*, stereo view of the complex model of human CYP27B1 and 25-$(OH)D_3$. Overall folding of CYP27B1 is represented by a *ribbon-loop* drawing. Sixteen amino acid residues where point mutation causes VDDR1 (atom type color), heme (*red*), and 25-$(OH)D_3$ (*yellow*) are depicted as a *ball and stick* model. *b*, the 25-hydroxyl group of 25-$(OH)D_3$ forms pincer-type hydrogen bond with Gln^{65} (2.83 Å) and Thr^{409} (2.82 Å), and the hydrogen at the 1α position (*cyan*), which will be subjected to hydroxylation, orients to an iron atom of the heme. The distance between C(1) and iron is 4.3 Å and that between hydrogen at the 1α-position and iron is 3.3 Å. *c*, conformation of 25-$(OH)D_3$ docked into the substrate binding pocket of CYP27B1. *d*, Gln^{65} may interact with Tyr^{87} on the β-sheet but not with the 25-hydroxyl group of the substrate.

Gln^{65} and Thr^{409} whose mutations cause VDDR1, we selected the substrate binding site where 25-$(OH)D_3$ can form the hydrogen bond between the 25-OH group and Gln^{65} and/or Thr^{409}. We docked 25-$(OH)D_3$ as follows: 1) the A-ring of 25-$(OH)D_3$ was superimposed on 1R-camphor accommodated in the substrate binding pocket of the P450cam protein (Protein Data Bank code 1DZ4) (19), because, structurally and biologically, the best characterized P450 is P450cam and we analyzed the docking modes of camphor into P450cam and found the modes being approximately conserved. In addition, P450cam belongs to the class 1 enzyme in the P450 superfamily as well as mitochondrial CYPs. 2) The side chain of 25-$(OH)D_3$ was positioned near Gln^{65} and Thr^{409}. 3) Spatial location of 25-$(OH)D_3$ was manually adjusted so as to minimize the van der Waals bump between the substrate vitamin and the amino acid residues lining the substrate binding pocket. The resulting structure of CYP27B1 and 25-$(OH)D_3$ complex is shown in Fig. 2*a*. The distances between the 25-hydroxyl group and Gln^{65} and the 25-hydroxyl group and Thr^{409} are 2.83 and 2.82 Å, respectively. This suggests that the 25-hydroxyl group forms pincer-type hydrogen bonds with Gln^{65} and Thr^{409}. The 1α-hydrogen of 25-$(OH)D_3$, which will be subjected to hydroxylation, orients to the iron atom as a constituent of heme in the CYP (Fig. 2*b*).

Conformation of 25-$(OH)D_3$ Accommodated in CYP27B1—As shown in Fig. 2*c*, 25-$(OH)D_3$ is docked with a stable conformation in which the A-ring adopts the chair form and the side chain adopts the gauche(+) conformation (43°) at C(16–17-20–22) and the following anti-conformation from C(20) to the terminal methyl group. A-ring adopts β-form. In this conformation, the distance between C(1) and iron is 4.3 Å and between hydrogen at the 1α-position and iron is 3.3 Å (Fig. 2*b*), which are consistent with the distances observed in the crystal structures: C(5)-iron (4.2 Å) and H(5)-iron (3.2 Å) in the camphor-P450cam complex (1DZ4) (19); C(5)-iron (3.9 Å) and H(5)-iron (3.3 Å) in the camphor-P450cam complex (1AKD) (20); C(1)-iron (3.8 Å) and H(1)-iron (2.9 Å) in the androstenedione-P450eryF complex (1EUP) (21). If the A-ring of 25-$(OH)D_3$ adopts the α-form, distances of C(1)-iron and C(2)-iron are 3.9 and 3.8 Å, respectively, resulting in the absence of a rational explanation for the selective hydroxylation that occurred at the 1α-position but not the 2-position. Thus, our docking model well explains the stereospecific hydroxylation at the 1α-position of 25-$(OH)D_3$.

Expression of Wild Type and CYP27B1 Mutants with GroEL/ES Co-expression System—Molecular modeling study of CYP27B1 strongly suggests that Ser^{408} of mouse CYP27B1 corresponding to Thr^{409} of human CYP27B1, and/or Gln^{65} are involved in substrate binding (Fig. 3). To reveal each function of the mutated amino acid residues, we generated multiple forms of CYP27B1 mutants at positions 408 (409 in human CYP27B1) and 65. As shown in Fig. 4, mutant S408I showed the reduced CO-difference spectra similar to wild type. S408T and S408A, and S408V, also showed similar spectra (data not shown). The expression level of the wild type of CYP27B1 was 200–300 nmol/liter of culture, as described previously (13). The

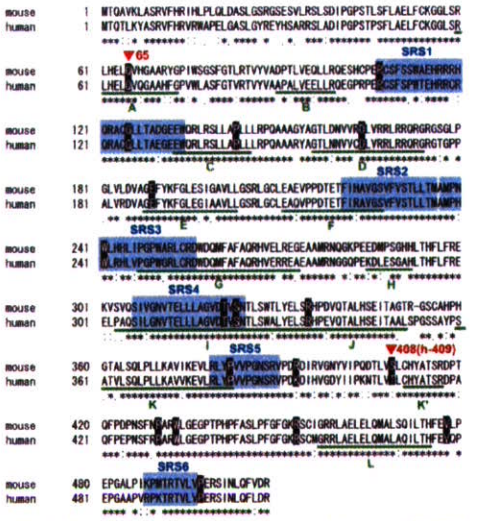

FIG. 3. **Sequence alignment of mouse and human CYP27B1.** The A to L helices are labeled as defined by Williams *et al.* (15). *Blue boxes* and *green bars* represent the substrate recognition site (*SRS*) and α-helix, respectively. *Black boxes* show the amino acid residues where the point mutation causes VDDR1.

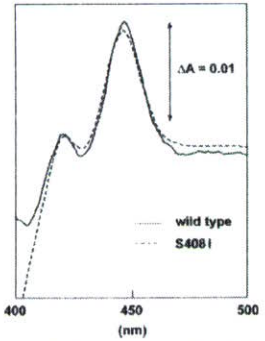

FIG. 4. **Reduced CO-difference spectra of wild type mouse CYP27B1 (—), and the mutant S408I (- - -).**

expression levels of Ser^{408} mutants, S408I and S408A, were nearly the same as the wild type, whereas those of S408T and S408V were higher (400–450 nmol/liter of culture). On the other hand, the expression levels of Gln^{65} mutants (Q65H, Q65E, Q65A, Q65L, Q65N) were too low to be determined by the reduced CO-difference spectra. However, Q65E showed a substrate-induced difference spectrum. Thus, the expression level of the Q65E hemoprotein was estimated to be 10 nmol/liter based on the assumption that Q65E shows a substrate-induced difference spectrum similar to wild type. In contrast, Western blot analysis showed that the distinct bands reacted with anti-CYP27B1 antiserum in the Gln^{65} mutants. The expression levels of the Gln^{65} mutants were not so different from that of the wild type (Fig. 5). These results suggest that most Gln^{65} mutants are expressed as apoproteins without a heme molecule in *E. coli* cells.

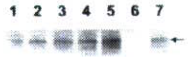

FIG. 5. **Western blot analysis of wild type and Gln^{65} mutants of mouse CYP27B1.** The solubilized fractions expressing each of the mutants Q65A (*lane 1*), Q65E (*lane 2*), Q65H (*lane 3*), Q65L (*lane 4*), Q65N (*lane 5*), control (*lane 6*: prepared from the control DH5α/pGro12 cells), and the wild type (*lane 7*) were analyzed as described under "Experimental Procedures."

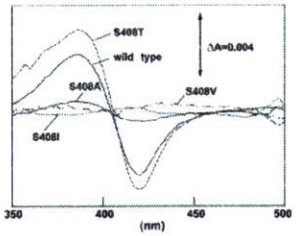

FIG. 6. **Substrate-induced difference spectra of wild type and CYP27B1 mutants with 1.0 μM 25-(OH)D_3.** The difference spectra of wild type and CYP27B1 mutants were measured in 100 mM Tris-HCl buffer (pH 7.4) containing 0.1% CHAPS. Enzyme concentrations were 160 nM (wild type, S408T, S408I) and 190 nM (S408A, S408V), respectively.

TABLE II
Kinetic parameters of wild type and CYP27B1 mutants for 25(OH)D_3 1α-hydroxylation activity

CYP27B1	k_{cat}	K_m	k_{cat}/K_m
	min^{-1}	μM	
Wild type	23.1 ± 0.9	0.28 ± 0.06	84 ± 19
S408T	5.9 ± 1.6	0.13 ± 0.03	46 ± 11
S408A	0.34 ± 0.06	0.24 ± 0.04	1.5 ± 0.3
S408V	0.78 ± 0.40	0.54 ± 0.18	1.5 ± 0.7
S408I	0.050 ± 0.020	0.18 ± 0.06	0.31 ± 0.10

TABLE III
Kinetic parameters of wild type and mutant S408V for 1α(OH)D_3 25-hydroxylation activity

CYP27B1	k_{cat}	K_m	k_{cat}/K_m
	min^{-1}	μM	
Wild type	0.60 ± 0.12	0.52 ± 0.05	1.1 ± 0.1
S408V	0.022 ± 0.010	0.66 ± 0.09	0.033 ± 0.009

Analysis of Substrate Binding of Wild Type and Ser^{408} Mutants of CYP27B1 with 25-(OH)D_3—As shown in Fig. 6, substrate-induced difference spectra of wild type and CYP27B1 mutants with 25-(OH)D_3 showed Type I spectra, indicating the change of spin state of heme iron of CYP27B1 from low spin to high spin. The magnitude of $\Delta A_{390-420}$ in S408T was slightly larger than the wild type of CYP27B1. In contrast, the magnitude of $\Delta A_{390-420}$ in S408V and S408A was quite small, but S408I showed no detectable spectral change. These results suggest that the substrate, 25-(OH)D_3, can remove the H_2O molecule as the sixth axial ligand of the heme iron of wild type CYP27B1 and mutant S408T. In addition, the hydroxyl group at the side chain of the amino acid at position 408 appears to be essential for removal of the H_2O molecule. It should be noted that S408I corresponding to T409I from patients with VDDR1 cannot remove the H_2O molecule by 25-(OH)D_3.

Analysis of 1α-Hydroxylation Activity of Wild Type and CYP27B1 Mutants toward 25-(OH)D_3—The 1α-hydroxylation activity toward 25-(OH)D_3 was examined using solubilized CYP27B1 by CHAPS as described under "Experimental Procedures." As shown in Table II, kinetic parameters, K_m and k_{cat}, of the wild type CYP27B1 were estimated to be 0.28 μM and 23.1 min^{-1}, respectively. The k_{cat} and K_m values of S408T were significantly lower than those of the wild type CYP27B1. However, S408T appeared to have enough activity as a 1α-hydroxylase for 25-(OH)D_3 based on its k_{cat}/K_m value. On the other hand, S408A and S408V showed much smaller k_{cat} values than the wild type. As expected by spectral analysis, S408I showed the smallest activity among the mutants. Note that S408A, S408V, and S408I showed K_m values not so different from the wild type.

In the same way, 1α-hydroxylation activity toward 25-(OH)D_3 of Gln^{65} mutants was measured. Mutant Q65E showed only a small activity, although other Gln^{65} mutants showed no detectable activity. The K_m value of Q65E was estimated to be 0.80 μM, which is considerably higher than those of Ser^{408} mutants (Table II). Because the concentration of Q65E hemoprotein was not determined from reduced CO-difference spectrum probably because of its unstability, the k_{cat} value was not determined. On the assumption that Q65E shows a substrate-induced difference spectrum similar to wild type, k_{cat} was estimated to be 0.55 min^{-1}.

Analysis of 1α-(OH)D_3 25-Hydroxylation Activity of the Wild Type and S408V—We consider that the mutant T409I of human CYP27B1 corresponds to S408I of mouse CYP27B1. However, it might be possible that the conversion of Thr to Ile corresponds to the conversion of Ser to Val, judging from their chemical structure. Thus, enzymatic properties of S408V were compared with those of the wild type. As shown in Table III, the kinetic parameters, K_m and k_{cat}, of the wild type for 1α-(OH)D_3 25-hydroxylation was estimated to be 0.52 μM and 0.60 min^{-1}, respectively. Thus, the k_{cat}/K_m value was only 1.3% 1α-(OH)D_3 25-hydroxylation. Ser^{408} showed a similar K_m value but a much smaller k_{cat} value than wild type. These results are quite similar to those for 25-(OH)D_3 1α-hydroxylation, suggesting that Ser^{408} is involved in the binding of not only 25-(OH)D_3 but also 1α-(OH)D_3.

Vitamin D_3 Metabolism by the Wild Type and S408V—Fig. 7 shows the HPLC profiles of vitamin D_3 by wild type CYP27B1 and S408V. Both 1α-(OH)D_3 and 1-α,25(OH)$_2D_3$ were detected in the metabolism by the wild type. However, 25-(OH)D_3 was not detected as reported previously (13). On the other hand, S408V showed a clear peak of 25-(OH)D_3 in addition to those of 1α-(OH)D_3 and 1α,25-(OH)$_2D_3$. LC-MS analysis confirmed that this metabolite is 25-(OH)D_3 (data not shown). It is possible to assume that 25-(OH)D_3 is not detected as an intermediate because of its rapid conversion to 1α,25-(OH)$_2D_3$ by the wild type CYP27B1, but 25-(OH)D_3 is detected because of its slow conversion by S408V. Fig. 8 shows the time courses of vitamin D_3 metabolism. In the metabolism of wild type CYP27B1, 1α-(OH)D_3 increased up to 10 min and thereafter reached plateau, whereas 1α,25-(OH)$_2D_3$ continued increasing. On the other hand, 25-(OH)D_3 was not detected as described previously (13). In contrast, 25-(OH)D_3 was detected as a metabolite of vitamin D_3 by S408V. As shown in Fig. 7, 25-(OH)D_3 increased up to 10 min and thereafter reached plateau, whereas 1α-(OH)D_3 continued increasing. On the other hand, 1α,25-(OH)$_2D_3$ appeared at 10 min, and then the rate of 1α,25-(OH)$_2D_3$ formation increased with increasing time. Vitamin D_3 metabolism together with 25-(OH)D_3 1α-hydroxylation and 1α-(OH)D_3 25-hydroxylation by S408V strongly indicated that S408V has a dual pathway to produce 1α,25-(OH)$_2D_3$ from vitamin D_3 as shown in Fig. 9. Although 25-(OH)D_3 was not detected in the wild type-dependent metabolism of vitamin D_3, it is possible that the wild type has a dual pathway as well as S408V.

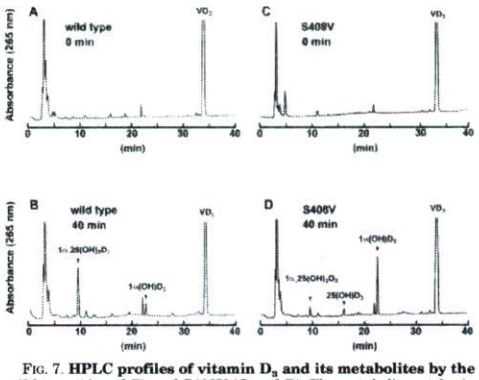

FIG. 7. **HPLC profiles of vitamin D_3 and its metabolites by the wild type (*A* and *B*) and S408V (*C* and *D*).** The metabolites at 0 min (*A* and *C*) and 40 min (*B* and *D*) were analyzed by HPLC according to "Experimental Procedures."

FIG. 8. **Time courses of vitamin D_3 metabolism by wild type (*A*) and S408V (*B*).** The amounts of metabolites of vitamin D_3 at 5, 10, 15, and 20 min was measured according to "Experimental Procedures."

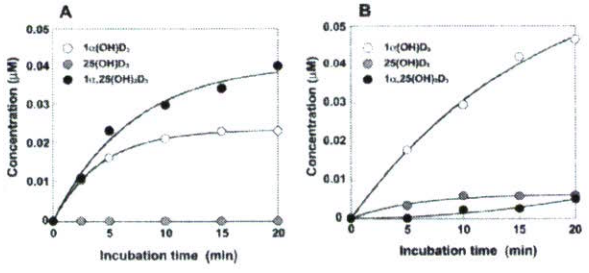

DISCUSSION

Kitanaka *et al.* (6, 7) cloned eight types of missense mutations and one nonsense mutation from Japanese VDDR1 patients, and other groups identified nine missense mutations from patients (8, 9). None of the CYP27B1 mutants expressed in mammalian cells (6) and *E. coli* cells (11, 12) showed 1α-hydroxylase activity toward 25-(OH)D_3. Thus, the mutated amino acid residues seemed to play important roles in the function of 1α-hydroxylase. Our previous study (11) suggested that Arg^{107}, Gly^{125}, and Pro^{497} destroyed the tertiary structure of the substrate-heme pocket. It was also suggested that Arg^{389} and Arg^{453} of CYP27B1 were involved in heme-propionate binding and that Asp^{164} stabilized the 4-helix bundle consisting of D, E, I, and J helices, possibly by forming a salt bridge. Thr^{321} was found to be responsible for the activation of molecular oxygen.

As shown in Fig. 1, amino acid residues at positions 65, 143,

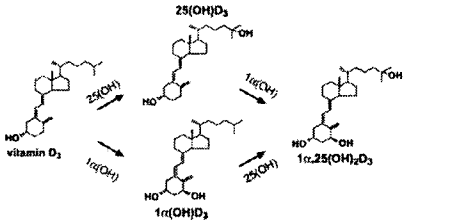

FIG. 9. **Metabolic pathway of vitamin D_3 by CYP27B1 and the mutant S408V.**

189, 323, 409, and 429 of human CYP27B1 were not conserved among mitochondorial P450s. Of these mutations, P143L, E189G(K,L), and R429P are assumed to disrupt protein folding because Pro and Gly residues are known to be helix breakers. In addition, S323Y in the I helix appears to play an important role in protein folding because the side chain of the amino acid residue at position 323 is oriented to the opposite side of a heme molecule, buried inside the protein structure (14). The three-dimensional structure model of CYP27B1 implied that Gln^{65} and/or Thr^{409} interacts with 25-(OH)D_3, probably by forming a hydrogen bond with the 25-hydroxyl group of the substrate. We have not successfully overexpressed human CYP27B1 yet, but we have successfully overexpressed mouse CYP27B1 by using a GroEL/ES co-expression system. Thus, we generated mouse CYP27B1 mutants for Gln^{65} and Ser^{408}, corresponding to Thr^{409} of human CYP27B1. The substitution of Ser^{408} to Thr did not cause significant alterations in substrate binding and 1α-hydroxylation activity toward 25-(OH)D_3. However, the substitutions to Ala, Val, and Ile dramatically decreased 1α-hydroxylation activity and changed the substrate binding manner. Judging from the K_m values of S408A, S408V, and S408I, these mutants have significant affinity for 25-(OH)D_3. However, based on their substrate-induced manner, their binding mode of the substrate appears unsuitable for displacement of H_2O as the distal ligand. Because the displacement of the H_2O molecule by the substrate is essential for P450 reactions, good correlation between the magnitude of $\Delta A_{390-420}$ in Fig. 5 and k_{cat} value in Table II is quite reasonable. Note that S408V has much lower activity than S408T. The difference in the side chain of Val from Thr is the difference between a methyl and a hydroxyl group. Thus, the hydroxyl group is responsible for substrate binding for the P450 reaction. It is possible to assume that the hydroxyl group of Ser^{408} of mouse CYP27B1 or Thr^{409} of human CYP27B1 interacts with the 25-OH group of the substrate through a hydrogen bond. The high affinity of S408A, S408V, and S408I for 25-(OH)D_3 may suggest that another amino acid residue takes the place of Ser^{408} through a hydrogen bond with the substrate.

It is noted that not only 25-(OH)D_3 1α-hydroxylation but also 1α-(OH)D_3 25-hydroxylation by S408V was much less than those of the wild type CYP27B1. These results suggest that the hydroxyl group of Ser^{408} of mouse CYP27B1 is involved in substrate binding of both substrates. Note that the substrate is fixed in the opposite direction in the substrate binding pocket of CYP27B1 between 1α- and 25-hydroxylations. Thus, it appears that the hydroxyl group of Ser^{408} interacts with the 1α-hydroxyl group of 1α-(OH)D_3. On the other hand, 1α-hydroxylation and 25-hydroxylation activities of S408V toward vitamin D_3 appear to be similar to those of the wild type, based on the time courses of the metabolites shown in Fig. 7. These results are consistent with the fact that vitamin D_3 has no hydroxyl groups at positions C-1α and C-25 to interact with the hydroxyl group of the amino acid at position 408.

The significantly higher K_m and lower k_{cat} values of Q65E than the wild type are consistent with an involvement of Gln^{65} in binding of the substrate. However, Western blot and spectral analyses of Gln^{65} mutants indicated that most Gln mutants were expressed as apoproteins without heme molecules, whereas Q65E showed a small amount of hemoprotein and the activity. These results strongly suggest that Gln^{65} is involved in protein folding.

In this study, we revealed that Ser^{408} and Gln^{65} play important roles in substrate binding and the folding of mouse CYP27B1, respectively. The reasons why mutations T409I and Q65H of human CYP27B1 cause VDDR1 were also clearly understood. It is noteworthy that the predictions derived from the three-dimensional model showed good agreement with the experimental data. Thus, this three-dimensional model gives essential information on the structure-function relationship of CYP27B1.

REFERENCES

1. Feldman, D., Glorieux, F. H., and Pike, J. W. (eds) (1997) *Vitamin D*, Academic Press, New York
2. Takeyama, K., Kitanaka, S., Sato, T., Kobori, M., Yanagisawa, J., and Kato, S. (1997) *Science* **277**, 1827–1830
3. Fu, G. K., Lin, D., Zhang, M. Y. H., Bikle, D. D., Shackleton, C. H. L., Miller, W. L., and Portale, A. A. (1997) *Mol. Endocrinol.* **11**, 1961–1970
4. Shinki, T., Shimada, H., Wakino, S., Anazawa, H., Hayashi, M., Saruta, T., DeLuca, H. F., and Suda, T. (1997) *Proc. Natl. Acad. Sci. U. S. A.* **94**, 12920–12925
5. St-Arnaud, R., Messerlian, S., Moir, J. M., Omdahl, J. L., and Glorieux, F. H. (1997) *J. Bone Miner. Res.* **12**, 1552–1559
6. Kitanaka, S., Takeyama, K., Murayama, A., Sato, T., Okumura, K., Nogami, M., Hasegawa, Y., Niimi, H., Yanagisawa, J., Tanaka, T., and Kato, S. (1998) *N. Engl. J. Med.* **338**, 653–661
7. Kitanaka, S., Murayama, A., Sakaki, T., Inouye, K., Seino, Y., Fukumoto, S., Shima, M., Yukizane, S., Takayanagi, M., Niimi, H., Takeyama, K., and Kato, S. (1999) *J. Clin. Endocrine Metab.* **84**, 4111–4117
8. Portale, A. A., and Miller, W. L. (2000) *Pediatr. Nephrol.* **14**, 620–625
9. Yoshida, T., Monkawa, T., Tenenhouse, H. S., Goodyer, P., Shinki, T., Suda, T., and Wakino, S. (1998) *Kidney Int.* **54**, 1437–1443
10. Omdahl, J. L., Borovnikova, Choe, S., Dwivedi, P. P., and May, B. K. (2001) *Steroids* **66**, 381–389
11. Sawada, N., Sakaki, T., Kitanaka, S., Kato, S., and Inouye, K. (2001) *Eur. J. Biochem.* **268**, 6607–6615
12. Sawada, N., Sakaki, T., Kitanaka, S., Takeyama, K., Kato, S., and Inouye, K. (1999) *Eur. J. Biochem.* **265**, 950–956
13. Uchida, E., Kagawa, N., Sakaki, T., Urushino, N., Sawada, N., Kamakura, M., Ohta, M., Kato, S., and Inouye, K. (2004) *Biochem. Biophys. Res. Commun.* **323**, 505–511
14. Yamamoto, K., Masuno, H., Sawada, N., Sakaki, T., Inouye, K., Ishiguro, M., and Yamada, S. (2004) *J. Steroid Biochem. Mol. Biol.* **89-90**, 167–171
15. Williams, P. A., Comse, J., Sridhar, V., Johnson, E. F., and McRee, D. E. (2000) *Mol. Cell* **5** 121–131
16. Kondo, S., Sakaki, T., Ohkawa, H., and Inouye, K. (1999) *Biochem. Biophys. Res. Commun.* **257**, 273–278
17. Omura, T., and Sato, R. (1964) *J. Biol. Chem.* **118**, 397–404
18. Hiwatashi, A., Nishi, Y., and Ichikawa, Y. (1982) *Biochem. Biophys. Res. Commun.* **105**, 320–327
19. Schlichting, I., Berendzen, J., Chu, K., Stock, A. M., Maves, S. A., Benson, D. E., Sweet, R. M., Ringe, D., Petsko, G. A., and Sligar, S. G. (2000) *Science* **287**, 1615–1622
20. Schlichting, I., Jung, C., and Schulze, H. (1997) *FEBS Lett.* **415**, 253–257
21. Cupp-Vickery, J., Anderson, R., and Hatziris, Z. (2000) *Proc. Natl. Acad. Sci. U. S. A.* **97**, 3050–3055

Biochem. J. (2005) **390**, 325–331 (Printed in Great Britain) doi:10.1042/BJ20041799

Role of the vitamin D receptor in FGF23 action on phosphate metabolism

Yoshio INOUE*†, Hiroko SEGAWA*, Ichiro KANEKO*, Setsuko YAMANAKA*, Kenichiro KUSANO‡, Eri KAWAKAMI*, Junya FURUTANI*, Mikiko ITO*, Masashi KUWAHATA*, Hitoshi SAITO‡, Naoshi FUKUSHIMA‡, Shigeaki KATO§, Hiro-omi KANAYAMA† and Ken-ichi MIYAMOTO*[1]

*Department of Molecular Nutrition, Institute of Health Bioscience, The University of Tokushima Graduate School, Kuramoto-cho 3, Tokushima 770-8503, Japan, †Department of Urology, The University of Tokushima School of Medicine, 3-18-15, Kuramoto-Cho, Tokushima 770-8503, Japan, ‡Chugai Pharmaceutical Co. Ltd., Gotenba 412-8513, Japan, and §Institute of Molecular and Cellular Biosciences, University of Tokyo, Yayoi 1-1-1, Bunkyo-ku, Tokyo 113-0032, Japan

FGF23 (fibroblast growth factor 23) is a novel phosphaturic factor that influences vitamin D metabolism and renal re-absorption of P_i. The goal of the present study was to characterize the role of the VDR (vitamin D receptor) in FGF23 action using VDR(−/−) (VDR null) mice. Injection of FGF23M (naked DNA encoding the R179Q mutant of human FGF23) into VDR(−/−) and wild-type VDR(+/+) mice resulted in an elevation in serum FGF23 levels, but had no effect on serum calcium or parathyroid hormone levels. In contrast, injection of FGF23M resulted in significant decreases in serum P_i levels, renal Na/P_i co-transport activity and type II transporter protein levels in both groups when compared with controls injected with mock vector or with FGFWT (naked DNA encoding wild-type human FGF23). Injection of FGF23M resulted in a decrease in 25-hydroxyvitamin D 1α-hydroxylase mRNA levels in VDR(−/−) and VDR(+/+) mice, while 25-hydroxyvitamin D 24-hydroxylase mRNA levels were significantly increased in FGF23M-treated animals compared with mock vector control- or FGF23WT-treated animals. The degree of 24-hydroxylase induction by FGF23M was dependent on the VDR, since FGF23M significantly reduced the levels of serum 1,25(OH)$_2$D$_3$ [1,25-hydroxyvitamin D$_3$] in VDR(+/+) mice, but not in VDR(−/−) mice. We conclude that FGF23 reduces renal P_i transport and 25-hydroxyvitamin D 1α-hydroxylase levels by a mechanism that is independent of the VDR. In contrast, the induction of 25-hydroxyvitamin D 24-hydroxylase and the reduction of serum 1,25(OH)$_2$D$_3$ levels induced by FGF23 are dependent on the VDR.

Key words: fibroblast growth factor 23, kidney, phosphate transport, vitamin D receptor.

INTRODUCTION

P_i (inorganic phosphate) is required for cellular function and skeletal mineralization. P_i re-absorption in the renal proximal tubule is a major mechanism in the maintenance of overall P_i homoeostasis; it is a Na^+-dependent, secondary active process involving Na/P_i co-transport across the renal brush-border membrane as rate-limiting step, particularly via the Na/P_i co-transporter [1–3]. Mammalian Na/P_i co-transporters have been subdivided into types I–III. The type II Na/P$_i$ co-transporter isoforms (a–c) are the major functional Na/P_i co-transporters [1–3]. The type IIa and IIc co-transporters are expressed in the proximal tubules of the kidney, whereas type IIb is expressed in tissues such as the lung and small intestine [1–3]. Serum phosphate concentrations are maintained within a defined range by expression of type II Na/P_i co-transporters, which is, in turn, regulated by PTH (parathyroid hormone) and vitamin D [1–3]. The actions of vitamin D and PTH are important for the control of intestinal P_i absorption or renal P_i excretion. However, adequate systemic phosphate homoeostasis is likely to require the presence of additional bioactive molecules [1,2].

Studies on patients with tumour-induced osteomalacia and ADHR (autosomal dominant hypophosphataemic rickets) resulted in the identification of FGF23 (fibroblast growth factor 23), a protein that shares sequence identity with other FGFs and which results in hypophosphataemic osteomalacia and inappropriately low serum levels of 1,25(OH)$_2$D$_3$ (1,25-dihydroxyvitamin D$_3$) [3–6]. The FGF23 protein is a secreted protein of 251 amino acids, including a putative N-terminal signal peptide (residues 1–24) [3,4,6]. ADHR is caused by missense mutations at Arg^{176} and Arg^{179} of FGF23, which are present in the consensus proteolytic cleavage sequence RXXR [3–6]. Since mutations at Arg^{176} and Arg^{179} prevent proteolytic cleavage, a large amount of the mutant protein may escape proteolytic degradation [3,4].

XLH (X-linked hypophosphataemia) is the most common form of inherited rickets, and is caused by inactivating mutations in the *PHEX* (phosphate regulating endopeptidase homologue, X-linked) gene [3,4]. XLH is characterized by hypophosphataemia due to increased renal phosphate clearance, low or inappropriately normal levels of circulating 1,25(OH)$_2$D$_3$ and rickets/osteomalacia [3,4]. Studies have demonstrated high serum levels of FGF23 in patients with XLH; in addition, levels of FGF23 mRNA expression in bone were significantly increased in the Hyp mouse (which is analogous to the human XLH patient), [7,8]. Thus current evidence indicates that FGF23 may be involved in the pathogenesis of XLH.

Continuous exposure to recombinant FGF23 was shown to cause increased renal P_i clearance resulting from decreased renal expression of type II Na/P_i co-transporters [9–14]. These animals showed paradoxically low/normal 1,25(OH)$_2$D$_3$ levels [9–15]. These reports indicate that FGF23 is an important regulator of P_i homoeostasis and vitamin D metabolism.

Vitamin D plays a central role in modulating P_i homoeostasis and P_i uptake by the small intestine and the kidney [1,2]. It is

Abbreviations used: ADHR, autosomal dominant hypophosphataemic rickets; BBMV, brush-border membrane vesicle; FGF, fibroblast growth factor; FGF23M, naked DNA encoding the R179Q mutant of human FGF23; FGF23WT, naked DNA encoding wild-type human FGF23; GAPDH, glyceraldehyde-3-phosphate dehydrogenase; 1α(OH)ase, 25-hydroxyvitamin D$_3$ 1α-hydroxylase; 24(OH)ase, 25-hydroxyvitamin D 24-hydroxylase; 1,25(OH)$_2$D$_3$, 1,25-dihydroxyvitamin D$_3$; PTH, parathyroid hormone; RT-PCR, reverse transcription–PCR; VDR, vitamin D receptor; XLH, X-linked hypophosphataemia.

[1] To whom correspondence should be addressed: Nutritional Science, Department of Nutrition, School of Medicine, Tokushima University, Kuramoto-Cho 3, Tokushima City 770-8503, Japan (email miyamoto@nutr.med.tokushima-u.ac.jp).

possible that the inappropriately low levels of $1,25(OH)_2D_3$ may suppress the expression of renal and intestinal Na/P_i co-transporters. Indeed, we demonstrated previously that levels of type IIa and type IIb Na/P_i co-transporter proteins were significantly decreased in VDR(−/−) (vitamin D receptor null) mice [16].

Further, targeted ablation of FGF23 [FGF23(−/−) mice] resulted in increased serum phosphate levels and renal phosphate re-absorption, and an elevation in serum $1,25(OH)_2D_3$ levels secondary to enhanced expression of renal 1α(OH)ase (25-hydroxyvitamin D 1α-hydroxylase). These results indicated that FGF23 is essential for normal phosphate and vitamin D metabolism [17]. In contrast, plasma PTH levels were normal, suggesting that hyperphosphataemia in FGF23(−/−) mice occurs via a PTH-independent mechanism [17]. Shimada et al. [14] suggested that FGF23 suppresses renal 1α(OH)ase expression by co-operating or competing with several humoral factors, such as PTH and $1,25(OH)_2D_3$. Thus, while the mechanisms responsible for the high serum phosphate and $1,25(OH)_2D_3$ levels in FGF23(−/−) mice remain unclear, it is possible that high serum $1,25(OH)_2D_3$ levels stimulate the intestinal absorption and renal re-absorption of P_i via the apical Na/P_i co-transporter. This is supported by the fact that levels of the type IIa Na/P_i co-transporter protein were markedly increased in the apical membranes of renal proximal tubule cells in FGF23(−/−) mice [17].

In our previous studies, we examined the effects of administration of FGF23WT (naked DNA encoding wild-type human FGF23) or FGF23M (naked DNA encoding the R179Q mutant of human FGF23) into rats [12]. Injection of FGF23M into rats resulted in significant decreases in plasma P_i levels, renal Na/P_i co-transport activity and type II Na/P_i co-transporter levels. However, injection of FGF23WT into rats had no significant effects. Rats injected with either FGF23WT or FGF23M highly expressed the human *FGF23* transcript in the liver. The levels of plasma human FGF23 protein were markedly increased in rats injected with FGF23M. However, this was not the case in rats injected with FGF23WT [12]. Thus wild-type FGF23 protein may be degraded in the liver or the blood.

The goal of the present study was to use VDR(−/−) mice to determine (i) whether vitamin D is involved in the regulation of renal P_i re-absorption by FGF23, and (ii) whether the VDR is required for the down-regulation of 1α(OH)ase activity by FGF23.

EXPERIMENTAL

Animals and diet

VDR(−/−) mice were generated by gene targeting as described previously [18]. VDR genotypes were confirmed by analysing the DNA obtained from each mouse approx. 3 weeks after birth. Genomic DNA was extracted from tail clippings and amplified by PCR using primers specific for VDR(+/+) exon 2 or the neomycin-resistance gene, as described previously [16].

VDR(+/+) and VDR(−/−) mice were weaned at 3 weeks of age, and given free access to water and a control diet containing 0.5 % P_i and 0.5 % Ca for 5 weeks. After 5 weeks, naked DNA (encoding FGF23 or FGF23 R179Q) or the empty vector was administered by intravenous injection [12,15].

FGF23 mutant construct and injection of naked DNA

DNA encoding human FGF23 or the FGF23 R179Q mutant was subcloned into the pCAGGS3 expression plasmid vector at a unique EcoRI site between the CAG promoter and a 3′-flanking sequence of rabbit β-globin. The empty pCAGGS3 plasmid (kindly provided by Dr J.-i. Miyazaki, Osaka University, Osaka, Japan) was used as a mock control. Next, 1.5 ml of DNA solution containing 10 μg of each expression plasmid [pCGF23 (wild-type human FGF23), pCGFM2 (human FGF23 R179Q mutant) or pCAGGS3 vector] was administered intravenously, as described previously [12,15]. At 4 days after the injection of naked DNA, blood samples were obtained from the abdominal vein, and tissues were rapidly removed under anaesthesia.

Quantitative analysis of FGF23 mRNA

Total RNA was extracted from the livers of transfected animals using ISOGEN (Nippon Gene, Tokyo, Japan), and cDNA was synthesized using M-MLV (Moloney murine leukaemia virus) Reverse H reverse transcriptase (Superscript; Invitrogen) and an $oligo(dT)_{12-18}$ primer. The amount of human FGF23 cDNA relative to GAPDH (glyceraldehyde-3-phosphate dehydrogenase) cDNA was determined by competitive RT-PCR (reverse transcription–PCR) using a 7700 Sequence Detector (PE Applied Biosystems) [12,15]. The PCR primers used for these experiments did not amplify cDNA of the endogenous mouse FGF23 homologue.

Detection of serum FGF23

The serum concentration of exogenous human FGF23 in mice was determined using the Human FGF23 (C-term) ELISA kit (Immunotopics, San Clemente, CA, U.S.A.), which only detects human FGF23 [12,15]. The serum concentration of endogenous mouse FGF23 was determined using the FGF-23 ELISA kit (KAINOS Laboratories, Inc., Tokyo, Japan). We analysed the cross-reactivity of FGF23 proteins between mouse and human (see Figure 1b). The human FGF-23 (C-term) ELISA kit did not detect endogenous mouse FGF23 in either VDR(+/+) or VDR(−/−) mice. In contrast, the mouse FGF23 ELISA kit clearly detected endogenous mouse FGF23 in both VDR(+/+) and VDR(−/−) mice. Serum FGF23 protein levels were significantly lower in VDR(−/−) than in VDR(+/+) mice. These results indicated that the human FGF23 (C-term) ELISA kit did not cross-react with the endogenous mouse FGF23.

Serum calcium, P_i, PTH and $1,25(OH)_2D_3$ levels

The serum concentrations of Ca^{2+} and P_i were determined by the Calcium-E test and the Phospha-C test (both from Wako, Osaka, Japan) respectively. Serum concentrations of PTH were determined using the mouse PTH ELISA kit (Immunotopics) [16,17]. Serum concentrations of $1α,25(OH)_2D_3$ were determined by a radioreceptor assay (Mitsubishi BCL, Tokyo, Japan) [15].

Northern blot analysis

Poly(A)$^+$ RNA (3 μg/lane) isolated from mouse intestine or kidney was separated on a 1 % (w/v) agarose gel in the presence of 2.2 M formaldehyde and blotted on to a Hybond N$^+$ membrane (Amersham Pharmacia Biotech) as described previously [12,16,19]. Specific probes for 1α(OH)ase, 24(OH)ase (25-hydroxyvitamin D 24-hydroxylase) and each Na/P_i co-transporter were labelled with [^{32}P]dCTP using the Megaprime DNA Labeling System (Amersham Pharmacia Biotech) [12,16,19]. The specific probes for 1α(OH)ase and 24(OH)ase were similar to those used for RT-PCR. Hybridization proceeded for 3 h at 65 °C, and the blot was evaluated by autoradiography using a Fujix BAS-1500 bioimaging analyser (Fujifilm, Tokyo, Japan).

RT-PCR for 1α(OH)ase and 24(OH)ase

Kidney total RNA extraction and cDNA synthesis were performed as described above. The PCR primers were designed for 1α(OH)ase and 24(OH)ase as follows: 1α(OH)ase (forward/reverse; 5′-3′), CCGCGGGCTATGCTGGAAC/CTCTGGGCAAAGGCAAACATCTGA; 24(OH)ase (forward/reverse; 5′-3′), TGGGAAGATGATGGTGACCC/ACTGTTCCTTTGGGTAGCGT. PCR were performed for 32 cycles, with cycle conditions of 94 °C for 1 min, 58 °C for 1 min, and 72 °C for 1 min. All amplicons were sequenced to confirm the specificity of amplification.

Preparation of BBMVs (brush-border membrane vesicles) and transport assay

BBMVs were prepared from mouse kidney or intestine by the Ca^{2+} precipitation method, as described previously [12,16,19]. BBMV ^{32}P uptake was measured by the rapid filtration technique. A sample of 10 μl of vesicle suspension was added to 90 μl of incubation solution (100 mM NaCl, 100 mM mannitol, 20 mM Hepes/Tris and 0.1 mM $KH_2{}^{32}PO_4$), and the preparation was incubated at 20 °C. Transport was terminated by rapid dilution with ice-cold saline, and the reaction mixture was transferred immediately to a remoistened filter (0.45 μm) and maintained under a vacuum [12,16].

Immunoblotting

Protein samples were heated at 95 °C for 5 min in sample buffer in the presence of 2-mercaptoethanol and subjected to SDS/PAGE. The separated proteins were transferred by electrophoresis to a Hybond-P PVDF transfer membranes and then treated with diluted affinity-purified antibodies against type IIa (1:4000) or type IIc (1:1000) Na/P_i co-transporters [17,18]. Mouse anti-actin monoclonal antibody (CHEMICON) was used as an internal control. Horseradish peroxidase-conjugated anti-rabbit or anti-mouse IgG was utilized as the secondary antibody (Jackson Immuno-Research Laboratories), and signals were detected using the ECL Plus® system (Amersham Pharmacia Biotech) [12,16,19].

Statistical analysis

One-way ANOVA (*post hoc* Scheffé *F*-test) and two-factor factorial ANOVA were performed. Data are expressed as means ± S.E.M. Statistical analysis of endogenous serum FGF23 measurements in VDR(−/−) and VDR(+/+) mice was performed using Welch's test. $P < 0.05$ was considered significant.

RESULTS

Effects of FGF23 on food intake in VDR(+/+) and VDR(−/−) mice

VDR(−/−) and VDR(+/+) mice were weaned at 3 weeks of age, housed in plastic cages, and given free access to water (distilled water) and diet containing 0.5 % calcium and 0.5 % phosphorus for 5 weeks, as described in the Experimental section. We measured the dietary intake of all VDR(−/−) and VDR(+/+) mice used in the study. As shown in Table 1, there were no differences in food intake between VDR(+/+) and VDR(−/−) mice for up to 4 days after the injection of naked DNA.

Expression of mutant FGF23 mRNA and protein

We demonstrated previously that injection of naked DNA plasmids encoding the human *FGF23* gene into animals resulted in the expression of FGF23 protein in the liver for at least 4 days [12,15]. To determine if the effect of FGF23 on intestinal and renal phosphate transport is dependent on vitamin D, naked DNA plasmids encoding the human *FGF23* gene were injected into VDR(+/+) and VDR(−/−) mice. At 4 days after injection, wild-type human FGF23 and mutant FGF23-R179Q mRNAs were present in liver tissue at relatively high levels in both VDR(+/+) and VDR(−/−) mice, as shown by quantitative PCR (Figure 1a).

Using the human FGF23 (C-term) ELISA kit, we demonstrated that protein levels of human FGF23 were markedly increased in both VDR(+/+) and VDR(−/−) mice injected with FGF23M, but not in mice injected with FGF23WT (Figure 1c).

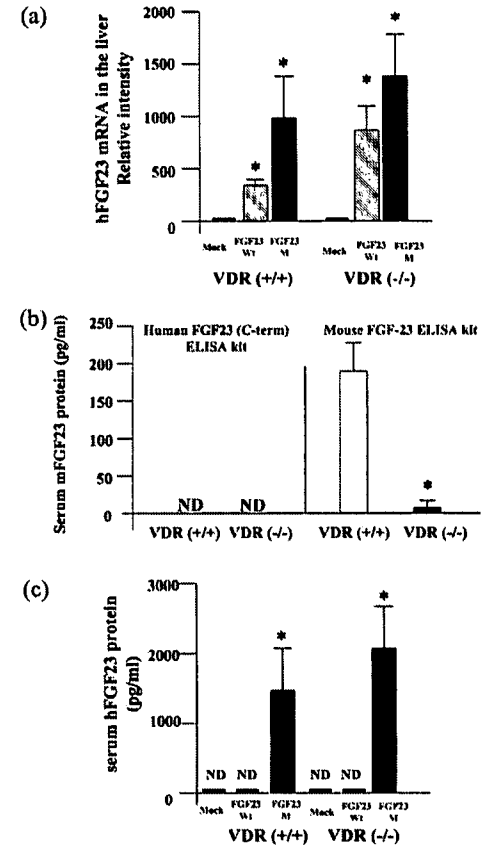

Figure 1 Expression of FGF23 in VDR(+/+) and VDR(−/−) mice

At 4 days after administration of FGF23WT, FGF23M or empty vector to VDR(+/+) mice and VDR(−/−) mice, we analysed the expression of human FGF23 mRNA and protein. (**a**) Expression of FGF23 in the liver, as assessed by competitive RT-PCR (see the Experimental section). FGF23 mRNA levels are shown relative to those of GAPDH mRNA. One-way ANOVA (*post hoc* Scheffé *F*-test) and two-factor factorial ANOVA were performed. Values are means ± S.E.M. ($n = 5$–6); *$P < 0.05$ compared with mock vector control. (**b**) Serum concentrations of endogenous mouse FGF23 (mFGF23) protein in VDR(+/+) and VDR(−/−) mice were determined using two separate ELISA kits, as described in the Experimental section. Statistical analysis of endogenous serum FGF23 levels in VDR(−/−) and VDR(+/+) mice was performed using Welch's test. Values are means ± S.E.M. ($n = 10$); *$P < 0.05$ for VDR(+/+) compared with VDR(−/−) mice. (**c**) Serum concentrations of exogenous human FGF23 protein (hFGF23) were determined by ELISA in VDR(+/+) and VDR(−/−) mice injected with naked DNA. One-way ANOVA (*post hoc* Scheffé *F*-test) and two-factor factorial ANOVA were performed. Values are means ± S.E.M. ($n = 5$–6); *$P < 0.05$ compared with mock vector control. ND, not detected.

Table 1 Effects of FGF23 on food intake in VDR(+/+) and VDR(−/−) mice

One-way ANOVA (*post hoc* Scheffé *F*-test) and two-factor factorial ANOVA were performed. Values are means ± S.E.M. ($n = 6–10$).

Mice	Injection	No. of days of injection ...	Food intake (g/day)					
			−1	0	1	2	3	4
VDR(+/+)	Mock		4.2 ± 0.8	3.6 ± 1.0	4.7 ± 0.9	3.8 ± 0.9	5.3 ± 0.8	4.2 ± 0.8
	FGF23WT		3.9 ± 0.9	3.5 ± 1.1	4.5 ± 0.6	3.7 ± 0.9	5.2 ± 0.8	3.9 ± 0.9
	FGF23M		4.1 ± 0.9	3.8 ± 0.9	4.8 ± 0.5	3.5 ± 0.9	4.7 ± 0.5	4.1 ± 0.9
VDR(−/−)	Mock		4.5 ± 0.8	3.7 ± 1.2	4.3 ± 0.8	3.8 ± 0.8	4.6 ± 0.8	3.9 ± 1.2
	FGF23WT		4.2 ± 0.9	3.9 ± 0.9	4.7 ± 0.6	3.5 ± 1.0	4.9 ± 0.8	3.6 ± 1.0
	FGF23M		4.4 ± 0.8	3.6 ± 0.9	4.2 ± 0.9	4.1 ± 1.1	4.7 ± 0.8	3.5 ± 0.9

Table 2 Effects of FGF23 on serum levels of calcium, P_i, 1,25(OH)$_2$D$_3$ and PTH in VDR(+/+) and VDR(−/−) mice at 4 days after injection

One-way ANOVA (*post hoc* Scheffé *F*-test) and two-factor factorial ANOVA were performed. Values are means ± S.E.M. ($n = 6–10$). Significance of differences: * $P < 0.05$ compared with VDR(+/+) (mock); † $P < 0.005$ compared with VDR(+/+) (FGF23WT); ‡ $P < 0.005$ compared with VDR(−/−) (mock); § $P < 0.05$ compared with VDR(−/−) (FGF23WT).

	VDR(+/+)			VDR(−/−)		
	Mock	FGF23WT	FGF23M	Mock	FGF23WT	FGF23M
Calcium (mg/dl)	9.02 ± 0.14	9.03 ± 0.23	9.24 ± 0.24	6.61 ± 0.52*	6.90 ± 0.39	7.46 ± 0.16
P_i (mg/dl)	7.43 ± 0.40	7.43 ± 0.31	5.87 ± 0.16*†	5.73 ± 0.27*	5.12 ± 0.30	3.59 ± 0.36‡§
1,25(OH)$_2$D$_3$ (pg/ml)	82 ± 16	130 ± 47	6 ± 0.16*†	630 ± 6*	617 ± 16	610 ± 8
PTH (pg/ml)	19.3 ± 3.0	18.5 ± 2.3	16.0 ± 1.0	343 ± 25.9*	281 ± 47.6	277 ± 25.3

Table 3 Effects of injection of FGF23M on intestinal and renal Na^+-dependent P_i transport activity in VDR(+/+) and VDR(−/−) mice

Na^+-dependent P_i co-transport activity was assessed by the measurement of P_i uptake into intestinal or renal BBMVs. One-way ANOVA (*post hoc* Scheffé *F*-test) and two-factor factorial ANOVA were performed. Values are means ± S.E.M. ($n = 5–6$). Significance of differences: * $P < 0.05$ compared with mock; † $P < 0.05$ compared with FGF23WT.

	P_i uptake (nmol/30s per mg of protein)					
	VDR(+/+)			VDR(−/−)		
	Mock	FGF23WT	FGF23M	Mock	FGF23WT	FGF23M
Intestine	0.533 ± 0.03	0.467 ± 0.070	0.304 ± 0.050*†	0.338 ± 0.040	0.364 ± 0.020	0.315 ± 0.060
Kidney	1.024 ± 0.133	0.984 ± 0.100	0.743 ± 0.040*†	1.104 ± 0.171	0.960 ± 0.161	0.733 ± 0.060*†

Effects of FGF23M on serum levels of calcium, P_i, PTH and vitamin D

Serum calcium, P_i, PTH and 1,25(OH)$_2$D$_3$ levels were determined 4 days after injection of FGF23WT, FGF23M or mock vector in VDR(+/+) and VDR(−/−) mice (Table 2). Serum calcium and P_i levels were significantly decreased in VDR(−/−) mice compared with VDR(+/+) mice, as described previously [16,18]. In contrast, serum PTH and 1,25(OH)$_2$D$_3$ levels were markedly increased in VDR(−/−) mice compared with VDR(+/+) mice [16,18]. Injection of FGF23M resulted in a significant decrease in serum P_i, but did not affect serum calcium or PTH, in both VDR(+/+) and VDR(−/−) mice. However, FGF23M resulted in a significant decrease in 1,25(OH)$_2$D$_3$ levels only in VDR(+/+) mice. There were no significant differences in any serum parameter when comparing mice injected with FGF23WT and those injected with mock vector.

Effects of FGF23M on renal and intestinal Na/P_i transport activity in VDR(+/+) and VDR(−/−) mice

We reported previously that intestinal Na/P_i co-transport activity in VDR(−/−) mice was reduced to 60% of that seen in VDR(+/+) mice, and that expression of intestinal Na/P_i co-transporter (type IIb) protein was markedly suppressed in VDR(−/−) mice when compared with VDR(+/+) mice [16]. Further, whereas renal BBMV Na/P_i co-transport activity was similar when comparing VDR(−/−) mice and VDR(+/+) mice, expression of type IIa Na/P_i protein was slightly and significantly decreased in VDR(−/−) mice, and there was no difference in type IIc Na/P_i protein expression between VDR(−/−) and VDR(+/+) mice [16].

In the present study, injection of FGF23M resulted in a significant reduction in intestinal Na/P_i co-transport activity in VDR(+/+) mice, but had no such effect in VDR(−/−) mice (Table 3). Injection of FGF23M also resulted in a significant reduction in renal Na/P_i co-transport activity in both VDR(+/+) and VDR(−/−) mice.

Effects of FGF23M on renal type II Na/P_i co-transporter proteins in VDR(+/+) and VDR(−/−) mice

Injection of FGF23M resulted in significant attenuation of type IIa and type IIc renal Na/P_i co-transporter protein expression in both VDR(+/+) and VDR(−/−) mice (Figures 2I and 2II, left panels). As shown in Figure 2 (right panels), the levels of type IIa Na/P_i co-transporter protein in BBMVs were decreased to 50% and those of type IIc protein were markedly reduced, compared with BBMVs from mock vector control-injected animals, in both VDR(+/+) and VDR(−/−) mice. However, injection of FGF23M had no effect on type IIa or type IIc transporter mRNA levels in VDR(+/+) or VDR(−/−) mice (Figure 3). As described previously [12,15], injection of mock vector or FGF23WT had no effect on intestinal or renal Na/P_i co-transport activity, or transporter protein or mRNA levels, in VDR(+/+) or VDR(−/−) mice (Table 2, Figures 2 and 3).

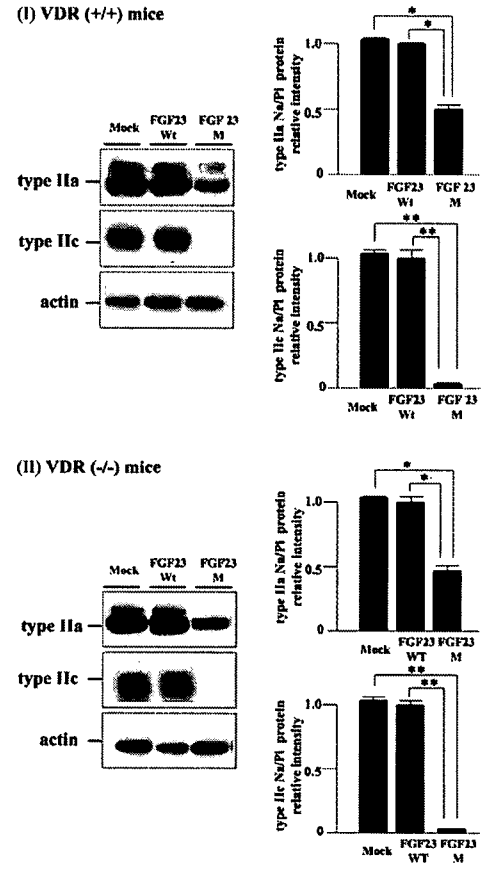

Figure 2 Western blot analysis of renal type II Na/P_i co-transporters

BBMVs (20 μg/lane) isolated from the kidneys of VDR(+/+) and VDR(−/−) mice injected with empty vector, FGF23WT or FGF23M were loaded into each lane. Upper panels, type IIa co-transporter; middle panels, type IIc Na/P_i co-transporter; lower panels, actin (internal control). The immunoreactive band intensity for mice injected with the empty vector was 1.0. One-way ANOVA (*post hoc* Scheffé *F*-test) and two-factor factorial ANOVA were performed. Values are means ± S.E.M. ($n = 5–6$); the significance of differences is indicated by * $P < 0.05$ and ** $P < 0.01$.

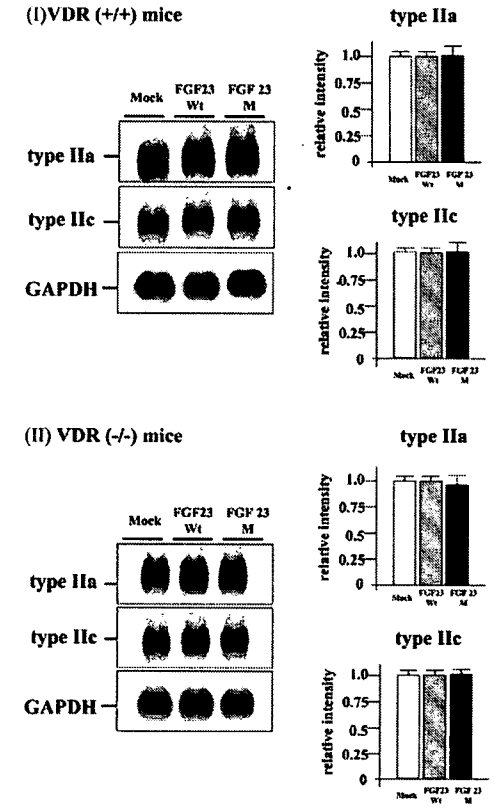

Figure 3 Northern blot analysis of renal Na/P_i co-transporters

Poly(A)$^+$ RNA was extracted from the kidneys of VDR(+/+) and VDR(−/−) mice that had been injected with FGF23WT, FGF23M or the empty vector. Each lane was loaded with 3 μg of RNA. Upper panels, type IIa co-transporter; middle panels, type IIc Na/P_i co-transporter; lower panels, GAPDH (internal control). The visualized band intensity for the mice injected with the empty vector expression was designated as 1.0, and all other band intensities were expressed relative to this value. One-way ANOVA (*post hoc* Scheffé *F*-test) and two-factor factorial ANOVA were performed. Values are means ± S.E.M. ($n = 5–6$).

Effects of FGF23 on 1α(OH)ase and 24(OH)ase mRNA levels

VDR(−/−) mice have higher 1α(OH)ase mRNA levels and lower 24(OH)ase mRNA levels when compared with VDR(+/+) mice [20,21]. Injection of FGF23M resulted in a marked reduction in 1α(OH)ase mRNA levels (Figure 4) and a significant increase in 24(OH)ase mRNA levels (Figure 4) in both VDR(+/+) and VDR(−/−) mice. However, the increase in 24(OH)ase mRNA levels was much less in VDR(−/−) mice than in VDR(+/+) mice.

DISCUSSION

The present study used VDR(+/+) and VDR(−/−) mice to investigate whether vitamin D is involved in the FGF23-mediated

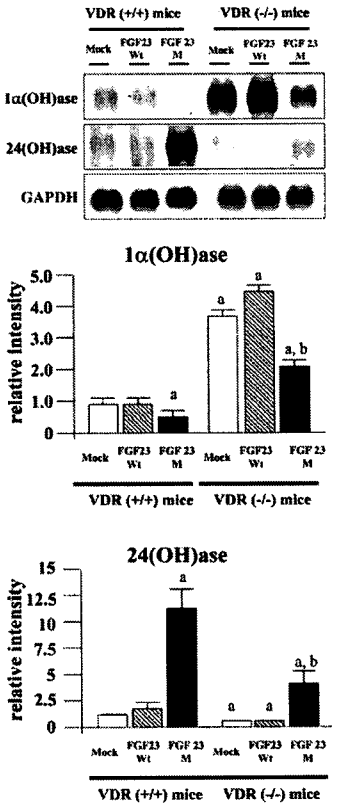

Figure 4 Effects of injection of FGF23M on 1α(OH)ase and 24(OH)ase mRNA levels

Poly(A)$^+$ RNA was extracted from the kidneys of VDR(+/+) and VDR(−/−) mice that had been injected with FGF23WT, FGF23M or the empty vector. Each lane was loaded with 3 μg of RNA. Upper panel, 1α(OH)ase; middle panel, 24(OH)ase; lower panel, GAPDH (internal control). In the histograms, the visualized band intensity for the VDR(+/+) mice injected with the empty vector was designated as 1.0, and all other band intensities are expressed relative to this value. One-way ANOVA (*post hoc* Scheffé *F*-test) and two-factor factorial ANOVA were performed. Values are means ± S.E.M. ($n = 5$–6); $^a p < 0.05$ compared with VDR(+/+) mock vector control., $^b p < 0.05$ compared with VDR(−/−) mock vector control.

regulation of renal P_i re-absorption, and whether the VDR is required for the FGF23-mediated down-regulation of $1,25(OH)_2D_3$ levels. The key findings are: (1) VDR may affect the hepatic expression of exogenous FGF23 mRNA, (2) VDR is not involved in the FGF23-mediated suppression of renal Na/P_i co-transport activity, (3) VDR may be involved in the FGF23-mediated down-regulation of intestinal Na/P_i co-transport activity, (4) VDR is involved in the FGF23-mediated induction of renal 24(OH)ase mRNA, and (5) VDR is important in the FGF23-mediated regulation of plasma $1,25(OH)_2D_3$ levels.

Previous studies demonstrated that injection of FGF23WT into rats resulted in an increase in the hepatic expression of FGF23 mRNA, but not in serum FGF23 levels [12]. This lack of a change in serum FGF23 levels may result from protein degradation of wild-type FGF23 in the liver or the circulation, since rats that received FGF23M showed high levels of mRNA in the liver, and serum FGF23 protein levels also increased. Indeed, the present study demonstrated that wild-type FGF23 was degraded in VDR(+/+) and VDR(−/−) mice. Moreover, the expression of both wild-type and mutant FGF23 in the liver was higher in VDR(−/−) than in VDR(+/+) mice (Figure 1a), which suggests that VDR may control the stability of FGF23 mRNA in the liver. Further studies are needed to clarify the mechanisms underlying the hepatic expression of of FGF23.

Recent studies reported that administration of FGF23 resulted in decreases in type II Na/P_i co-transporter mRNA and proteins levels in the kidney [11,12,14], suggesting that FGF23 may affect the transcriptional step of type II transporter synthesis. However, the present study demonstrated that down-regulation of type II Na/P_i co-transporter expression was not dependent on transcriptionally regulated changes in mRNA. Murer et al. [2] found that changes in type II Na/P_i co-transporter mRNA levels were either rather small or occurred only after prolonged stimulation by thyroid hormone (3,3′,5-tri-iodothyronine) and feeding of a low-P_i diet; furthermore, they occurred after changes in specific transporter protein content, suggesting that changes in mRNA represent a phenomenon secondary to the primary event (i.e. down-regulation or up-regulation of brush border type IIa co-transporter expression) [2]. Thus FGF23 may directly modulate trafficking of the transporter from the apical membrane to the intracellular organelles.

Injection of FGF23M decreased intestinal Na/P_i co-transport activity in VDR(+/+) mice, but not in VDR(−/−) mice, which suggests that the action of the mutant FGF23 on intestinal P_i transport is VDR-dependent. Further, VDR(−/−) mice were characterized by hypophosphataemia, hypocalcaemia and high PTH and $1,25(OH)_2D_3$ levels, which may also affect the action of FGF23M. In a previous study, we investigated the effects of FGF23 in hypophosphataemic animals (fed a low-P_i diet) [12]. After injection of naked FGF23 DNA, renal Na/P_i co-transport activity and type II phosphate transporter protein levels were significantly deceased in hypophosphataemic rats [12]. 1α(OH)ase mRNA levels and intestinal Na/P_i co-transport activity were also deceased in those animals. These data suggested that hypophosphataemia itself does not affect the function of FGF23 in VDR(−/−) mice. Further investigations aimed at characterizing the regulation of intestinal Na/P_i co-transporter (type IIb) gene expression by VDR and mutant FGF23 would be of benefit.

FGF23 acts to decrease 1α(OH)ase mRNA levels and increase 24(OH)ase mRNA levels. Renal 1α(OH)ase and 24(OH)ase are regulated by several factors, including PTH, calcium, P_i and $1,25(OH)_2D_3$ [3–5]. In target tissues, $1,25(OH)_2D_3$ exerts most of its biological actions by binding to the VDR, and feedback regulation of 1α(OH)ase gene expression by $1,25(OH)_2D_3$ has been reported [22–24]. Thus VDR may be important in the regulation of 1α(OH)ase and 24(OH)ase mRNAs by FGF23.

In the present study, injection of FGF23M induced a decrease in 1α(OH)ase mRNA and an increase 24(OH)ase mRNA levels in both VDR(+/+) and VDR(−/−) mice. These results suggest that the actions of FGF23 are independent of the VDR-mediated decrease in 1α(OH)ase mRNA and increase in 24(OH)ase mRNA. The lack of a decrease in serum $1,25(OH)_2D_3$ levels in VDR(−/−) mice injected with FGF23M may be for several reasons. First, degradation of $1,25(OH)_2D_3$ may be insufficient in VDR(−/−) mice, as expression of 24(OH)ase, which is required for the inactivation and degradation of vitamin D metabolites, was relatively low in these mice. Secondly, the serum calcium concentration may directly regulate serum $1,25(OH)_2D_3$ levels.

Panda et al. [25] studied groups of VDR(−/−) mice exposed to (1) a high-calcium diet, (2) a high-calcium diet plus injection of $1,25(OH)_2D_3$, and (3) a rescue diet (high calcium, high phosphate and high lactose), and showed that only VDR(−/−) mice receiving a rescue diet had normal plasma calcium levels. Further, VDR(−/−) mice had normalized plasma P_i, $1,25(OH)_2D_3$ and PTH concentrations, as well as increased 24(OH)ase mRNA and decreased in 1α(OH)ase mRNA levels [25]. These data suggest that the normalization in serum calcium levels may be related to normalization of serum $1,25(OH)_2D_3$ in mice fed the rescue diet. In the present study, injection of FGF23M did not affect serum calcium levels in either VDR(+/+) or VDR(−/−) mice. Since serum calcium levels remained low in VDR(−/−) mice, high levels of $1,25(OH)_2D_3$ may persist in these mice. Further studies to investigate the FGF23 signalling pathway would be of benefit in clarifying the physiological role of FGF23 in vitamin D metabolism.

In conclusion, the present study has demonstrated that injection of FGF23M lowered renal P_i transport and 1α(OH)ase levels by a mechanism that is independent of the VDR. In contrast, the induction of 24(OH)ase and reduction in serum $1,25(OH)_2D_3$ levels by FGF23 is dependent on the VDR.

We thank Miss Kazuyo Shiozawa for technical support. This work was supported by grants from the Ministry of Education, Science, Sports and Culture of Japan (grants 15790430 to H.S. and 11557202 to K.M.) and the 21st Century COE Program, Human Nutritional Science on Stress Control, Tokushima, Japan.

REFERENCES

1 Miyamoto, K., Segawa, H., Ito, M. and Kuwahata, M. (2004) Physiological regulation of renal sodium-dependent phosphate cotransporters. Jpn. J. Physiol. **54**, 93–102
2 Murer, H., Hernando, N., Forster, I. and Biber, J. (2000) Proximal tubular phosphate reabsorption: molecular mechanisms. Physiol. Rev. **80**, 1373–1409
3 Tenenhouse, H. S. and Sabbagh, Y. (2002) Novel phosphate-regulating genes in the pathogenesis of renal phosphate wasting disorders. Pflugers. Arch. **444**, 317–326
4 Quarles, L. D. (2003) FGF23, PHEX, and MEPE regulation of phosphate homeostasis and skeletal mineralization. Am. J. Physiol. Endocrinol. Metab. **285**, E1–E9
5 The ADHR Consortium (2000) Autosomal dominant hypophosphatemic rickets is associated with mutations in FGF23. Nat. Genet. **26**, 345–348
6 White, K. E., Jonsson, K. B., Carn, G., Hampson, G., Spector, T. D., Mannstadt, M., Lorenz-Depiereux, B., Miyauchi, A., Yang, I. M., Ljunggren, O. et al. (2001) The autosomal dominant hypophosphatemic rickets (ADHR) gene is a secreted polypeptide overexpressed by tumors that cause phosphate wasting. J. Clin. Endocrinol. Metab. **86**, 497–500
7 Liu, S., Simpson, L. G., Xiao, Z. S., Burnham, C. E. and Quales, L. D. (2003) Regulation of fibroblastic growth factor 23 expression but not degradation by PHEX. J. Biol. Chem. **278**, 37419–37426
8 Yamazaki, Y., Okazaki, R., Shibata, M., Hasegawa, Y., Satoh, K., Tajima, T., Takeuchi, Y., Fujita, T., Nakahara, K., Yamashita, T. and Fukumoto, S. (2002) Increased circulatory level of biologically active full-length FGF-23 in patients with hypophosphatemic rickets/osteomalacia. J. Clin. Endocrinol. Metab. **87**, 4957–4960
9 Bai, X. Y., Miao, D., Goltzman, D. and Karaplis, A. C. (2003) The autosomal dominant hypophosphatemic rickets R176Q mutation in fibroblast growth factor 23 resists proteolytic cleavage and enhances in vivo biological potency. J. Biol. Chem. **278**, 9843–9849
10 Bai, X. Y., Miao, D., Li, J., Goltzman, D. and Karaplis, A. C. (2004) Transgenic mice overexpressing human fibroblast growth factor 23 (R176Q) delineate a putative role for parathyroid hormone in renal phosphate wasting disorders. Endocrinology **145**, 5269–5279
11 Larsson, T., Marsell, R., Schipani, E., Ohlsson, C., Ljunggren, O., Tenenhouse, H. S., Juppner, H. and Jonsson, K. B. (2003) Transgenic mice expressing fibroblast growth factor 23 under the control of the α1(I) collagen promoter exhibit growth retardation, osteomalacia and disturbed phosphate homeostasis. Endocrinology **145**, 3087–3094
12 Segawa, H., Kawakami, E., Kaneko, I., Kuwahata, M., Ito, M., Kusano, K., Saito, H., Fukushima, N. and Miyamoto, K. (2003) Effect of hydrolysis-resistant FGF23-R179Q on dietary phosphate regulation of the renal type-II Na/Pi transporter. Pflugers Arch. **446**, 585–592
13 Shimada, T., Mizutani, S., Muto, T., Yoneya, T., Hino, R., Takeda, S., Takeuchi, Y., Fujita, T., Fukumoto, S. and Yamashita, T. (2001) Cloning and characterization of FGF23 as a causative factor of tumor-induced osteomalacia. Proc. Natl. Acad. Sci. U.S.A. **98**, 6500–6505
14 Shimada, T., Hasegawa, H., Yamazaki, Y., Muto, T., Hino, R., Takeuchi, Y., Nakamura, K., Fukumoto, S. and Yamashita, T. (2004) FGF-23 is a potent regulator of vitamin D metabolism and phosphate homeostasis. J. Bone Miner. Res. **19**, 429–435
15 Saito, H., Kusano, K., Kinosaki, M., Ito, H., Hirata, M., Segawa, H., Miyamoto, K. and Fukushima, N. (2003) Human fibroblast growth factor-23 mutants suppress Na^+-dependent phosphate co-transport activity and 1α,25-dihydroxyvitamin D3 production. J. Biol. Chem. **278**, 2206–2211
16 Segawa, H., Kaneko, I., Yamanaka, S., Ito, M., Kuwahata, M., Inoue, Y., Kato, S. and Miyamoto, K. (2004) Intestinal Na/Pi cotransporter adaptation to dietary Pi content in vitamin D-receptor (VDR) null mice. Am. J. Physiol. Renal Physiol. **287**, F39–F47
17 Shimada, T., Kakitani, M., Yamazaki, Y., Hasegawa, H., Takeuchi, Y., Fujita, T., Fukumoto, S., Tomizuka, K. and Yamashita, T. (2004) Targeted ablation of FGF23 demonstrates an essential physiological role of FGF23 in phosphate and vitamin D metabolism. J. Clin. Invest. **113**, 561–568
18 Yoshizawa, T., Handa, Y., Uematsu, Y., Takeda, S., Sekine, K., Yoshihara, Y., Kawakami, T., Arioka, K., Sato, H., Uchiyama, Y. et al. (1997) Mice lacking the vitamin D receptor exhibit impaired bone formation, uterine hypoplasia and growth retardation after weaning. Nat. Genet. **16**, 391–396
19 Ohkido, I., Segawa, H., Yanagida, R., Nakamura, M. and Miyamoto, K. (2003) Cloning, gene structure and dietary regulation of the type-IIc Na/Pi cotransporter in the mouse kidney. Pflugers Arch. **446**, 106–115
20 Li, X., Zheng, W. and Li, Y. C. (2003) Altered gene expression profile in the kidney of vitamin D receptor knockout mice. J. Cell. Biochem. **89**, 709–719
21 Takeyama, K., Kitanaka, S., Sato, T., Kobori, M., Yanagisawa, J. and Kato, S. (1997) 25-Hydroxyvitamin D3 1α-hydroxylase and vitamin D synthesis. Science **277**, 1827–1830
22 Barletta, F., Dhawan, P. and Christakos, S. (2004) Integration of hormone signaling in the regulation of human 25(OH)D3 24-hydroxylase transcription. Am. J. Physiol. Endocrinol. Metab. **286**, E598–E608
23 Christakos, S., Dhawan, P., Liu, Y., Peng, X. and Porta, A. (2003) New insights into the mechanisms of vitamin D action. J. Cell. Biochem. **88**, 695–705
24 Christakos, S., Barletta, F., Huening, M., Dhawan, P., Liu, Y., Porta, A. and Peng, X. (2003) Vitamin D target proteins: function and regulation. J. Cell. Biochem. **88**, 238–244
25 Panda, D. K., Miao, D., Bolivar, I., Li, J., Huo, R., Hendy, G. N. and Goltzman, D. (2004) Inactivation of the 25-hydroxyvitamin D 1alpha-hydroxylase and vitamin D receptor demonstrates independent and interdependent effects of calcium and vitamin D on skeletal and mineral homeostasis. J. Biol. Chem. **279**, 16754–16766

Received 26 October 2004/25 April 2005; accepted 10 May 2005
Published as BJ Immediate Publication 10 May 2005, doi:10.1042/BJ20041799

JB Minireview—Reproductive / Urogenital Organ Development and Molecular Genetic Cascades *J. Biochem.* **138**, 105–110 (2005)
DOI: 10.1093/jb/mvi118

Study of Androgen Receptor Functions by Genetic Models

Takahiro Matsumoto[1,2], Ken-ichi Takeyama[1], Takashi Sato[1] and Shigeaki Kato[1,2,*]

[1]*Institute of Molecular and Cellular Biosciences, University of Tokyo, 1-1-1 Yayoi, Bunkyo-ku, Tokyo, 113-0032; and* [2]*ERATO, Japan Science and Technology Agency, 4-1-8 Honcho, Kawaguchi, Saitama, 332-0012*

Received April 6, 2005; accepted April 20, 2005

Androgens exert most of their biological activities through binding to the androgen receptor (AR). The AR belongs to the nuclear receptor superfamily and acts as a ligand-inducible transcriptional factor. AR dysfunction causes a diverse range of clinical conditions, such as testicular mutation (Tfm) syndrome, prostate cancer, and spinal and bulbar muscular atrophy (SBMA). However, the molecular basis of the AR function underlying these AR-related disorders remains largely unknown due to the lack of stable genetic models. Here we review recent results of our studies into genetic models of the loss of AR function in mice and the gain of AR function in *Drosophila*.

Key words: androgen receptor (AR), androgen receptor knockout (ARKO), *Drosophila*-eye model, polyQ repeat, spinal and bulbar muscular atrophy (SBMA), testicular feminization mutation (Tfm).

Abbreviations: AR, androgen receptor; ARE, androgen response element; KO, knockout; SBMA, spinal and bulbar muscular atrophy; Tfm, testicular feminization mutation.

Androgens as male sex hormones have a critical role in wide rage biological processes (*1*, *2*). These include spermatogenesis, virilization of genitalia and brain functions. Most actions of androgens are mediated by the nuclear androgen receptor (AR), which acts as ligand-inducible transcription factor (*3*, *4*). Liganded AR forms homodimers and binds specific DNA elements in the target gene promoter. The DNA element that binds AR is the common sequence 5′-AGAACANNNTGTTCT-3′, referred to as the consensus androgen response element (*ARE*). To date, a number of clinical disorders of the AR have been reported. Classical AR functional abnormalities cause a spectrum of disorders of androgen insensitivity syndrome (AIS) or testicular feminization mutation (Tfm) (*5–9*). AR mutations underlying these disorders include amino acid substitutions in the DNA or ligand binding domains, point mutations leading to premature stop codons, and deletions of the AR gene (*6*, *8*, *9*). In addition, expansion of a polyQ repeat region within AR has been implicated in the pathogenesis of a motor neuron disease called spinal and bulbar muscular atrophy (SBMA) (*5*, *7*). AR is a relatively large protein compared to other steroid receptors, due to its long N-terminal A/B domain that contains this polyQ repeat. However, the molecular basis of AR function underlying these AR-related disorders remains largely unknown due to the lack of stable genetic models. In this article, we present recent results of our studies into genetic models of loss of AR function in mice (*10–12*) and gain of AR function in *Drosophila* (*13*).

*To whom correspondence should be addressed at: Institute of Molecular and Cellular Biosciences, University of Tokyo, Yayoi, Bunkyo-ku, Tokyo 113-0032. Fax: +81-3-5841-8477, Tel: +81-3-5841-8478, E-mail: uskato@mail.ecc.u-tokyo.ac.jp

Domain features of androgen receptor

In the late 1980s, the cloning the human AR opened an avenue for understanding the molecular mechanism of androgen actions (*14*). The AR gene comprises eight exons that encode a 110-kDa protein. In common with other members of the nuclear receptor superfamily, the AR contains distinct structural and functional domains referred to as domains A to E(F) (*3*, *4*). The highly conserved middle region (C domain) acts as a DNA binding domain, while the ligand binding domain (LBD) is located in the C-terminal E/F domain. The LBDs of most nuclear receptors, including AR, have been analyzed and are comprised of 12 α helixes that form a pocket to capture cognate ligands (*15*, *16*). Upon ligand binding, the C-terminal α helix 12 (H12) in the LBD shifts position to create a space, with helixes 3 to 5 serving as the key interface following dissociation of corepressor complexes and association of coactivator complexes (*3*, *17*). During ligand-induced transactivation, the N-terminal domains A/B and the steroid receptor LBD act as interacting regions for the co-activator complexes. The autonomous activation function-1 (AF-1) within the A/B domain is ligand-independent, while AF-2 within the LBD is induced upon ligand binding (*18*). While unliganded LBD appears to suppress the function of the A/B domain, ligand binding to the LBD is thought to evoke LDB function and restore A/B domain function through an as yet undescribed intramolecular alteration of the entire steroid receptor structure.

Generation of AR-null mutant mice by gene targeting using the Cre-loxP system

Although androgens seem to exert beneficial effects in males, the physiological role of AR-mediated androgen signaling in male physiology and behaviors has not been established. This is because estrogens are locally converted from serum androgens by aromatase in target

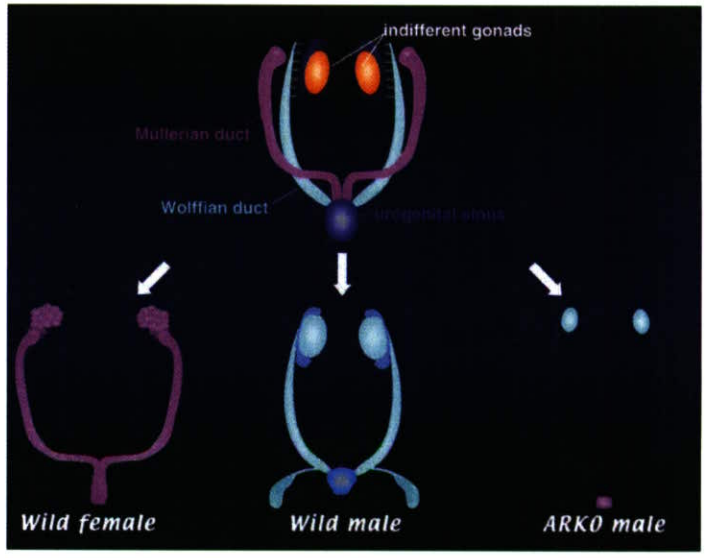

Fig. 1. **Schematic representation of reproductive organs in male ARKO mice.** Male ARKO mice are characterized by female-typical appearance, including a clitoris-like phallus and a vagina with a blind end, as well as the absence of internal male and female reproductive organs, except for the presence of atrophic testes.

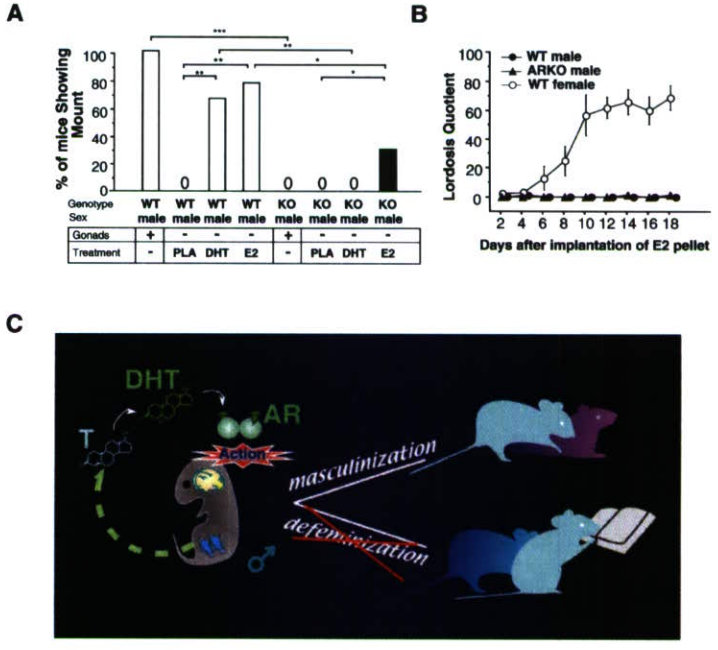

Fig. 2. **Ablation of AR in male mice resulted in the lack of both male and female sexual behaviors.** (A) Loss of all components of male sexual behavior in intact (Gonads: +) 10-week-old ARKO mice. (B) Lordosis was not induced in gonadectomized ARKO male mice after treatment with E2. (C) Schematic representation of AR function in perinatal brain masculinization and defeminization.